

2011

A Different Kind of Garden: Seeding the Growth of TaS₂ Nanostructures with 3d Transition Metals

Kayla Rose Boyle
University of Northern Iowa

Let us know how access to this document benefits you

Copyright ©2011 Kayla Rose Boyle

Follow this and additional works at: <https://scholarworks.uni.edu/hpt>

Recommended Citation

Boyle, Kayla Rose, "A Different Kind of Garden: Seeding the Growth of TaS₂ Nanostructures with 3d Transition Metals" (2011). *Honors Program Theses*. 835.

<https://scholarworks.uni.edu/hpt/835>

This Open Access Honors Program Thesis is brought to you for free and open access by the Student Work at UNI ScholarWorks. It has been accepted for inclusion in Honors Program Theses by an authorized administrator of UNI ScholarWorks. For more information, please contact scholarworks@uni.edu.

Offensive Materials Statement: Materials located in UNI ScholarWorks come from a broad range of sources and time periods. Some of these materials may contain offensive stereotypes, ideas, visuals, or language.

A DIFFERENT KIND OF GARDEN:
SEEDING THE GROWTH OF TaS₂ NANOSTRUCTURES
WITH 3d TRANSITION METALS

A Thesis
Submitted
in Partial Fulfillment
of the Requirements for the Designation
University Honors

Kayla Rose Boyle
University of Northern Iowa
May 2011

This Study by: Kayla Rose Boyle

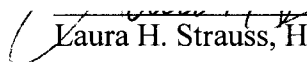
Entitled: A Different Kind of Garden: Seeding the Growth of TaS₂ Nanostructures with
3d Transition Metals

has been approved as meeting the thesis requirement for the Designation

University Honors

5/6/2011

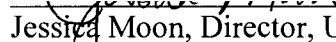
Date



Laura H. Strauss, Honors Thesis Advisor, Chemistry and Biochemistry

5/6/11

Date



Jessica Moon, Director, University Honors Program

ABSTRACT

An investigation into the synthesis of TaS₂ nanostructures was performed through the comparison of four growth methods. Each method utilized a 3d metal, Mn or Cr, or a comparable metal sulfide compound as a potential nucleating compound to seed the growth of these nanostructures, and all samples were produced using similar heating conditions. Sample imaging of the final products was performed using scanning electron microscopy (SEM), while the chemical compositions were determined by x-ray diffraction (XRD) and energy dispersive x-ray spectroscopy (EDS). From these analyses it was determined that the most effective growth process for these TaS₂ nanostructures resulted from the direct seeding of the elemental powders Mn or Cr and the dispersion of the initial powders across the sample ampoules. This elemental nucleation also resulted in the successful intercalation of Mn into the crystalline TaS₂ structure, altering the natural structure of these materials. Attempts to nucleate nanostructure growth from the metal sulfide powders were unsuccessful. The rigidity of these nanostructures was also shown to improve when samples were grown from a nucleated substance, compared to those synthesized without a seeding material.

ACKNOWLEDGEMENTS

I would like to begin by thanking the faculty and staff of the UNI Chemistry and Biochemistry and Physics departments, the professors who shared their knowledge with me during classes or just in passing conversations and the staff who helped fill in the “how to”s and “what to do”s while saving my experiments over the years. Most especially, I would like to thank Dr. Laura Strauss for the incredible instruction and guidance through three years of research, including this final thesis. Thank you for showing me the flaming passion to chemistry! Also, many thanks to Dr. Tim Kidd of UNI Physics for the many recommendations during this and other research projects over the last two years.

Also, I would like to extend my appreciation to the College of Natural Sciences for its assistance in the completion of this thesis project through the funding of a SOAR (Student Opportunities for Academic Research) award.

Finally, and most importantly, I would like to thank my parents, John and Jo Kay. It was through your guidance that I opened myself to see the many opportunities available to me at UNI. You have been my ever-present encouragers and the constant inspiration for my success throughout this and every project—“thank you” does not seem good enough. I love you!

TABLE OF CONTENTS

	PAGE
LIST OF FIGURES	v
LIST OF TABLES	vii
1. INTRODUCTION	1
1.1. Thesis overview	1
1.1.1. Research purpose	1
1.1.2. Hypotheses tested.....	1
1.2. Literary overview.....	2
1.2.1. Basic TMDC 2D crystal structures	2
1.2.2. Intercalated TMDC 2D crystals	3
1.2.3. 1D Nanostructure formation of TMDC combinations.....	5
2. MATERIALS AND METHODS.....	10
2.1. Materials	10
2.2. Random growth samples.....	11
2.2.1. Method A	11
2.2.2. Method B	12
2.3. Base growth samples	13
2.3.1. Method C	13
2.3.2. Method D	15
3. RESULTS AND DISCUSSION	17
3.1. Pure Samples	17
3.1.1. Method A (KB Pr A).....	17

3.1.2. Method B (KB Pr B).....	19
3.1.3. Method C (KB Pr C).....	22
3.1.4. Method D (KB Pr D).....	23
3.2. Mn and MnS Samples.....	25
3.2.1. Method A (KB Mn A).....	25
3.2.2. Method B (KB Mn B).....	28
3.2.3. Method C (KB Mn C).....	31
3.2.4. Method D (KB Mn D).....	32
3.3. Cr and Cr ₂ S ₃ seeded samples.....	33
3.3.1. Method A (KB Cr A).....	33
3.3.2. Method B (KB Cr B).....	35
3.3.3. Method C (KB Cr C).....	37
3.3.4. Method D (KB Cr D).....	38
4. CONCLUSIONS.....	40
4.1. Research conclusions.....	40
4.2. Limitations and recommendations for future study.....	42
REFERENCES	45
APPENDIX A: ACQUIRED X-RAY DIFFRACTION SPECTRA	47
APPENDIX B: IDENTIFIED DATA CARDS FROM THE INTERNATIONAL CENTER FOR DIFFRACTION DATA.....	57
APPENDIX C: ENERGY DISPERSIVE X-RAY SPECTROSCOPY REPORTS	63

LIST OF FIGURES

FIGURE	PAGE
1 Model of crystalline packing structure for TaS ₂ samples	3
2 Overlaid x-ray diffraction spectra of samples KB Pr A1 and A2 with identified composition.....	18
3 Scanning electron microscope images KB Pr A sample.....	19
4 Overlaid x-ray diffraction spectra of samples Pr B1, B2 and B3 with identified composition.....	21
5 Scanning electron microscope image of KB Pr B sample	21
6 Scanning electron microscope image of KB Pr C sample	23
7 Overlaid x-ray diffraction spectra of samples Pr C1 and D1 with identified composition.....	24
8 Super-imposed x-ray diffraction spectra of all four pure classes	25
9 Overlaid x-ray diffraction spectra of samples KB Mn A1 and A2 with identified composition.....	26
10 Scanning electron microscope image of KB Mn A	28
11 Overlaid x-ray diffraction spectra of samples KB Mn B1 and B2 with identified composition.....	30
12 Scanning electron microscope image of KB Mn B	30
13 X-ray diffraction spectra of samples KB Mn C1 with identified composition.	31
14 Scanning electron microscope image of KB Mn C	32
15 Overlaid x-ray diffraction spectra of samples KB Mn C1 and D1 with identified composition.....	33

16	Overlaid x-ray diffraction spectra of samples KB Cr A1 and A2 with identified composition.....	34
17	Overlaid x-ray diffraction spectra of samples KB Cr B1 and B2 with identified composition.....	36
18	Scanning electron microscope image of KB Cr B.....	36
19	Scanning electron microscope image of KB Cr C.....	37
20	Overlaid x-ray diffraction spectra of samples KB Cr C1 and D1 with identified composition.....	39
21	Super-imposed x-ray diffraction spectra of all four Cr classes.....	39

LIST OF TABLES

TABLE	PAGE
1 Summary of the four studied growth methods.....	16

1. INTRODUCTION

1.1. Thesis overview

1.1.1. Research purpose

In early 2010, Dunnill, MacLaren and Gregory¹ expressed the need for “an understanding of growth and structure at the nanoscale” for the nano-sized materials formed by crystalline tantalum disulfide, TaS₂. Such knowledge is essential to determine which of the various structure-related properties existing for bulk dichalcogenide materials also translate to nano-sized structures and if any new structure-property relationships arise from nanoscale samples. One method that can assist in the identification of such structure-property relationships is intercalation, a process in which additional particles are integrated into a pure crystalline structure. This research sought to further the understanding of successful growth methods for TaS₂ nanostructures through variations in the reactant chemicals and growth parameters. Specifically, these experiments utilized the concept of intercalation by focusing on the effects of adding 3d metals manganese, Mn, or chromium, Cr, or their respective metal-sulfide counterparts to the reactant mixtures of tantalum, Ta, and sulfur, S. This focus allowed investigations into the extent to which the intercalating elements act as a nucleation material for the production of TaS₂ nanostructures.

1.1.2. Hypothesis tested

The information gathered from recent literature sources provided some basic insight into the growth of these materials. First, the synthesis of actual TaS₂ nanostructures is temperature dependent; annealing samples at temperatures too high or too low will yield other TaS_x compounds. Similarly, the TaS₂ polytype will also be

partially determined by heating and cooling rates, particularly the formation of 3R-TaS₂ from cooling more slowly. Finally, the specific microscale structure and structural consistency of these TaS₂ nanomaterials (nanorod, -tube, -tape, etc.) is likely a direct response to the material used for nucleation in the reaction. As a target temperature was already identified for these intercalated materials, this study investigated the validity of the following statements:

- Both pure Mn or Cr powders and commercial MnS or Cr₂S₃ powders will produce nucleation material for the formation of TaS₂ nanostructures.
- Introducing the commercial powders into the initial reaction in place of the pure metal powders will override the need for a metal-sulfide side product to form, causing the TaS₂ nanostructure growth to become more consistent.
- The uniform nature of the commercial powders will provide a consistent base from which the nanostructures will grow, thereby producing a more ordered arrangement for structure growth compared to those formed from the clusters of reaction side products.

It was believed that questions revolving around the synthesis of these nucleated nanostructures would be answered by concentrating on these specific concepts.

1.2. Literary overview

1.2.1. Basic TMDC 2D crystal structures

TaS₂ is one MCh₂ compound of approximately 60 combinations that are broadly categorized as transition metal dichalcogenide (TMDC) structures, where M could be nearly any group IVb, Vb, VIb, VIIb or VIIIb transition metal and Ch=S, Se or Te. In 1977, Lieth and Terhell considered all of these materials to fall into one of two

classifications, either layered or non-layered compounds.² Through an extensive review of TMDC preparation techniques and resulting sample structures, the two primary crystal

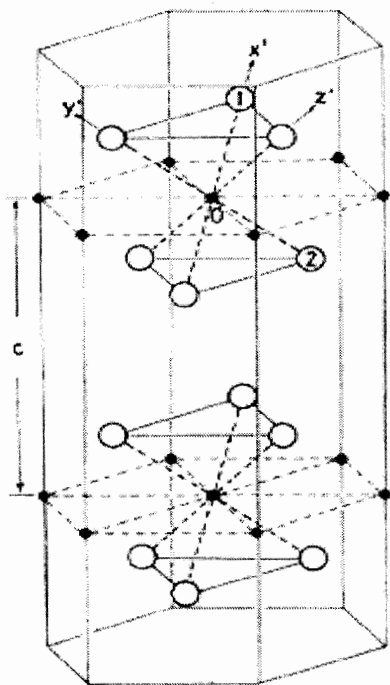


Figure 1. Structural model of 2H-TaS₂ crystalline structure. Small black circles denote Ta atoms, white circles S.¹⁶

structures that described the majority of these samples were hexagonal close packed systems and trigonal prismatic systems, both of a 6:3 coordination with the chalcogens surrounding the transition metals in the respective structural holes. The bulk crystal and powder materials were formed by weak interlayer van der Waals interactions between chalcogen atoms bonding together to hold multiple molecular layers together.² The coordination of the 2H-TaS₂ polytype, the primary structure found in nearly all studies involving TaS₂ materials and the structure shown in Figure 1, was described by Guo and Liang³ as being trigonal prismatic and belonging to the hexagonal

space group system. The sandwich-like molecular layers provided sufficient space for the transition metal in an intra-layer octahedral hole, while still providing vacant holes in which other materials may later be introduced.³

1.2.2. Intercalated TMDC 2D crystals

These vacant holes within the crystalline structures have been used to further enhance the natural electronic conduction properties of TMDCs.⁴ Guo and Liang were able to exploit the open octahedral holes of TaS₂ by introducing small Li atoms into the crystal structure, a process known as intercalation. The addition of the intercalant, Li,

had little effect on the resulting crystal dimensions, as the minute atoms were able to sit neatly in previously vacant locations; however, the addition resulted in the formation of a semiconductor of crystalline nature.³ Intercalation of the post-transition metals Pb and Sn had a greater effect on the physical properties of the TaS₂ structure, both in expanding the crystalline dimensions in the vertical (c-axis) direction by intercalating into the interlayer spacing and through the resulting increase in superconducting transition temperatures.³ Intercalation of TaS₂ has also been induced using organic compounds such as pyridine molecules,⁵ which lie in bilayers parallel to the TaS₂ layers. The resulting structures from the organic intercalation were without the structural distortion that was common for TMDC compounds of group Vb elements.⁵

Intercalation of TMDC structures with 3d transition metals, often noted as Z_xMCh₂ where Z=3d series and x<1.0, has also been a topic of great interest to researchers,⁶ even in the early stages of studies on these structures. Recent studies on the structures using a copper intercalant⁷ resulted in the successful intercalation of the 3d metal into the interlayer spacing, which created an observed competition between the inherent electronic and magnetic properties of the two materials, overall hindering the superconductivity established for these layered materials. Historically, it has been difficult to make general statements for the properties of 3d-intercalated TaS₂, as many of the elements resulted in different physical properties.⁶ For instance, Mn and Cr intercalation induced ferromagnetic behavior in the TMDC material, while Fe-intercalated samples presented antiferromagnetic behavior. However, as a whole, it appeared that intercalation of TaS₂ with 3d metals effectively eliminated the superconductivity of this layered dichalcogenide material.

1.2.3. 1D Nanostructure formation of TMDC combinations

As a result of the in-depth studies on numerous TMDC materials throughout the last five decades, various nanostructures of these materials have actually been synthesized for over 30 years; however, unfamiliarity to nanomaterials at the time meant these new TMDC forms were often classified by phrases like “poorly crystalline ‘rag’ structures”.⁸ It was not until after published discoveries of carbon nanostructures by H. W. Kroto⁹ and S. Iijima¹⁰ in 1987 and 1991, respectively, sparked world-wide interest in nano-sized structures that researchers began investigating the possibilities of nano-sized TMDC compounds. Most often the initial studies observed a wide variety of the MCh_2 compounds, varying the metal between any of the heavier group IVb, Vb or VIb transition metals with corresponding sulfur or selenium.^{11,12(a)} Newer studies became more focused on the relative structural compositions and uses for just one type of transition metal, such as the Group Vb compounds NbS_2 and TaS_2 .^{1,12(b),13}

In the last decade, studies by Nash and Rao,^{12(a),(b)} Dunnill et al.^{1,13} and Liu et al.¹¹ investigated the structures of nano- TaS_2 using various growth methods and come away with an array of conclusions. The conclusion of greatest variation between these three groups of authors was also the simplest: the terminology used to describe the macroscale structure formed by the common molecular structure of TaS_2 . While Liu made reference to the synthesis of nanotubes and nanorods of TaS_2 with hemispherical tips, Nash and Rao specified their growth process clearly resulted in hollow-core nanotubes with diameters of approximately 20-40nm and fairly rectangular tips.^{12(a)} Both groups reported the synthesis of 2H- TaS_2 structures through the application of a gas-solid reaction at elevated temperatures. In contrast, the first reported single-step synthesis of

TaS₂ nanostructures by Dunnill, Edwards, Brown and Gregory¹³ in 2006 resulted in nanowires of diameters 100-600nm that were identified as “clustered bundles of smaller individual nanofilaments”. When analyzed, the nanofilaments corresponded to the 2H polytype like their nanorod and nanotube predecessors; however, inspection of the bulk crystalline powder that accompanied these structures corresponded to the 3R polytype, indicating a mixed polytypic synthesis. Dunnill and Gregory’s more recent study with MacLaren¹ also produced nanoribbons, fine nanowires, platelets and nanotapes of various TaS_x combinations and polytypes. The variation in structure was related to different maximum annealing temperatures during the growth process. Shi et al.¹⁴ referred to both of these synthetic methods as well as many others in the review of the various approaches to TMDC synthesis. Mention of TaS₂ syntheses, however, is most strongly supported through the discussions of the above methods. Because the primary challenge for each of these research groups was to understand the growth mechanism of these materials, no mention was made of tested, applicable uses for these structures. Sample analyses for all studies were consistent, utilizing x-ray diffraction (XRD) to match sample composition and polytype to stored PDF files from the International Center for Diffraction Data (ICDD), while scanning electron microscopy (SEM), energy dispersive x-ray spectroscopy (EDS) and tunneling electron microscopy (TEM) provided the imaging and structural information to classify the sizes and structural aspects of the reaction products. Some studies also utilized selected area electron diffraction (SAED) to confirm the single-crystalline structure of materials.¹³

While the research of the last decade into the synthetic processes of TMDC nanostructures resulted in identifying a large collection of both micro- and

nanostructures, there is still much to learn about the growth mechanisms behind these minute structures for which a wide array of applications is imagined. Because such obstacles are still prevalent, little investigation has occurred involving the intercalation of the nano-scale compounds to parallel their bulk 2D counterparts. However, a study performed in 2009 at the University of Northern Iowa (UNI)¹⁵ originally focused on the synthesis of $Z_{0.25}\text{TaS}_2$ bulk materials, $Z=\text{Mn, Cr}$, effectively produced TaS_2 nanostructures resembling those synthesized in the single-step method by Dunnill et al.^{1,13} The integration of pure 3d metal intercalant powders into the reaction ampoule provided the necessary elements for nanostructure growth to readily occur during the annealing process and resulted in intercalated structures, some measuring several millimeters in length. While the nanostructures of the Cr samples presented inconsistent intercalation, with doping ranges varying from 0-17%, the nanomaterials of Mn-doped samples appeared relatively uniform in structure and, through XRD, were found to have experienced a slight c-axis spacing shift indicative of Mn storage between the crystalline molecular layers.¹⁵

Though the self-intercalation of these TaS_2 nanostructures was indeed a notable result of the synthetic method derived by researchers at UNI, it was not the only significant observation produced by these experiments. The microscopic clusters formed by the reaction side product, MnS or Cr_2S_3 were also a significant discovery. Side products were expected to form from the single-step reaction, however it was not expected that these clusters would be regularly located at the base of bundled nanostructures. In fact, SEM images suggested these intercalant-sulfide clusters actually

played a role in fueling the growth of nanostructures, that it was these clusters acting as a nucleation site for the nanostructures that stimulated the initial structural formation.

The idea of sample nucleation is not unique to intercalated samples, however, for each of the synthetic processes previously discussed also required some form of nucleation to initiate the growth of TaS₂ nanostructures. The earliest TaS₂ synthesis references utilized the gas-solid reaction method, forming the nanorods and nanotubes from the inside out.^{11,12(a)} This process prepared the dichalcogenide materials from the reduction of their trichalcogenide precursors by a stream of H₂ gas in elevated temperatures. In this instance, the TaS₃ precursors served as the nucleation surface from which the TaS₂ structures grew as H₂ gas passed, pulling the reduced nanostructures outward from the nucleation site. Liu et al.¹¹ reported SEM images of clustering trichalcogenide particles surrounded by TaS₂ nanotubes. In 2006, Dunnill et al.¹³ also utilized a nucleation stimulus in the form of pure Ta foil. This addition to the reaction ampoule was reported to significantly increase the yield of nanostructures grown.

The effects of nucleating these reactions did not seem to be limited to merely stimulating the formation of nanostructures, though. Of further interest was the fact that in these cases, the microstructures of each TaS₂ nano-sized product appeared to reflect the composition and structural appearance of their nucleation material. Inside-out growth methods^{11,12(a)} produced nanorods, readily formed by the streaming of H₂ gas through the precursor materials, taking with it reduced TaS₂ molecular crystals. Hollow-core nanotubes were likely synthesized by surrounding the trichalcogenide precursors with newly formed TaS₂ structures that, when aided by the constant stream of H₂ gas, extended outward to close only at the very tip of the nanotubes. Dunnill et al. also

observed needle-like nanostructures protruding from the Ta foil, seemingly growing perpendicular to the foil surface,¹³ and later identified TaS₂ structures as nanotapes that always grew from surfaces, likely resulting from the interactions between the sulfur-rich vapor phase and the Ta foil surface.¹ Likewise, the UNI samples protruded from randomly synthesized side products and displayed complete disorganization of the nanostructures, growing in every direction and tangled into large nests of interwoven material, which further supported the concept of a relationship between the seeding material and the organization of the nanostructure growth.

2. MATERIALS AND METHODS

2.1. Materials

This research comprised four distinct growth methods; the first was a replication of the method leading to the original production of TaS₂ nanotubes by the University of Northern Iowa laboratory group, while the remaining three series explored various growth methods utilizing the nucleation compounds MnS and Cr₂S₃. Every sample was grown using commercially purchased elemental and molecular powders of high purities (Alfa Aesar, 99+%) and regulated sizes. An analytical scale provided the masses of each powder in a plastic weigh boat before they were transferred into fused silica ampoules, 11mm inner diameter. A handcrafted glass funnel was used during this transfer to ensure that the powders reached the bases of the ampoules and did not remain above the level where the ampoule would be sealed. The samples from Methods A and B were grown in a three-zone tube furnace (Thermolyne 79600), and samples from Methods C and D were grown in a single-zone (Thermcraft) furnace. Every sample was analyzed by x-ray diffraction (XRD) using a bench-top RIGAKU Miniflex II X-ray Diffractometer, and scanning electron microscopy (SEM) and energy dispersive x-ray spectroscopy (EDS) analyses were acquired from an Evex MiniSEM. Composition identifications from XRD data utilized the previously published spectral data stored as PDF files by the International Center for Diffraction Data (ICDD). Appendix A contains the XRD identification of each sample individually and Appendix B the utilized ICDD PDF files. The composition reports and analyzed images for the EDS analyses are contained in Appendix C.

2.2. Random growth samples

2.2.1. Method A

Because Method A was intended to affirm the reproducibility of the method previously discovered to produce nanostructures with a basic TaS₂ crystalline structure, the growth procedure was copied from the earlier experiment.¹⁵ Each 0.5 g sample consisted of stoichiometric amounts of tantalum powder (-325 mesh, 99.9%) and sulfur powder (sublimed, 99.5%). Additionally, extra manganese (-325 mesh, 99.95%) or chromium (-60 mesh, 99.99%) powders were added to the samples in a 25% molar ratio to produce samples of Mn_{0.25}TaS₂ or Cr_{0.25}TaS₂. These samples were labeled as KB Mn A and KB Cr A, respectively, whereas the pure samples (those containing no 3d metal intercalant) were labeled as KB Pr A. Each of the three classes within this A series was duplicated to ensure that the resulting compounds were products of the growth method itself and not some unique trait of the ampoule, thus creating samples A1 and A2 for each class and a total of six samples grown from Method A.

After the powders were settled into the bottom of a fused silica ampoule, the ampoules were flame-sealed under vacuum using a natural gas torch to a length of approximately 15 cm. The sample tubes were allowed to cool before they were hand shaken to mix the layers of powders, and then the powder was loosely situated near the base of ampoule. Each of the six ampoules was then placed in a ceramic sleeve before it was laid on its side in the Thermolyne tube furnace. In the furnace, the sleeves containing ampoules labeled KB __ A2 were placed directly over their KB __ A1 counterparts.

The heating process for these samples began by heating the furnace to 125 °C and holding the temperature for 24 hours to ensure the ampoules would not burst from a quick build up of pressure as the sulfur powder vaporized. Next, the sample heating continued as the temperature rose to 700 °C at a rate of approximately 8.5 °C/h. The furnace was held at this temperature for five days before the samples began to cool back to room temperature over 15 hours.

Once the ampoules were removed from the furnace, a small line was etched into the tube using a dremel router, and the ampoule was popped open by applying pressure to the ampoule opposite the etching, breaking the vacuum inside. A portion of the resulting products was removed from each ampoule and placed in a labeled glass vial that was then capped and covered with parafilm. These samples were stored until SEM and EDS analyses could be performed. The remainder of each sample was stored in labeled plastic vials. These vials supplied the material used for XRD analysis. The samples analyzed by SEM/EDS were removed from their capped vials and mounted onto aluminum/nickel pin stubs using carbon tape. For this series alone, the XRD analyses were obtained using whole nanostructures on a silicon zero-background sample holder. Droplets of acetone were added to the sample plate to help hold the nanostructures secure during the analysis.

2.2.2. Method B

The creation of the samples produced from Method B varied little from those in Method A. Again, pure tantalum and sulfur powders were placed into fused silica ampoules stoichiometrically to create 0.5 g samples. With this series, though, the corresponding metal sulfide compounds (nucleation compounds) replaced the pure intercalant powders. This meant the samples labeled KB Mn B1 and B2 contained a fine,

green powder of commercial MnS (99.9%) in place of the Mn powder, and the samples KB Cr B1 and B2 contained commercial Cr₂S₃ powder (99%) rather than the Cr powder. KB Pr B1 and B2 still reflected the ampoules that held only pure tantalum and sulfur powders, as did the third pure sample KB Pr B3.

The seven samples from this B series were flame-sealed in the same manner as Method A, each measuring 16-18 cm. Once sealed, each of the ampoules was shaken to mix the various powders within, and the powder was distributed across the bottom of the tubes to provide a greater surface area from which the TaS₂ structures could grow. The six ampoules whose labels paralleled the samples of Method A were identically arranged in the tube furnace; KB Pr B3 was situated directly above KB Pr B2. The growth of these samples proceeded using the same heating pattern as in Method A, as did the process used to open each ampoule. Because of the consistency of these samples—primarily powder rather than nanostructures—each of these samples was ball-milled into a very fine powder after some of the initial product was removed and contained separately for SEM/EDS analysis. The ball-milled portion of these samples was then used to fill the 0.2 mm-deep well of an aluminum XRD sample holder. Again, droplets of acetone were added to the powder to pack the sample in the well and smooth the surface of the sample. The procedure for SEM/EDS analysis was identical to that of Method A.

2.3. Base growth samples

2.3.1. Method C

The preparation of the samples grown through Method C varied more from Method A than Method B did to create a direct comparison between the products of

Method C and Method D. The introduction of the commercial powders into the ampoule for this series began with the metal sulfide compounds where appropriate, potentially creating a base of nucleation material from which the TaS₂ structures could grow upward. Next, the tantalum powder was layered on top of the nucleation powders, followed by the sulfur powder at the top in amounts that created 0.3 g samples of TaS₂. Again, the molar ratios between these materials were 1/2/0.25 Ta/S/Mn or Cr in MnS or Cr₂S₃. Each ampoule was flame-sealed under vacuum at a length of 16-18 cm, and with this series care was taken to not shake the powders inside the ampoule so the nucleation base might stay intact.

The use of the single-zone furnace for this series rather than the three-zone furnace that grew the samples in Method A and B resulted in a still greater divergence between the growth patterns. First, no duplication samples (KB __ C2) were created because of limited space in the furnace. Also, the single-zone furnace was capable of being angled upward, so each sample was inserted into the furnace sitting more than 30° above horizontal, with the base of each ampoule closest to the bottom of the furnace. Finally, the growth program was altered slightly to lessen the time required for sample creation, and these variations occurred at each major step in the program.

The first change during heating process was to reduce the time the furnace remained at 125 °C from 24 to 6 hours. Since the sample size was reduced, there was little concern with also reducing this idling time. Next, the rate at which the temperature rose to 700 °C was increased from 8.5 °C/h to 12 °C/h. Also, from the differences between products of Method A and Method B it was evident that a macrostructure (nanomaterials or crystalline powders) would be apparent after even a short time at the

highest temperature, so the furnace was held at 700 °C for only 3 days rather than 5 days. The samples were then cooled to room temperature as the furnace ceased heating and allowed the heat to diffuse out over the next 15 hours. The procedures used to prepare the series B samples for XRD and SEM/EDS analysis were also utilized for this analysis.

2.3.2. Method D

The three samples that comprised Method D growth were prepared nearly identically to those grown by Method C. The only true difference between the two series is that Method C was a single-step growth method while Method D was a two-step method. This extra step occurred at the very beginning of the sample creation, though, before most of the preparations detailed above occurred. For this series the additional step indicated a difference in starting materials of the reaction. Rather than introducing both pure tantalum and sulfur powders into the ampoule on top of the nucleation material, Method D designated that 0.3 g of a previously synthesized sample of pure TaS₂ nanostructures was added to the ampoule. The pure TaS₂ materials used as the reactant for this series originated as the final products of samples KB Pr B1, B2 and B3. Beyond this difference, though, the synthesis and analysis of Method D samples was carried out in the same fashion as the samples of series C.

Table 1. Summary of the four studied growth methods

Method	A	B	C	D
Materials and Preparation	Elemental Ta, S and Mn or Cr powders Hand-shaken Laid flat in furnace	Elemental Ta, S and MnS or Cr ₂ S ₃ powders Hand-shaken Laid flat in furnace	Base of MnS or Cr ₂ S ₃ powders Ta, then S powders Angled up in furnace	Base of MnS or Cr ₂ S ₃ powders Pure TaS ₂ from Method B Angled up in furnace
125 °C Hold	24 h	24 h	6 h	6 h
Ramp rate	8.5 °C/h	8.5 °C/h	12 °C/h	12 °C/h
Anneal temp/time	700 °C/5 days	700 °C/5 days	700 °C/3 days	700 °C/3 days
Cool time	15 h	15 h	15 h	15 h
Sample Analysis	XRD of whole samples SEM/EDS of unaltered materials	XRD of ball-milled samples SEM/EDS of non-ground materials	XRD of ball-milled samples SEM/EDS of non-ground materials	XRD of ball-milled samples SEM/EDS of non-ground materials

3. RESULTS AND DISCUSSION

3.1. Pure Samples

3.1.1. Method A (KB Pr A)

The first step for the analysis of each sample was to record visual observations of the reaction product(s) both to the eye and under an optical microscope. When removed from the tube furnace the pure samples created by this method appeared to have a consistency like that of pulled cotton toward the flame-sealed end of the ampoule, while a large portion of the sample remained near the base of the ampoule and formed together, resembling a hard piece of sample, like an island surrounded by uncoated quartz. Under microscopic magnification the structures forming this island appeared furry from a top view. Also, though these structures are naturally silver colored, the light from the microscope was reflected back in an array of colors that changed across the visible spectrum as the ampoule was rotated.

The formal identification of the structural composition of these materials was performed through x-ray diffraction (XRD). The diffraction spectrum of the first pure sample (Pr A1) was identified as a 2H-TaS₂; the material was formally TaS₂ of a hexagonal structure (see Appendix A). The XRD spectrum for the second pure sample possessed a less intense signal through most of the spectrum because less material was provided for diffraction analysis. Still, the peaks of the spectrum were almost identical to that of Pr A1, so the two samples were classified as the same TaS₂ compound (see Figure 2 and Appendix B, PDF#01-071-3686). The broadness of many of the diffraction peaks reflected a small sampling size over which the diffraction occurred, meaning there were fewer layers of crystalline material available to diffract the initial x-ray than would be

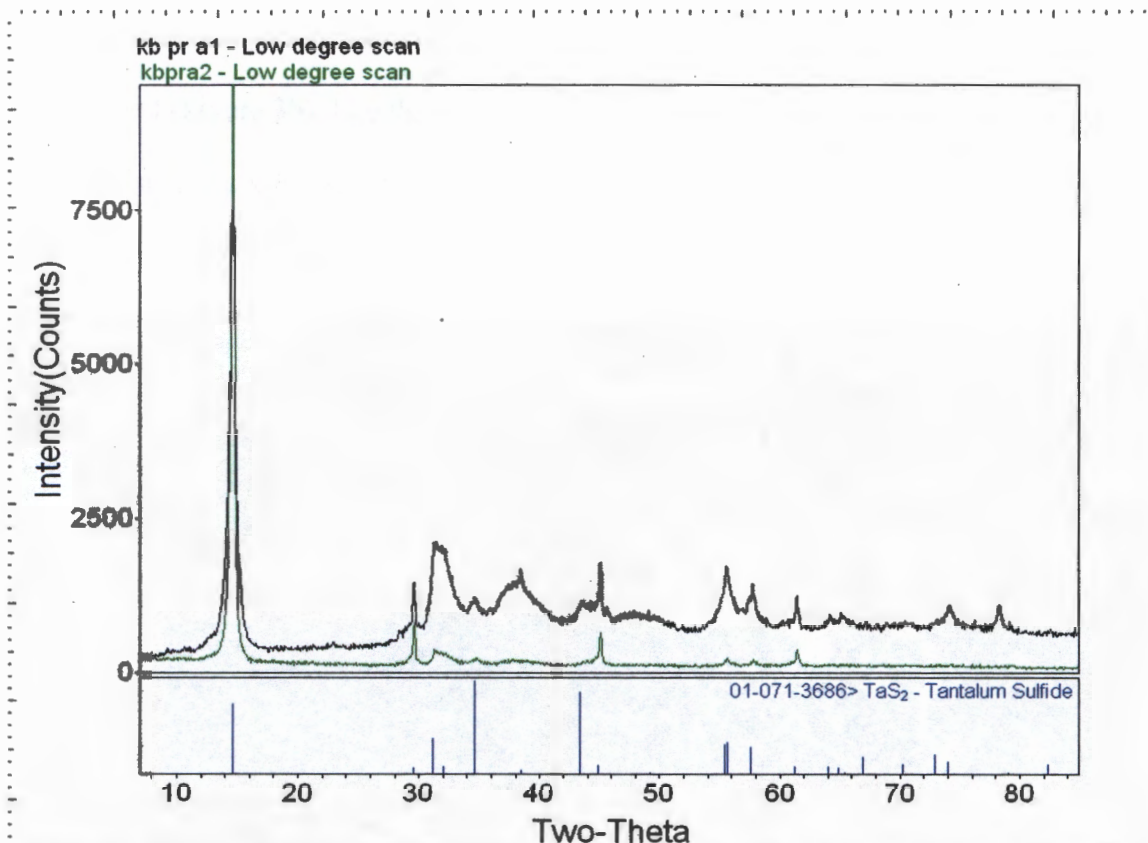


Figure 2. X-ray diffraction spectra overlays of KB PR A1 (black) and KB Pr A2 (green) show the matching peaks. Below (blue), the composition of the samples was identified as a hexagonal 2H form of TaS₂ using the database from the International Center for Diffraction Data (see Appendix B).

expected in a standard bulk crystal. This sampling reduction resulted in less precision of the diffraction angles, and therefore broader peak widths. The peak broadening seen in Figure 2 was indicative of analyzed samples composed of nanosized material, which further supported the production of TaS₂ nanostructures.

The Evex MiniSEM was used to image the two material types within these samples. Examples of the scanning electron microscope (SEM) images acquired from each end of the ampoule are displayed in Figure 3. From these images it was determined that the non-intercalated samples formed long nanostructures that resembled thin straws at the locations where the powders clustered (Figure 3a), and in those locations where the

material appeared pulled and wispy the structures were significantly smaller in size and less defined (Figure 3b), like the rag structures mentioned by early literature sources.⁸ Energy dispersive x-ray spectroscopy (EDS) data reports also showed evidence of TaS₂ structures (see Appendix C).

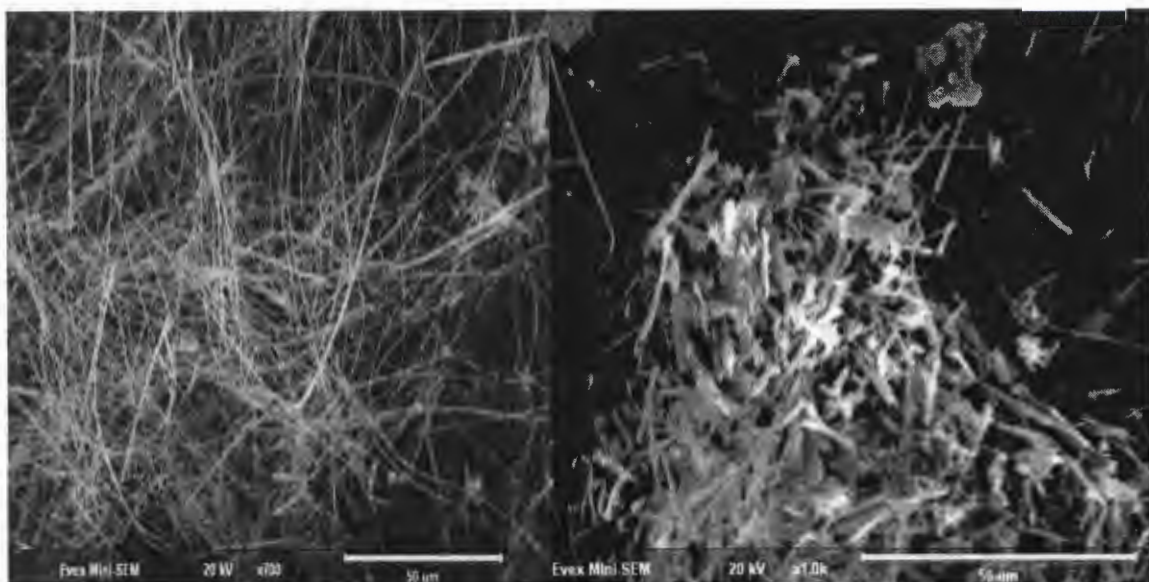


Figure 3 a.(left) Pure TaS₂ straw-like nanostructures from the base of the Method A pure ampoules, x700 mag. **b.**(right) Rag-like nanostructures of pure TaS₂ samples found near the flame-sealed end of the ampoules, x1.0k mag.

3.1.2. Method B (KB Pr B)

As the three pure samples of Method B were grown identically to the two Method A samples, it was not surprising that the products from this pure growth reflected the same results. The only variance in the results of this method from the preceding was the dispersion of the straw-like nanostructures throughout the entirety of the ampoules rather than clustered more toward the bases. This difference, though, was simply a result of the initial dispersion of the elemental powders across the entire length of the ampoules instead of containing the samples near the bases of their sample holders, as in Method A.

As a result of this dispersion, the quantity of rag-like material appeared to be reduced from the quantity grown during Method A.

The XRD analyses of the three samples also confirmed the duplication of the Method A products. When individually compared to the PDF files of the ICDD, each sample identified as the same 2H-TaS₂ material as was found the Method A products. As seen in Figure 4, the overlaid spectra of the products from this method exhibited identical broadening of the peaks at 31.2°, 32.1° and 38.5° (2θ) to the broadening seen in the pure sample A1, which again were indicative of nanostructure material within the samples.

The scanning electron microscope images from this sample greatly resembled Figure 3a. A reduction in the quantity of rag-like structures resulted in the acquired images displaying tangled nests of thin straw-type nanostructures. An observation of interest gained from the SEM images was the flexibility of these straw-like materials, an apparent ability of one strand to bend or curve through a nest of nanostructures, as the wave-shaped structure in Figure 5 demonstrates. The EDS data obtained for this sample also exhibited the electronic peaks corresponding to Ta, S and a minute quantity of C (see Appendix C). The tantalum and sulfur peaks confirmed the identity of the material, while the exposed carbon peak was a result of the carbon tape used to secure the samples to the sample holders during the analysis process.

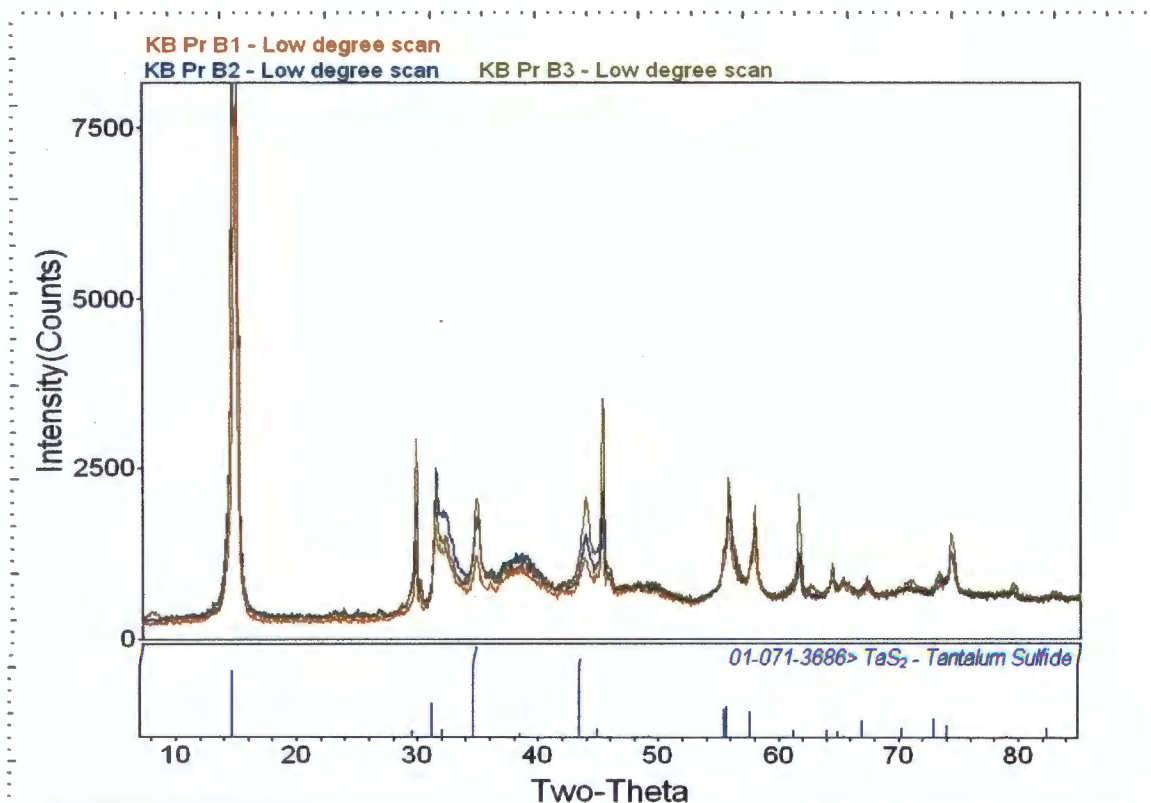


Figure 4. X-ray diffraction spectra overlays for pure samples B1 (orange), B2 (teal) and B3 (gold) show peaks matching the 2H-TaS₂ previously identified using the PDF database from the International Center for Diffraction Data (blue).

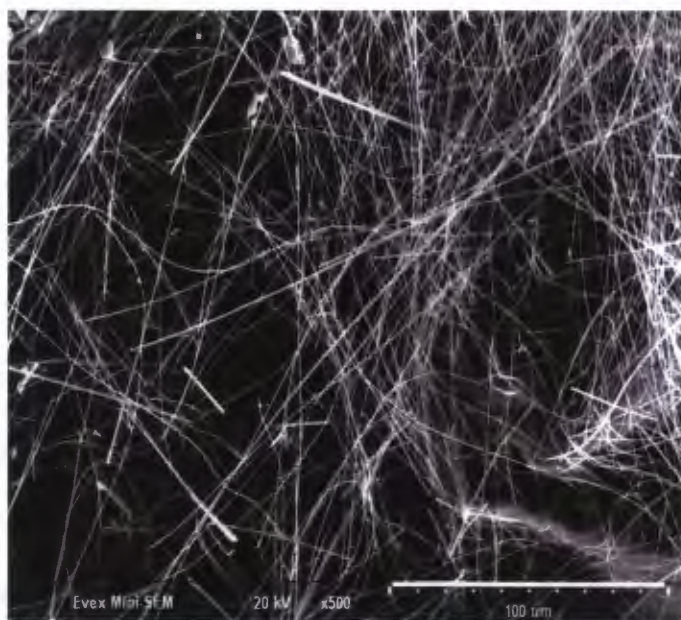


Figure 5. Scanning electron microscope image of Method B pure samples. Structural flexibility is demonstrated by a wave-shaped structure on the left of the image, x500 mag.

3.1.3. Method C (KB Pr C)

The macroscopic appearance of the Method C samples was unlike the material grown by the preceding methods. Where the samples synthesized through Methods A and B had clusters of fuzzy material that were nanostructures riddled through out the ampoules, the products of Method C existed as a fine black powder. This powder had a shiny appearance when the ampoule was rotated, a result of the light reflecting off of microscopic crystals within the sample. A microscopic view of the products only resulted in a further confirmation of the presence of microcrystals, making the basic hexagonally structure minutely visible under magnification.

The analysis of the material from XRD labeled the powder material as a new type of TaS₂. Rather than the 2H form that composed the nanoscale materials, this powder grew in a rhombohedral form, the 3R polytype (see Appendix A). Though somewhat surprising, this result was not altogether unexpected as a possible product, since other research groups also reported the synthesis of this polytype during single-step growth methods.¹ The difference from the previously reported process, however, was that these materials were still annealed at 700 °C, while the platelets reported earlier resulted from high temperature annealing at 1100 °C.

The unique formation of Method C samples was again confirmed through the SEM imaging. The images of this product, like Figure 6, showed collections of microcrystalline platelets of pseudo-hexagonal shape, appearing to have a basic hexagonal structure but with rounded edges. The growth of the platelets still appeared to be spurred by the presence of other structures like itself, similar to the nanostructures of Methods A and B growing from a central location, with these platelets growing one on

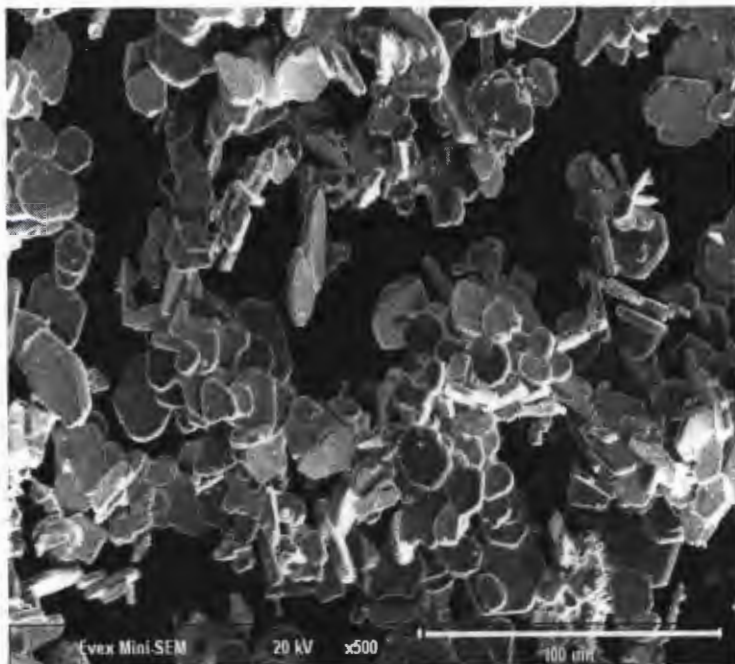


Figure 6. Scanning electron microscope images of the microcrystalline platelets synthesized by the Method C pure growth, x500 mag.

top of the other and, in some cases, out from crystalline clusters already formed. Still, these platelets varied from their nanostructure counterparts in more than just shape. The dimensionality of these microcrystals, seeming at most approximately 20 μm across any direction of the surface and a few microns

deep, was significantly different than the nanostructures that were likely less than 5 nm in diameter and could grow many hundred microns long.

3.1.4. Method D (KB Pr D)

The pure product of Method D also resulted in samples of an unexpected form, especially because the starting material of this method was pure nanostructures that had been previously synthesized. Visually the material appeared very similar to the counterpart Method C samples, a fine black powder that shined when the light reflected off certain surfaces inside the ampoule. A microscopic view of the loose sample showed microcrystal formation throughout the powder as well.

The resulting analysis from XRD on the ground powder sample (Figure 7) also confirmed the pure D sample was composed of the same 3R polytype of TaS_2 . The two spectra do not even vary in peak width, which was expected considering the state of the

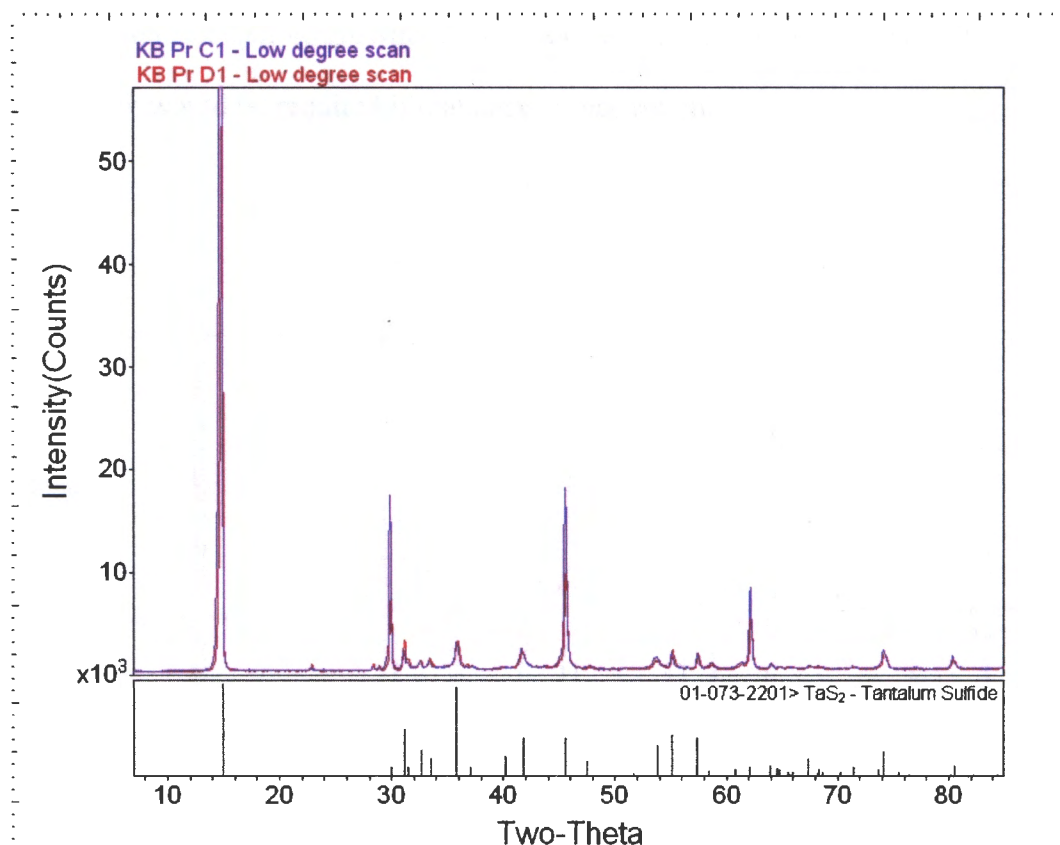


Figure 7. X-ray diffraction spectra of the powdered samples of Pr C1 (purple) and D1 (red) correlating to the referenced 3R-TaS₂ polytype, shown in black below the overlaid spectra. See Appendix B for the reference PDF from the International Center for Diffraction Data.

Method D starting material. Likewise, the SEM images revealed rounded pseudo-hexagonal platelets of similar dimensions as were seen in the Method C products. As a result of the observed similarities between these two methods it became clear that one of the two growth variations made from Methods A and B to C and D resulted in the rearrangement of the packing structures, forming 3R-platelets rather than the 2H-nanostructures of the earlier samples. To further demonstrate the spectral differences of these two polytypes, the x-ray diffraction spectra of each method were superimposed and offset across one domain, Figure 8. However, it could not be determined whether the resulting crystalline rearrangement in the pure samples was due to the angled, and

therefore compact, sample growth or the accelerated time scale of the annealing process; further study would be required if that answer was sought.

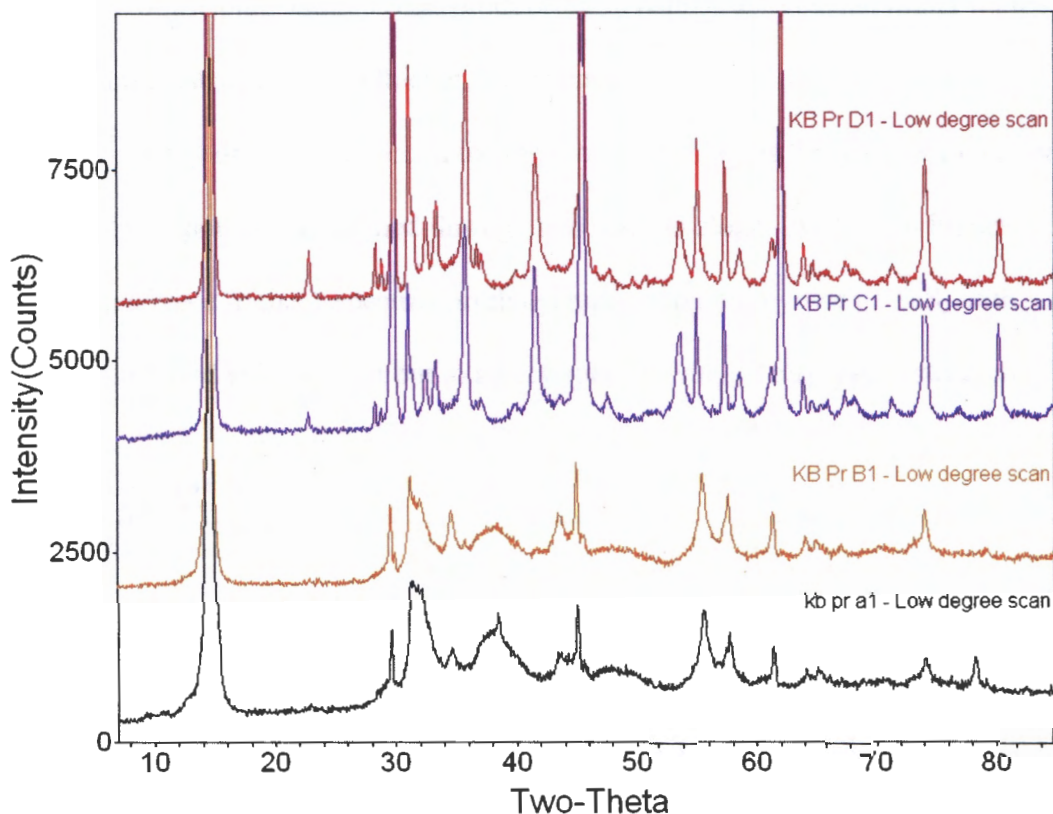


Figure 8. Super-imposed x-ray diffraction spectra of all methods of pure sample growth. The spectra of A1 and B1 correlated to 2H-TaS₂ structures, C1 and D1 to the 3R crystalline polytype.

3.2. Mn and MnS Samples

3.2.1. Method A (KB Mn A)

The Method A manganese-intercalated growth pattern produced samples unlike any other material grown during this study. Upon visual observation these samples appeared mold-like. Similar to their pure sample counterparts, the product was primarily black in color and protruded from a tight cluster of the same material that was centered

near the location of the original powder sample. Microscopic observations showed a slight deviation from the pure samples. These Mn-intercalated samples presented nanostructures sprouting from central nucleation sites that could be visibly distinguished one from another. In this way the material did not have the same tightly clustered, fuzzy appearance of the pure samples that produced thin nanostructures, but rather it presented individual nanostructures of a thicker consistency.

The x-ray diffraction spectra for the produced samples further confirmed that a distinctive compound was formed through this method alone. As seen in Figure 9, the products analyzed in these spectra correlated not to a pure polytype of TaS₂ with some form of Mn-based side product but to a very specific Mn_{0.25}TaS₂ crystal structure. The

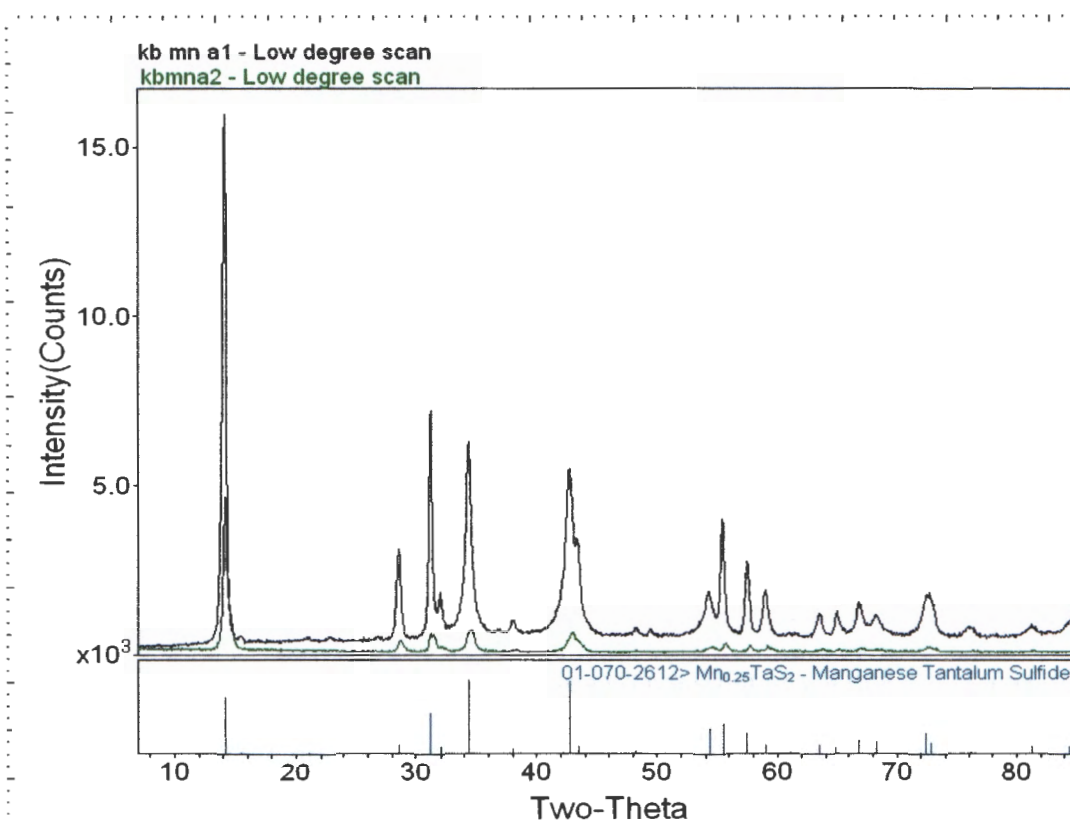


Figure 9. Experimental spectra of the Mn samples grown from Method A (KB Mn A). Using the PDF files provided by the International Center for Diffraction Data, Mn A1 (black) and Mn A2 (green) both identified as the intercalated crystal form Mn_{0.25}TaS₂.

identification of this material as such confirmed the successful and consistent intercalation of Mn into the crystalline structure of a TaS₂ nanomaterial. Also, both experimentally obtained spectra of the Mn A samples exhibited the same peak broadening at the baseline that was first acknowledged in the pure Method A samples, which was indicative of nanostructure formation. The relatively low intensity of Mn A2 compared to Mn A1 was once again a result of less sample material placed on the zero-background silicon sample holder.

If the x-ray diffraction analysis was not enough data to confirm the special consistency of these Mn-intercalated products, the images obtained on the SEM provided the last bit of evidence needed. The products from the Mn-seeded samples of Method A grew not only as intercalated structures, but also as nucleated materials, with many structures protruding from a very small, central location (Figure 10a). More interesting still was that these nucleation points were primarily large clusters of a synthesized MnS side product, not a tantalum and sulfur compound or some portion of the quartz ampoule surface as the pure samples used (Figure 10b). This discovery spurred the replacement of Mn powder with MnS powders as the seeding material for the remaining growth methods. Further, structural consistency of this product was unique to this class of materials. While the pure samples were only a few nanometers in diameter and were very thin and wavy, the intercalated samples truly formed straw-like structures. Each nanostructure appeared firm in shape; there was no potential to see this product bend or curve without breaking the straws. Rather, these nanostructures appear to hold a straight shape firmly (10b). The differences in structure from the pure nanomaterial to these intercalated samples became especially apparent when comparing Figure 10b to Figure 5.

Though both images were acquired at the same x500 magnification, the individual nanostructures of the Mn-intercalated samples appeared significantly thicker and firmer than the pure counterparts that were wavy and very narrow.

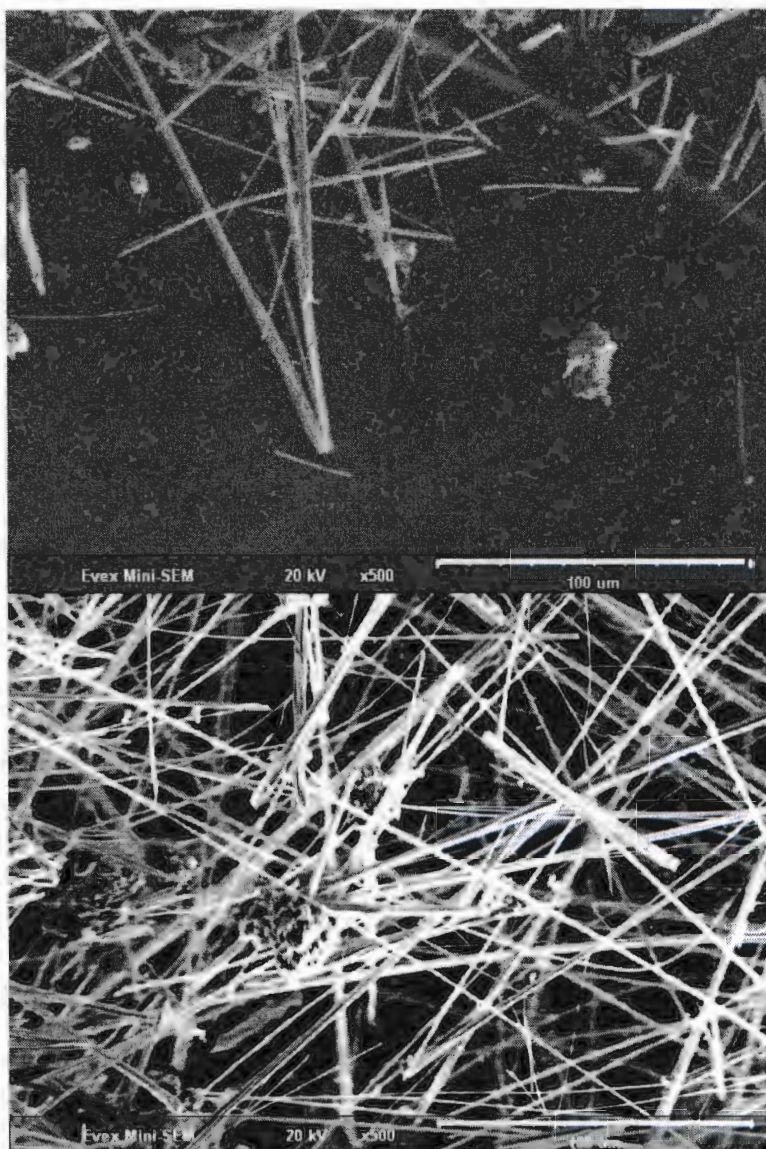


Figure 10a. $\text{Mn}_{0.25}\text{TaS}_2$ nanostructures growing from a central nucleation site, x500 mag. **10b.** Structurally firm nanostructures growing from a nucleation site of synthesized MnS, x500 mag.

3.2.2. Method B (KB Mn B)

Also unlike the pure counterparts, the class of samples grown in Method B using MnS did not result in products similar to the Mn-intercalated structures of Method A. Rather, seeding the samples of this method with MnS produced dark powder samples that occasionally shone with the reflecting light, suggesting only small amounts of

microcrystal growth. Observations using the optical microscope also suggested only a small quantity of microcrystallization based on the low levels of reflecting crystals throughout the samples. Instead of crystalline growth, it appeared that the majority of the sample products contained the original green MnS powder that could be observed still coating the interior of the ampoule and another side product.

The identity of this unknown side product was quickly identified as Hauerite, MnS_2 , from the obtained XRD spectra of these Method B Mn-class samples (Figure 11). In addition to the side product, the products were also determined to be a hexagonal form of TaS_2 and traces of the $\text{Mn}_{0.25}\text{TaS}_2$ compound seen in the Mn-class samples of Method A. It is likely that this combination of compounds and the relative quantities of each that were visually observed resulted from the elemental sulfur leaching onto the commercially synthesized MnS powder, leaving less material to form the targeted TaS_2 crystalline materials.

The images acquired of these samples also suggested a high prevalence of synthesized side product and comparatively low concentration of crystallite materials. As the SEM image of Figure 12 exemplified, a window at the comparable magnification of x500 presented only few hexagonal crystals within the entire window, and each of these crystals was covered in what was determined to be the MnS_2 side product. This scene was consistent throughout most imaging scans of the Mn B samples.

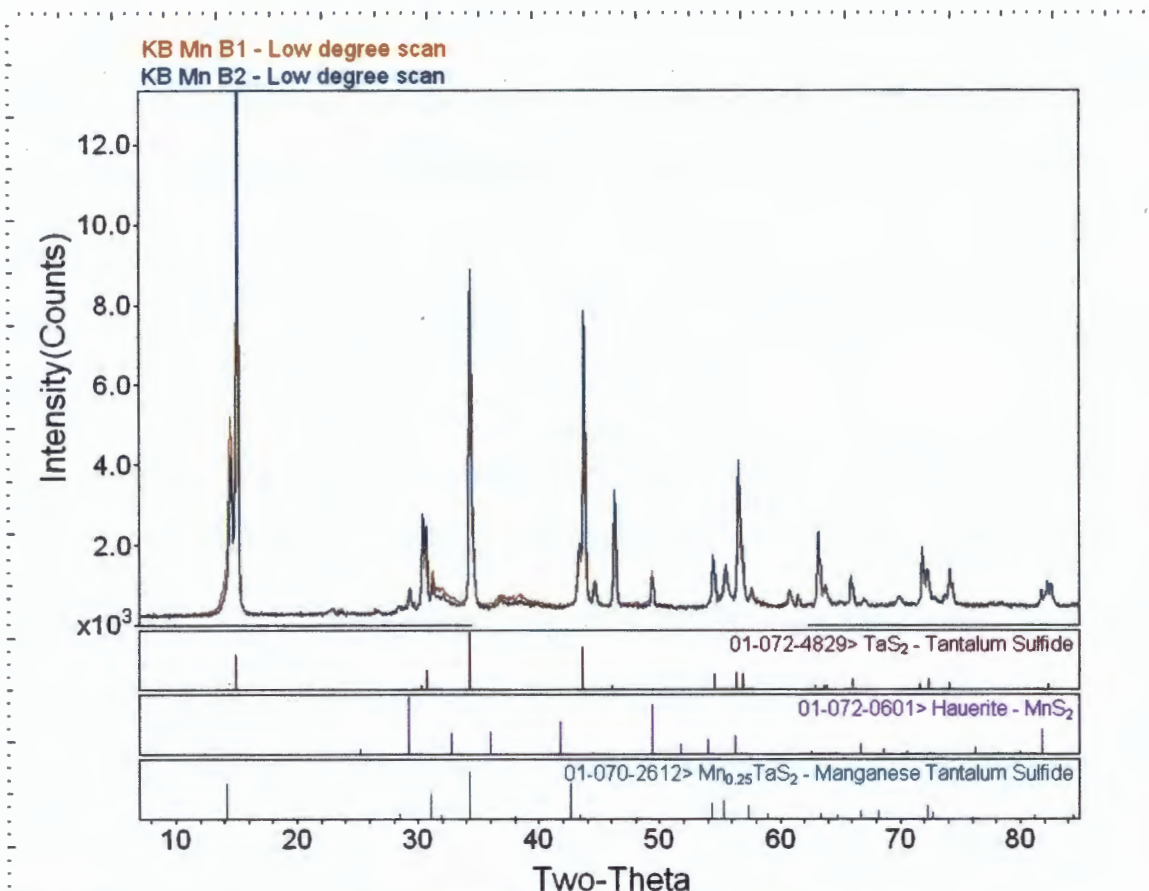


Figure 11. Overlaid x-ray diffraction spectra of KB Mn B1 (orange) and B2. Peak identification suggested the sample products consisted of hexagonal TaS₂, MnS₂ and Mn_{0.25}TaS₂, all identified from the International Center of Diffraction Data database.

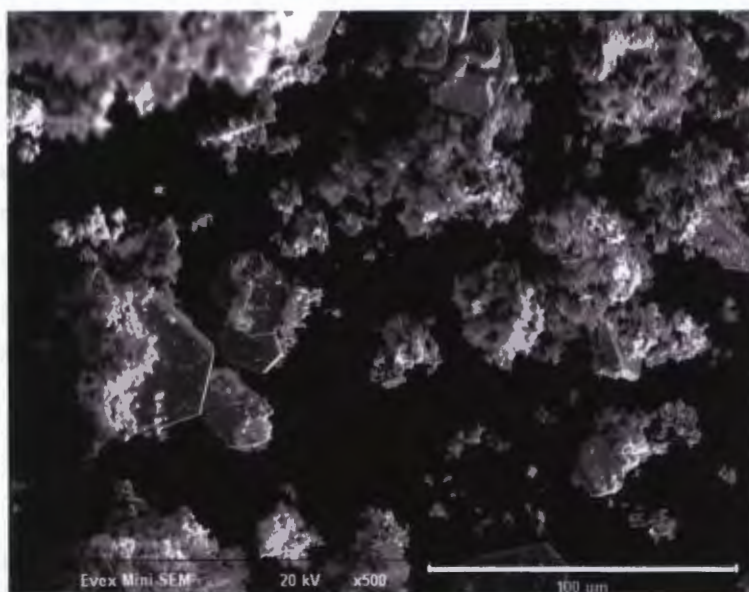


Figure 12. Scanning electron microscope image of the general appearance of a KB Mn B sample, x500 mag.

3.2.3. Method C (KB Mn C)

The first of the base growth samples containing MnS produced material very like what was seen in the pure class of Method C. The products looked like a blackish/gray powder, shining from portions of microcrystals. Viewing the sample under an optical microscope confirmed the presence of small crystals within the material while suggesting that there was a lack of nanostructures within the products.

Both the XRD and SEM analyses supported this conclusion. From the powder diffraction spectrum of Mn C1, Figure 13, it was determined that this product material was composed of the 2H-TaS₂ crystalline material that first appeared in nano form in the pure Method A class samples, as well as the same MnS material that was the commercially obtained seeding reactant (original XRD spectrum of the commercial product located in Appendix A). Once again, the sharp peaks within the spectrum

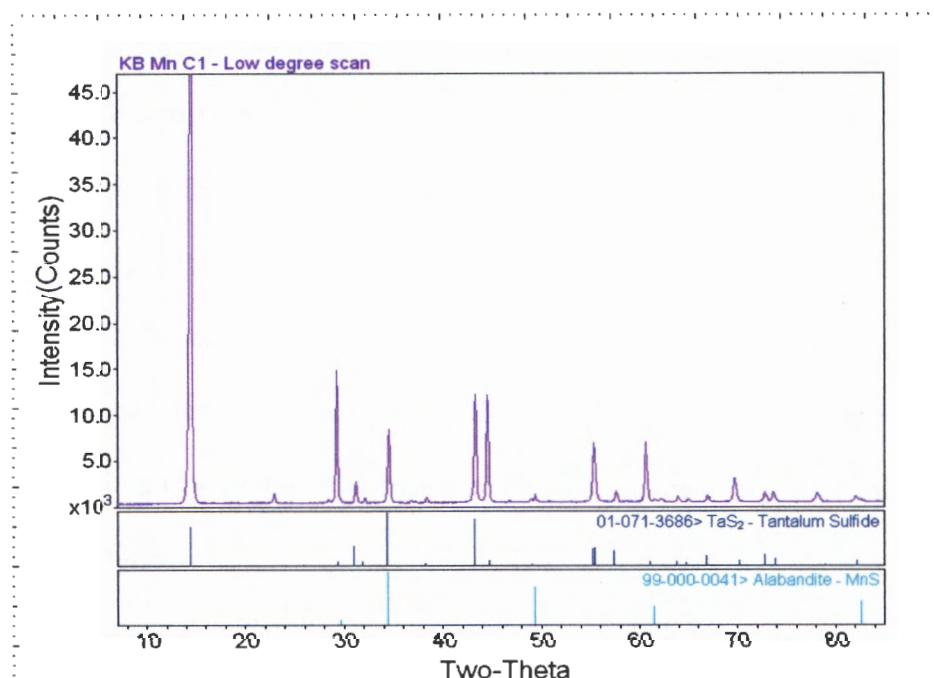


Figure 13. X-ray diffraction spectrum of KB Mn C1, identified as a combination of 2H-TaS₂ and Alabandite, the commercial MnS compound. Identification made using the database of crystalline files from the International Center for Diffraction Data.

negated the concept of nanostructure formation. In addition to the XRD, SEM imaging acquired for this sample showed that the base growth system used for this sample did, in fact, play a role in the large-scale arrangement of this material. Though

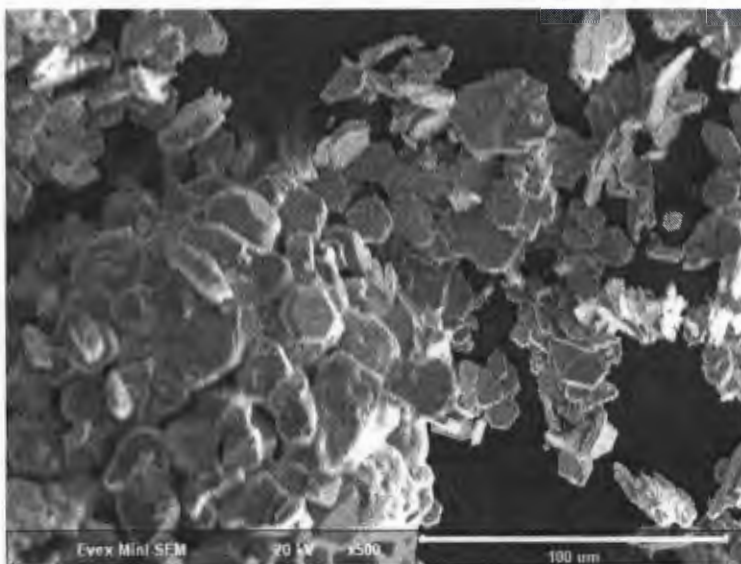


Figure 14. Scanning electron microscope image of a towering structure of TaS₂ microcrystals. Image displayed distinct hexagonal crystal structures, center at base, x500 mag.

the base growth did not result in the formation of ordered nanostructures as expected, this material grew the microcrystals in a towered formation, appearing to have aligned the similar axes of their crystalline structures (see Figure 14).

3.2.4. Method D (KB Mn D)

Though the Method D sample began as ball-milled nanostructures layered over the MnS base, the growth process resulted in fine black powder that appeared more microcrystalline than nanostructure filled. Similar to the Method C sample, the optical microscope showed microcrystals and little evidence of a nanomaterial, suggesting that the second annealing caused a reordering of the macrostructure to crystal, similar to the pure Method D sample.

The instrumental analyses of this sample also concluded that the products were of a similar form as the MnS based Method C sample. As demonstrated by Figure 15, the diffraction spectrum of this two-step sample aligned exactly with the Method C spectrum,

showing a composition of 2H-TaS₂ mixed with the commercial MnS base growth reactant. Again, the specificity to the diffraction angles suggested that the earlier nanostructures were no longer prevalent within the sample. The SEM scans of this sample also produced images much like Figure 14, further confirming this conclusion.

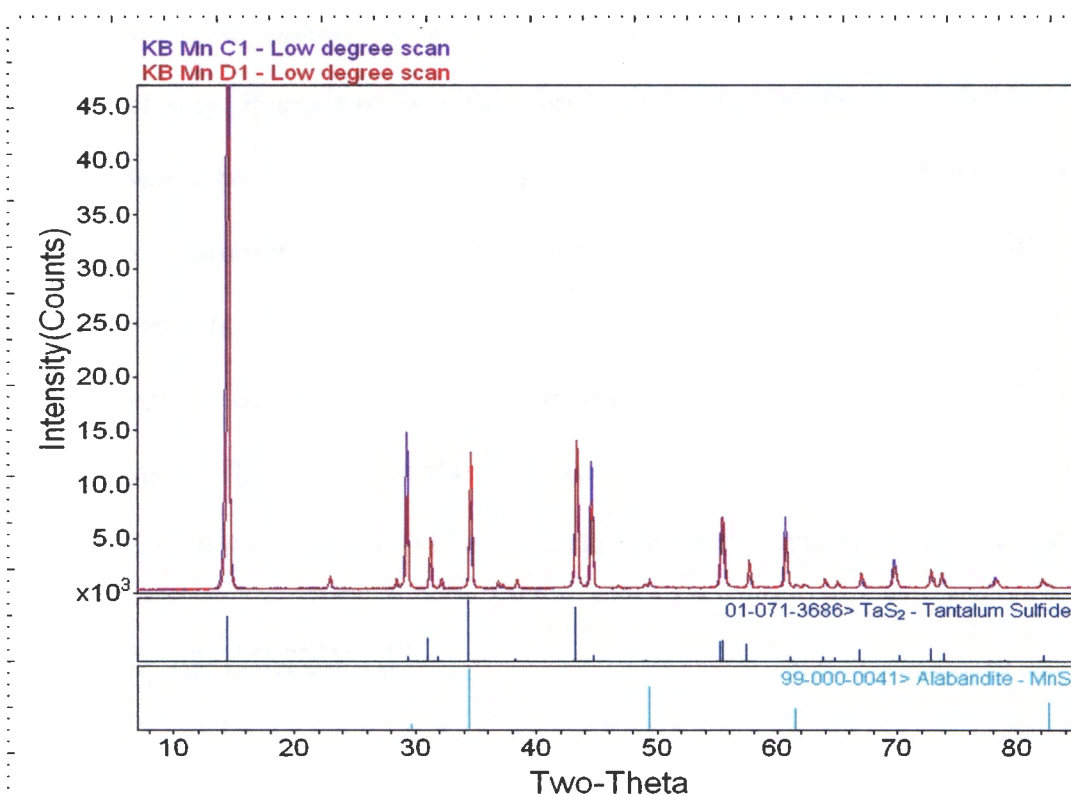


Figure 15. Overlaid x-ray diffraction spectra of Mn C1 (purple) and Mn D1 (red) identified at 2H-TaS₂ mixed with the commercially obtained Alabandite, MnS, according to the database of crystalline spectra from the International Center for Diffraction Data.

3.3. Cr and Cr₂S₃ Samples

3.3.1. Method A (KB Cr A)

Like both the pure and Mn-intercalated samples of Method A, the Cr-seeded materials grew as nanostructures. The original view of the clustered material reflected the look of the pure nanostructures; the majority of the sample was contained in an island of materials that appeared furry under an optical microscope. Also, though the basic

silver color of the other Method A structures was also present, these samples appeared to be missing the reflecting capacity of the pure class samples. Any rotation of the ampoule resulted in very little reflection of the input visible light.

After the results of the pure and Mn-intercalated samples were acquired, it was expected that these materials would reflect a combination of characteristics from the two preceding classes. Because of the visual observations the expectation was that these structures would be less solid than their Mn-seeded counterparts, but would likely have grown from a chromium sulfide compound and be partially intercalated. The XRD spectra for this class supported the similarities to the pure nanomaterials, identifying as $2H-TaS_2$ with no identifiable side product peaks, but the success of Cr-intercalation was left to question. The spectral overlays of Figure 16 exhibited the same peak broadening and aligned with the same ICDD PDF file as the pure nanostructures of the method.

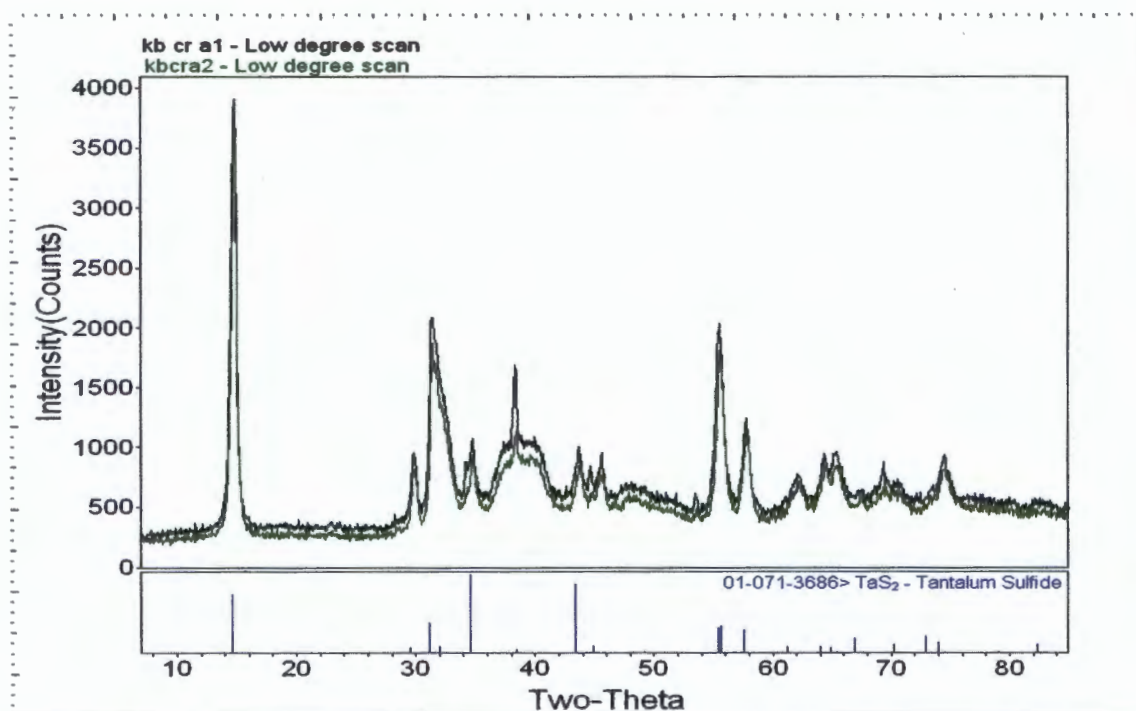


Figure 16. X-ray diffraction spectra of KB Cr A1 (black) and A2 (green) matched with $2H-TaS_2$ from the International Center for Diffraction Data PDF files.

The electron microscope images of these products further supported the combination of characteristics defined by Pr A and Mn A samples. These structures appeared as narrow wire-like segments of TaS₂ like the pure samples shown in Figure 3a, however the segments did not present the flexibility of the pure nanostructures. Rather, these thin nanostructures were short fragments, reflecting the inflexible nature of the Mn-intercalated samples. Using EDS it was determined that these structures were most likely unintercalated, since no Cr related voltages were detected (Appendix C).

3.3.2. Method B (KB Cr B)

The materials seeded with the commercial Cr₂S₃ as a replacement for elemental Cr powders resulted in products much like their MnS-seeded equivalent; the products removed from the tube furnace were powders of a dark brown/black color, presenting little shine as the ampoule was rotated to look for reflective microcrystals. Under the optical microscope the microcrystals were detected, however their relative concentration appeared low against the prevalent side product.

The x-ray diffraction spectra from this method classified the products as the same hexagonal form of TaS₂ seen in the Mn class of this method, as well as the commercial side product, Cr₂S₃ (Figure 17). The precision of the peaks once again suggested an absence of nanostructures, which was confirmed through SEM imaging. Rather than the wire-like nanomaterial of the Cr-seeded products, these images occasionally showed a clear view of small microcrystals, but more often the image contained indistinct views of these platelet structures clustered together with a coating of the side product, as seen in Figure 18. Therefore, it was concluded that, like its MnS-seeded counterpart, this

commercial material did not instigate nanostructure formation, nor did it assist in forming intercalated structures.

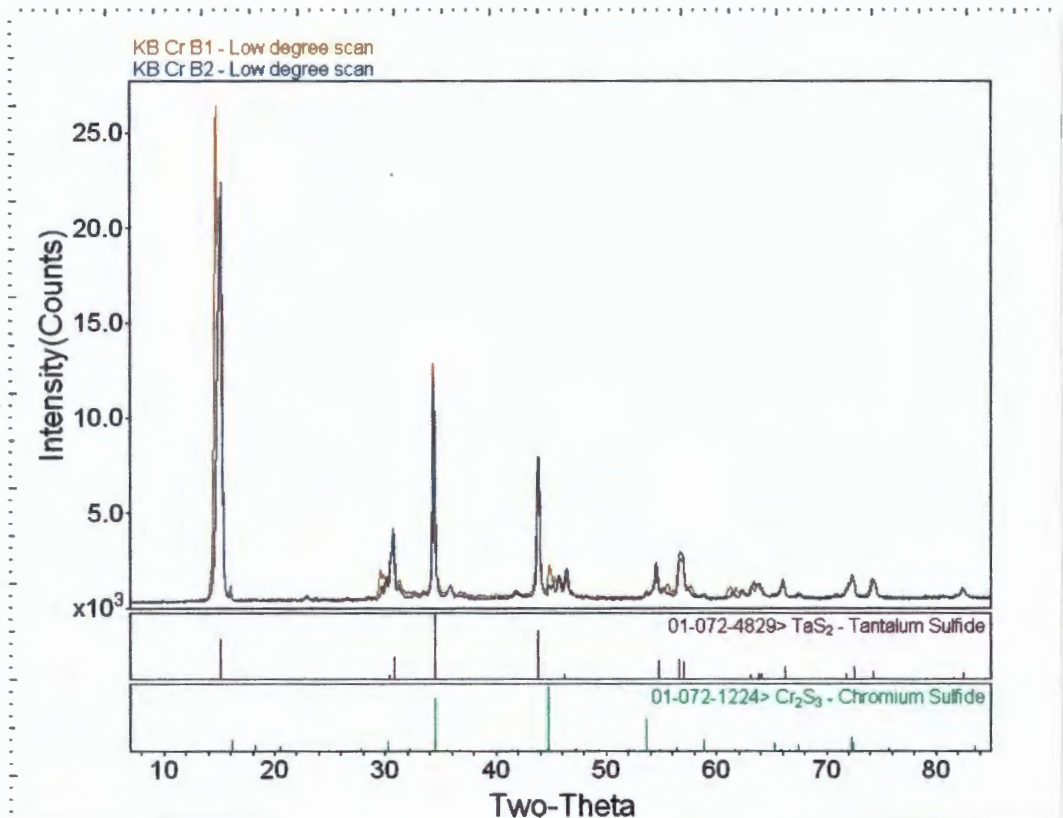


Figure 17. X-ray diffraction spectra of KB Cr B1 (orange) and B2 (teal) identified as hexagonal TaS_2 mixed with the commercial Cr_2S_3 seeding material.

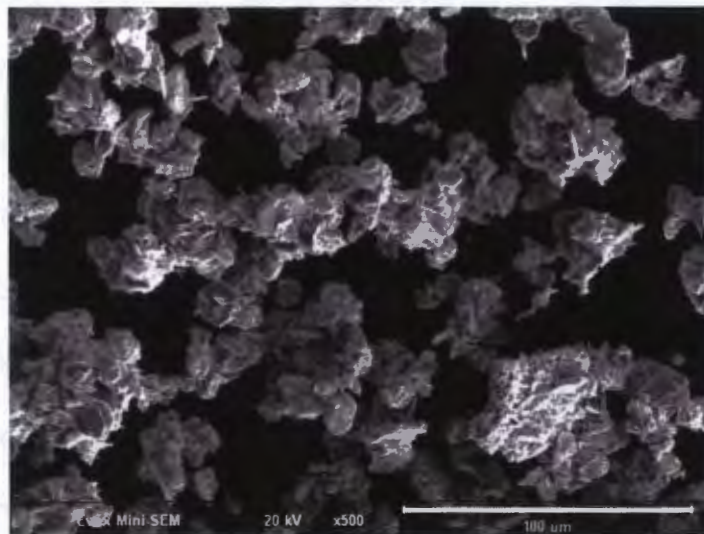


Figure 18. Electron microscope image of KB Cr B sample showing clusters of microscale TaS_2 platelets coated by commercial Cr_2S_3 side product, x500 mag.

3.3.3. Method C (KB Cr C)

The angled growth of these materials initially appeared to have no effect in changing the structure of single-step synthesis samples. When removed from the furnace, the observed material was a dark powder, clustered at the base of the ampoule as a result of its initial placement. Microscopic inspections proved the presence of microcrystals, although, once again these crystals appeared in low concentrations compared to the quantity of side product.

The differences between this sample composition and that of its Method B predecessor was made apparent through x-ray diffraction. The peaks of the spectrum aligned with the original 2H-TaS₂ polytype that was seen in the Cr-seeded nanostructures rather than the reordered form of the Method B products, though the lack of peak broadening also suggested that this product was in platelet form and not composed of nanostructures. In addition to TaS₂, the unidentified spectral peaks matched the commercial nucleation material, Cr₂S₃.

The final confirmation that the angled material differed from the previous seeding method using Cr₂S₃ came from the SEM images. As Figure 19 exemplified, the TaS₂ crystal structures produced from this angled growth were quite

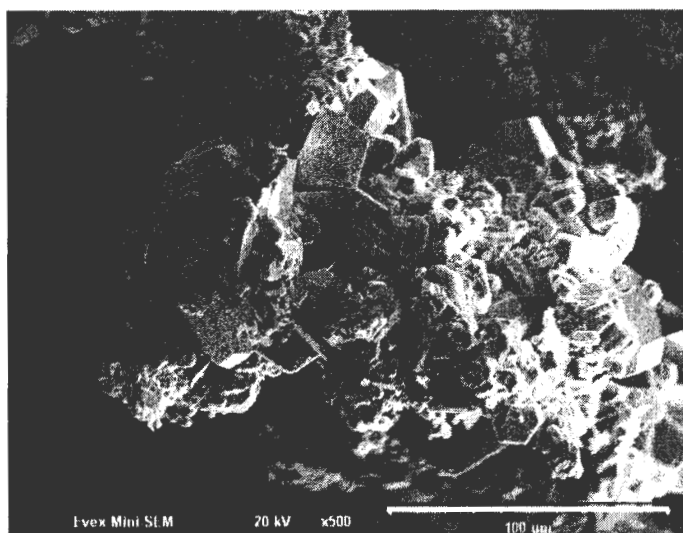


Figure 19. Electron microscope image of 2H-TaS₂ crystals with Cr₂S₃ grown in KB Cr C, x500 mag.

distinct. Like the MnS-seeded class products, this material grew vertically, building towers of thin TaS₂ crystals interspersed among Cr₂S₃ nucleation material.

3.3.4. Method D (KB Cr D)

Once again, the TaS₂ material produced from Method D did not resemble the macrostructure of its predecessor, pure nanostructures grown from Method B. Instead of a black mold-like material, the products looked like the Cr₂S₃-seeded structures of Method C; black sample clustered at the base of the ampoule as either loose or clumped powder. Once more, the microscopic view of the product, after it was dislodged from the ampoule base, showed signs of microcrystallization but little evidence of any nanomaterial.

The XRD spectrum for this sample also paired with the products of Method C, as in the MnS-seeded material, confirming the chemical composition of the sample (Figure 20). The similarities of these two methods while and the variations in the products of the four Cr-based methods were further illustrated by superimposing a spectrum from each method across the same domain (Figure 21). SEM images of the two-step product appeared similar to the image of Figure 19, which acted as the final supporting evidence for the conclusion that the product formation of these materials is more dependent on the exact growth parameters than the actual starting materials.

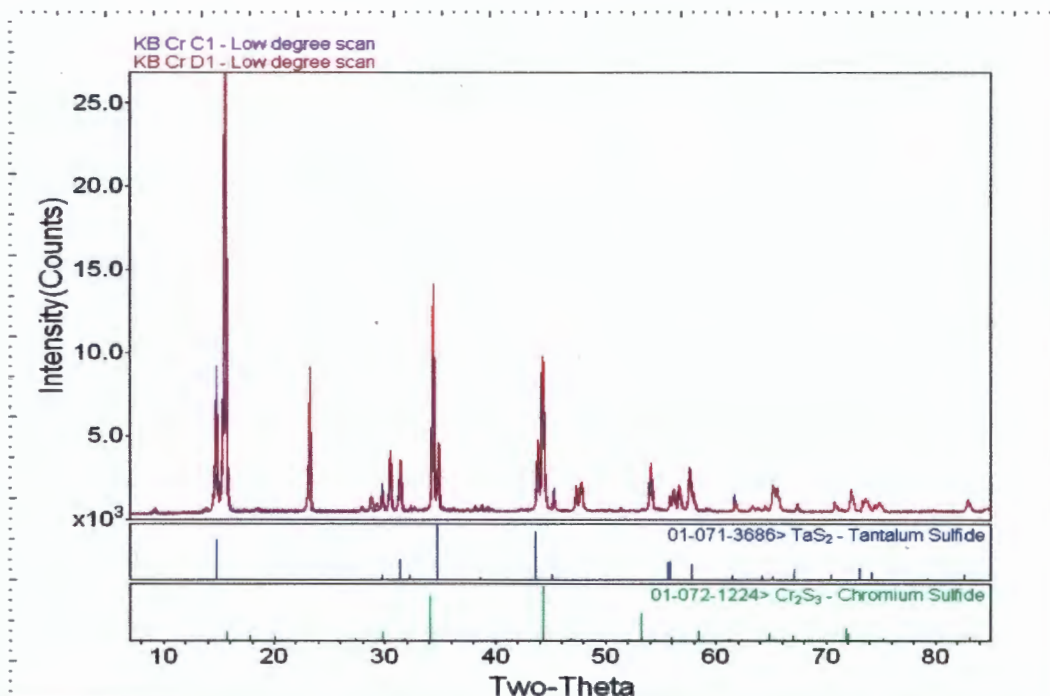


Figure 20. Overlaid x-ray diffraction spectra of KB Cr C1 (purple) and D1 (red) aligned with PDF spectra from the International Center for Diffraction Data. Contents were identified as 2H-TaS₂ and commercially obtained Cr₂S₃.

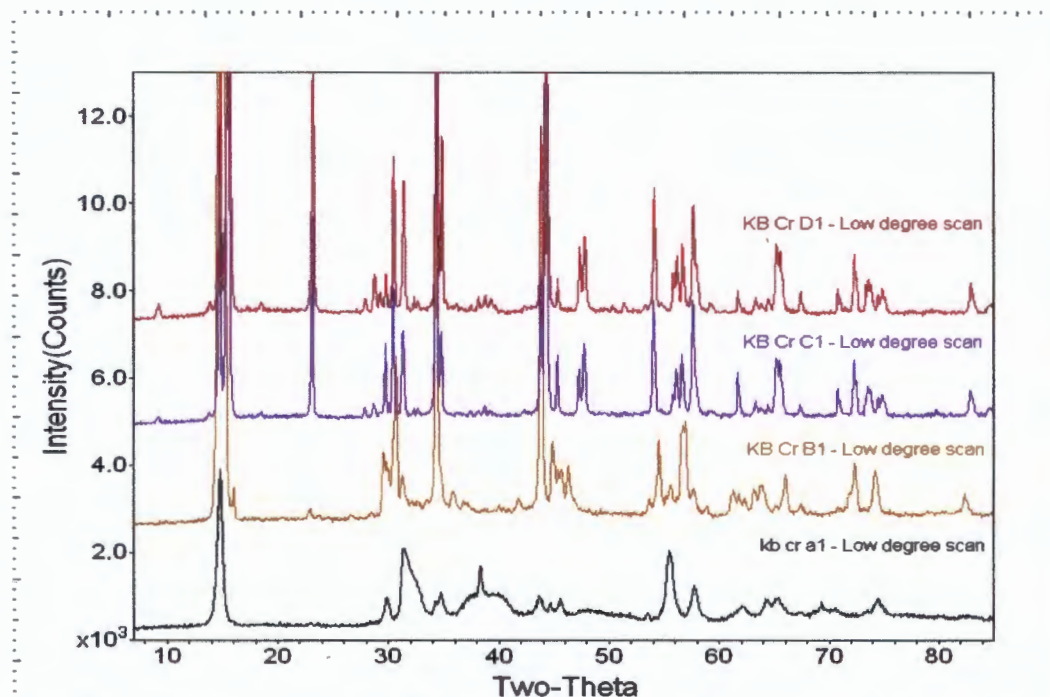


Figure 21. Superimposed x-ray diffraction spectra of all four growth methods for Cr- or Cr₂S₃-seeded materials. Products migrated from nano-structures of unintercalated 2H-TaS₂ (A) to a hexagonal form of TaS₂ mixed with Cr₂S₃ (B), and back to 2H-TaS₂ with commercial Cr₂S₃ (C and D).

4. CONCLUSIONS

4.1. Research conclusions

This study began with a goal of gaining a greater understanding of how TaS₂ nanostructures grow. The expectation through this process was that nanostructures could be grown using a seeding material of either an elemental 3d transition metal, Mn or Cr, or from a corresponding metal sulfide compound, MnS or Cr₂S₃. Additionally, it was predicted that the use of the metal sulfides would actually regulate the nanostructures growth, forming more consistent and ordered materials from a commercially refined nucleation material. However, these hypotheses were as far from the actual results as possible. Rather than forming ordered nanostructures of a consistent hexagonal TaS₂, the replacement of the 3d metal with metal sulfides stimulated the growth of platelet microcrystals of various polytypes. Also, these materials were even more disorganized and inconsistent than the interwoven nests of nanostructures found in Method A, as each of the six metal sulfide-seeded classes displayed products riddled with either the initial commercial side product or an even more sulfur-rich side product that was synthesized during the annealing process.

Further, even though each of the three classes from Method A grew nanostructures, the results did not exhibit any type of basic trend. The pure products contained two primary nanomaterials: the undefined rag-like materials and nanostructures that resembled extremely narrow wires that were a few nanometers in diameter at best and had a flexible property to them. In contrast, the Mn-seeded samples grew as thicker structures and almost no exhibited flexibility, as most images showed jagged breaks of the thick, straw-like material. These samples also incorporated the 3d metal into the

nanostructures, altering the basic crystal structure to include the elemental Mn. Because this discovery occurred relatively early in the research, it was hypothesized that the structural thickness and ability to intercalate was a result of the Mn-seeded structures growing from a cluster of MnS side product; products grown without a specific nucleation material would have less definition and stability to them. However, the results of the Cr-seeded class of samples did not strengthen this hypothesis as the nanostructures appeared significantly more like their pure nanowire counterparts and, even after each instrumental analysis was considered, it was unclear whether the Cr-nucleated materials were intercalated. What was clear from the Method A samples, though, was that 3d metal intercalation of TaS₂ nanostructures is possible in a single-step synthesis at a 25% intercalation ratio using elemental Mn.

Even though the initial hypotheses were shown to be incorrect, the study was not without important findings. In addition to the successful discovery of Mn-intercalated TaS₂ nanostructures, the inclusion of Methods C and D to the study provided two other significant points of interest. First, the formation of the sought-after nanostructures only occurred when the reaction materials were initially dispersed throughout the ampoule, as in Methods A and B. This dispersion provided the nanostructures room to grow outward whereas packing the reactant powders into one location forced a reorganization of the materials into microcrystals, and in some cases may have been the cause for the reformation of the crystal structure into a 3R-polytype rather than the more common 2H-TaS₂. Also, the direct comparison of Methods C and D provided the knowledge that, at least under the specified growth conditions, a two-step method including existing

nanostructures is no more effective in successfully synthesizing TaS₂ nanostructures than a single-step method.

4.2. Limitations and Recommendations for future study

The scope of this research was broad enough to provide many points of inquiry without imposing too many limitations to the study or requiring excessive methods to generally analyze the resulting material. One of the few limitations that did exist was the extent to which the analysis of the nanostructures was able to undergo as a result of the instrumentation. As previously mentioned, some research groups were able to successfully determine the size, structural characteristics and crystalline consistency of their reaction products using tunneling electron microscopy (TEM) and selected area electron diffraction (SAED).^{1,12-14} These techniques were not available for application during this current study. Additionally, as a result of instrumental limitations and technician inexperience the images acquired with the scanning electron microscope (SEM) were not of optimal magnification or resolution quality for some of the more refined elements of SEM analysis, such as dimensional determination of the various products.

The other significant limiting factor within the study was time. The placement of academic holidays and project deadlines became the regulating factor that determined when samples were created and the time allotted for the growth of each sample collection. This was the primary reason for the alteration of growth parameters for Methods C and D; a condensed timetable required a shorter growing period. Therefore, the first suggestion for further study would be to synthesize a series of pure samples using the materials and preparation techniques of Methods C and D but the annealing

specifications of Methods A and B. If nothing else, the results from this experiment ought to provide insight into which variable, the clustered and angled growth or the rate of temperature changes, led to the production of the 3R-polytype materials.

Additional studies could focus on investigating appropriate applications for the commercial metal sulfide compounds. Since the samples from Method B produced microcrystal platelets, this could first be achieved by altering preparations of the Method B samples to include a carrier agent, such as iodine, and attempt to grow macroscale crystals using metal sulfide nucleation. This targeted crystal growth would likely be best achieved using a temperature gradient of at least 50 °C above the recorded 700 °C. The contributions of metal sulfides in this reaction could also be explored by altering any of the growth methods with a precursor step, one that reacts the commercial metal sulfide with the identified quantity of sulfur before adding in the stoichiometric amount of tantalum powder. This could possibly provide an avenue for the metal sulfide side product to become sufficiently large and irregular in shape and size to nucleate the formation of nanostructures, as the side product clusters of KB Mn A were. However, this reaction could also have an adverse response and form a sulfur-rich side product that would coat any TaS₂ structures formed, as was seen in Mn B samples with the formation of Hauerite.

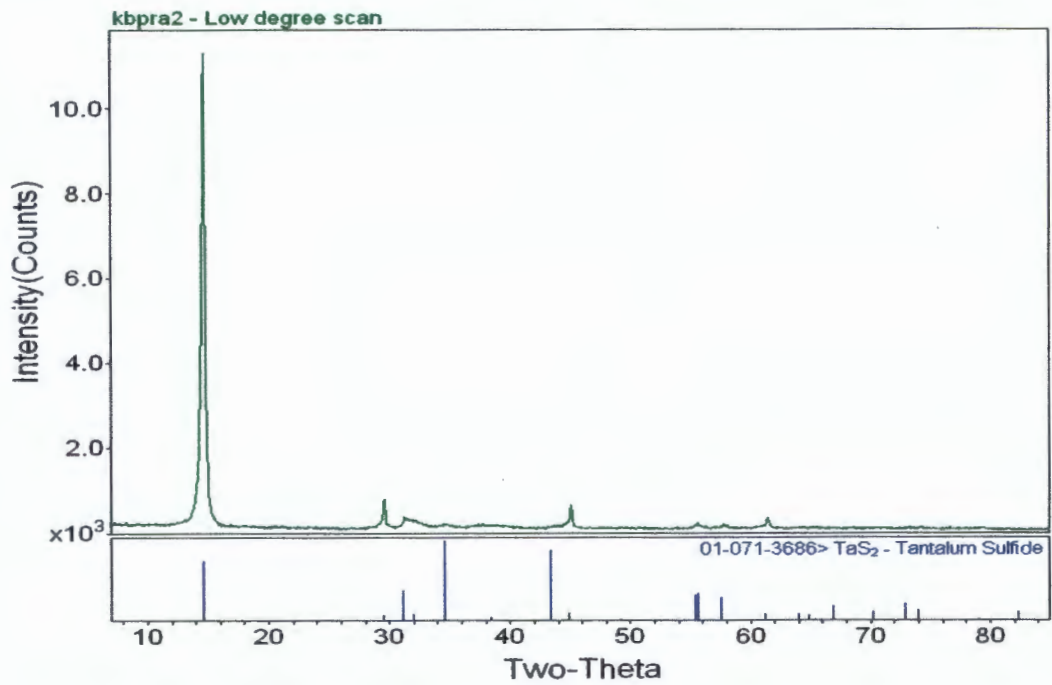
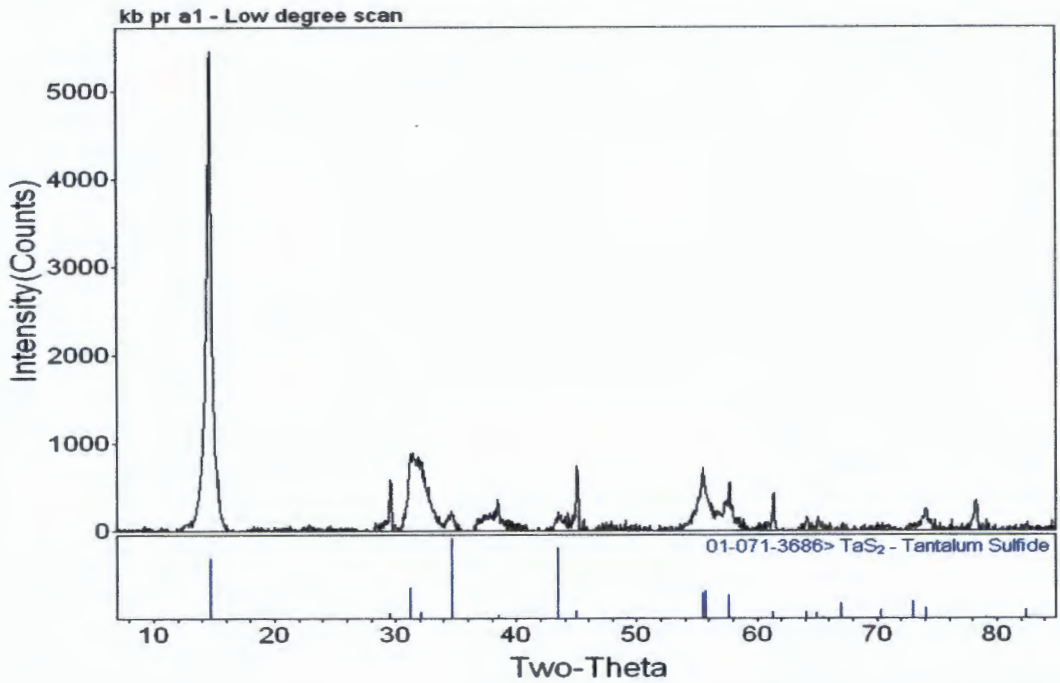
While each of the previously mentioned studies would bring about specific answers, they still lack a direct path to true application. Therefore, the recommendation for an extended study that holds the most merit would be to explore the formation of Mn-intercalated nanostructures across a variety of molar ratios using the Method A growth parameters. At the current time, examining Cr-intercalation samples does not appear to

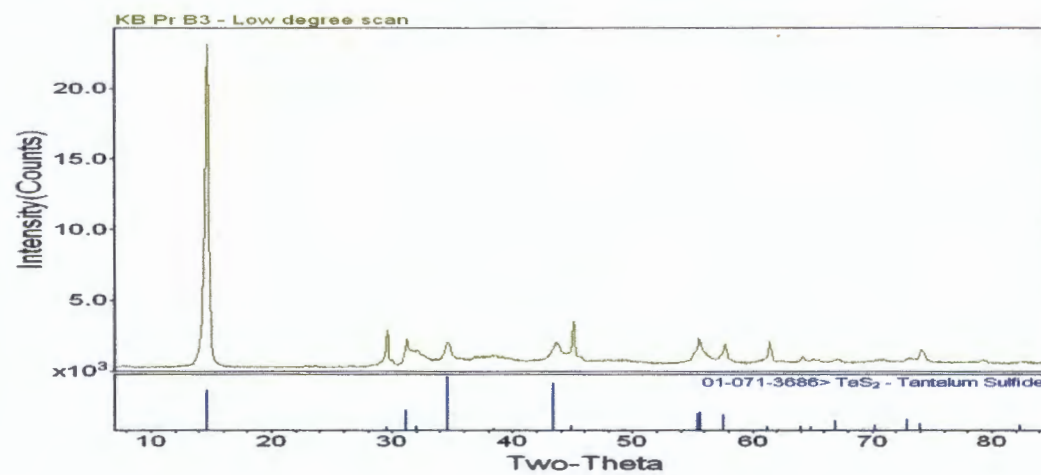
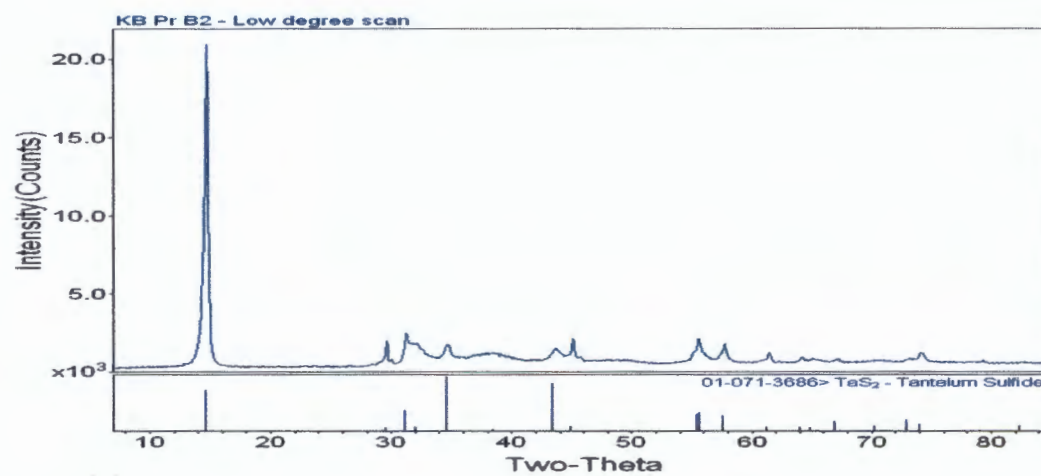
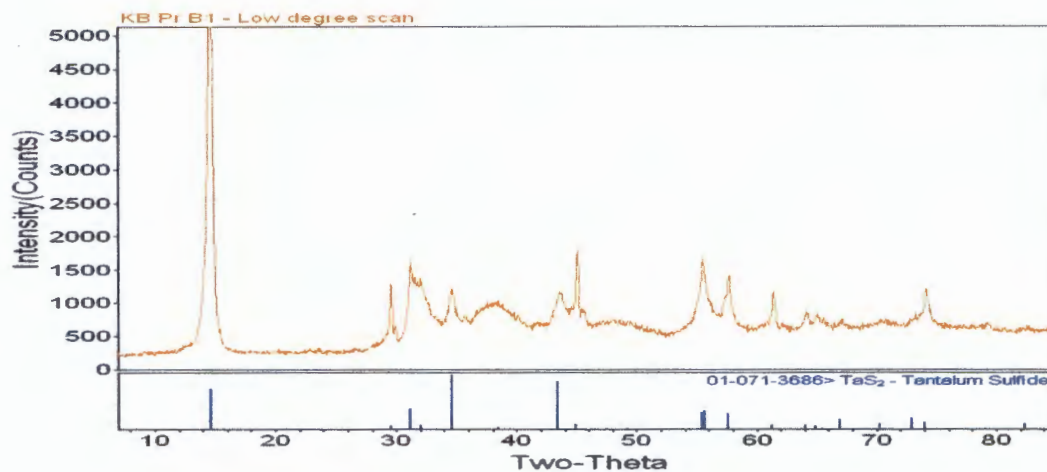
be a valuable use of resources because of the many uncertainties associated with these structures. However, an investigation into a variety of Mn-intercalated materials could potentially help researchers understand how these materials form during the annealing process, for instance whether the intercalation occurs simultaneously with the formation of the MnS side product or one growth precedes the other. These answers are important because it is only after these types of questions have been answered and a synthetic process has been refined to generate consistent products that researchers can begin to expand studies. It will likely be the differences of material properties like optics, magnetism and electronics between these intercalated samples and their pure nanostructure counterparts that the applications for these materials will be discovered, thus finally completing the extended challenge set by Charles Dunnill in 2010.

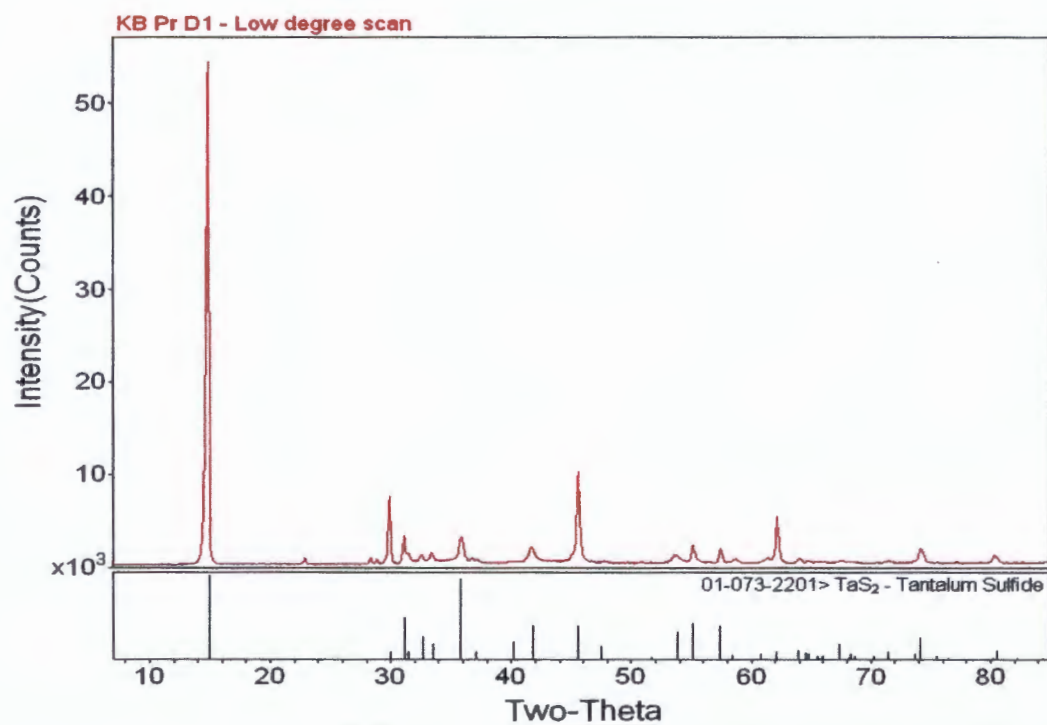
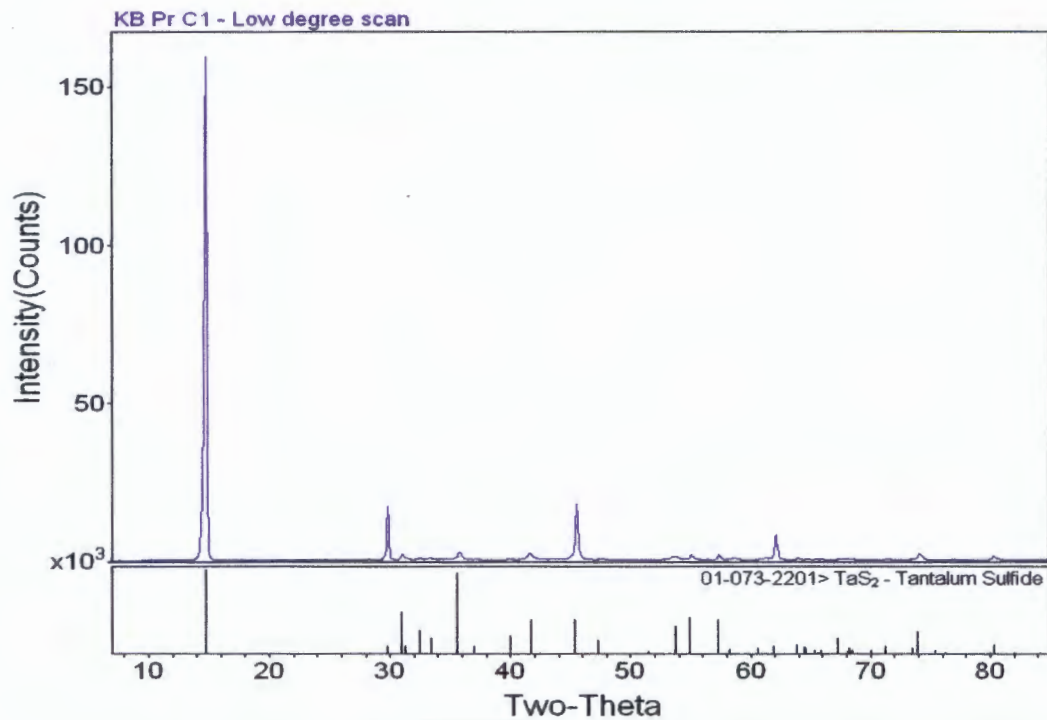
REFERENCES

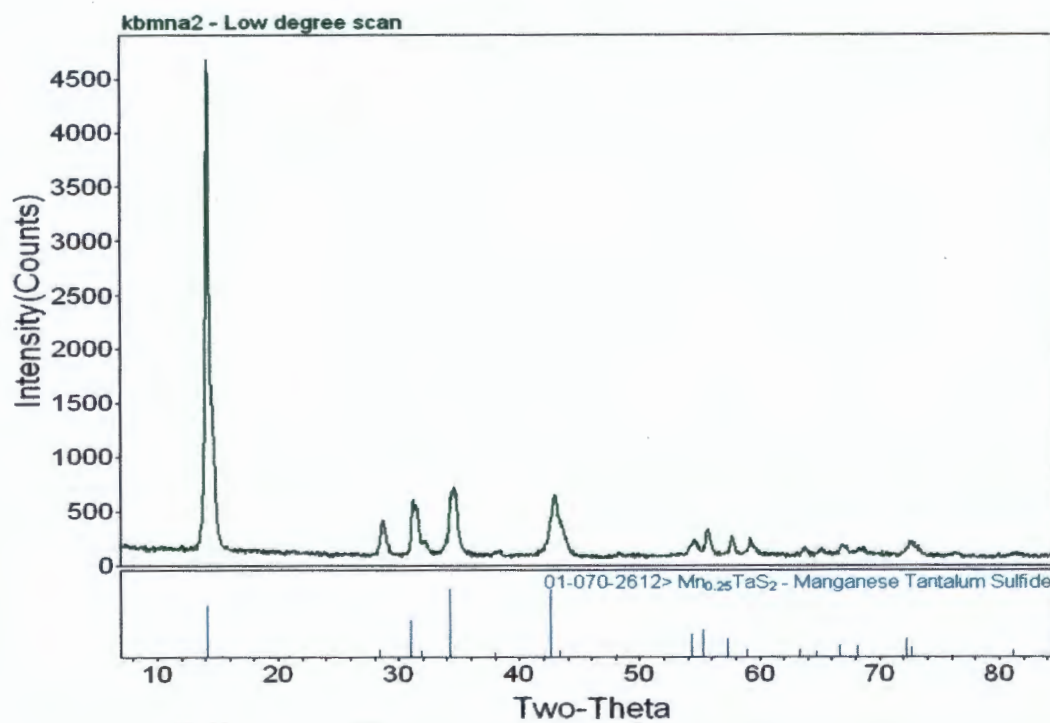
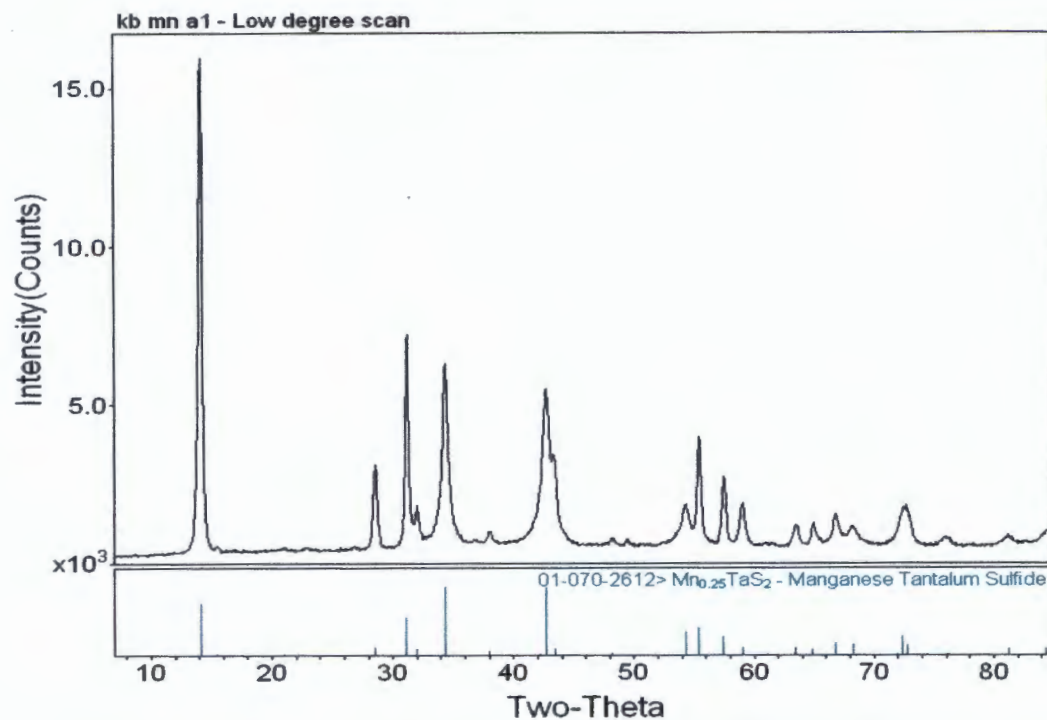
1. Dunnill, C. W.; MacLaren, I.; Gregory, D. H. *Nanoscale* **2010**, *2*, 90-97.
2. Lieth, R. M. A.; Terhell, J. C. J. M. Transition Metal Dichalcogenides. In *Preparation and Crystal Growth of Materials with Layered Structures*; Lieth, R. M. A., Ed.; Physics and Chemistry of Materials with Layered Structures, Vol. I; D. Reidel: Dordrecht, The Netherlands, 1977, pp. 142-145, 150, 186-188.
3. Guo, G. Y.; Liang, W. Y. *J. Phys. C: Solid State Phys.* **1987**, *20* (27), 4315-4334.
4. Miessler, G. L.; Tarr, D. A. The Crystalline Solid State. *Inorganic Chemistry*, 4; Prentice Hall: New York, 2011; pp.220-229.
5. Thompson, A. H.; Gamble, F. R. *J. Phys. Rev. B* **1972**, *5* (8), 2811-2816.
6. Subba Rao, G. V.; Shafer, M. W. Intercalation in Layered Transition Metal Dichalcogenides. In *Intercalated Layered Materials*; Lévy, F. A., Ed.; Physics and Chemistry of Materials with Layered Structures, Vol. VI; D. Reidel: Dordrecht, The Netherlands, 1979, pp.99-107, 131-139, 179-181.
7. Wagner, L. E.; Morosan, E.; Hor, Y. S.; Tao, J.; Zhu, Y.; Sanders, T. McQueen, T. M.; Zandbergen, H. W.; Williams, A. J.; West, D. V.; Cava, R. J. *Phys. Rev. B* **2008**, *78* 104520-1-104520-6.
8. Chianelli, R. R.; Prestridge, E. B.; Pecoraro, T. A.; DeNeufville, J. P. *Science* **1979**, *203*, 1105-1107.
9. Kroto, H. W. *Nature* **1987**, *329*, 529-531.
10. Iijima, S. *Nature* **1991**, *354*, 56-58.

11. Liu, Y.; Li, C.; Yang, J.; Hua, Z.; Li, J.; Yan, K.; Zhao, S. *J. Mater. Sci. Technol.* **2007**, *23* (2), 185-188.
12. (a) Nath, M.; Rao, C. N. R. *Pure Appl. Chem.* **2002**, *74* (9), 1545-1552. (b) *J. Am. Chem. Soc.* **2001**, *123*, 4841-4842.
13. Dunnill, C. W.; Edwards, H. K.; Brown, P. D.; Gregory, D. H. *Angew. Chem. Int. Ed.* **2006**, *45*, 7060-7063.
14. Shi, W.; Hughes, R. W.; Denholme, S. J.; Gregory, D. H. *Cryst. Eng. Comm.* **2010**, *12*, 641-659.
15. Kidd, T. E.; O'Shea, A. C.; Wallace, J.; Hummel, M.; Boyle, K. R.; Strauss, L. H. Synthesis of 1D tantalum disulfide nanostructures doped with 3d transition metals. To be submitted for publication.
16. Kidd, T. Photoemission Studies of Novel Charge Density Wave Systems. Ph.D. Thesis, University of Illinois Urbana-Champaign, Urbana, IL, 2002.

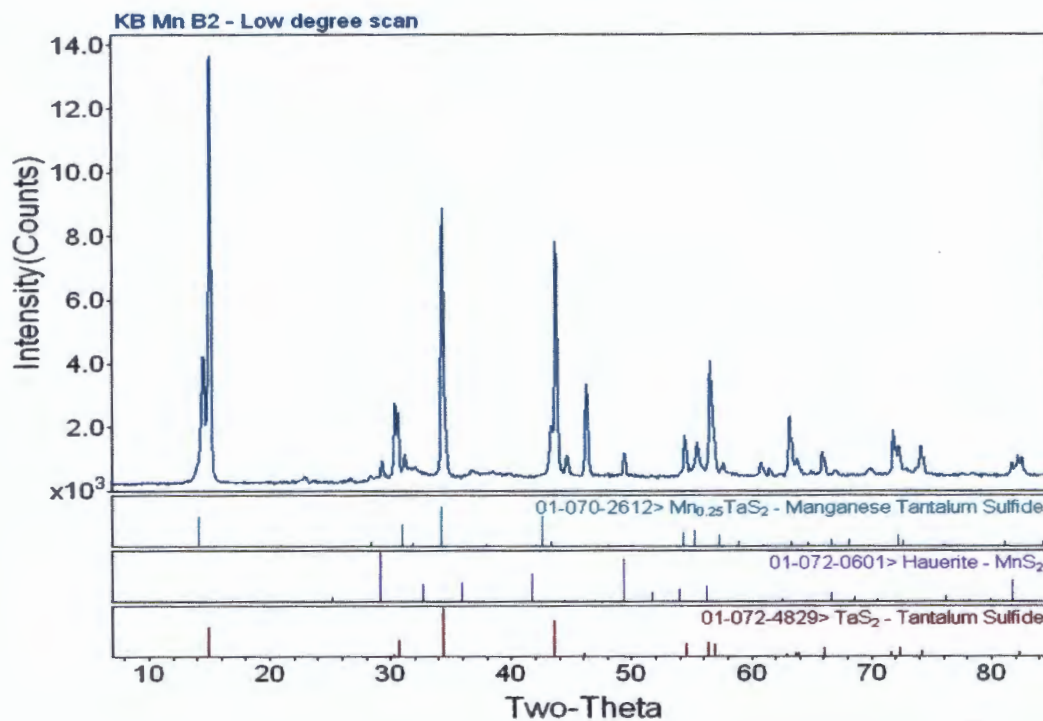
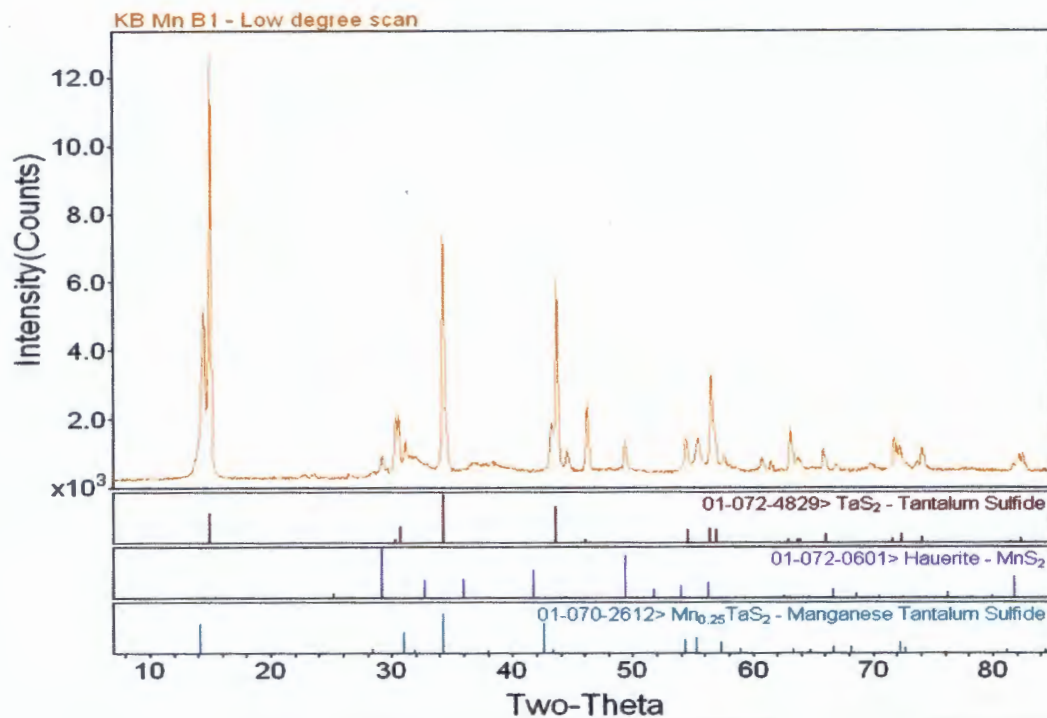
APPENDIX A: ACQUIRED X-RAY DIFFRACTION SPECTRA*Method A, Pure*

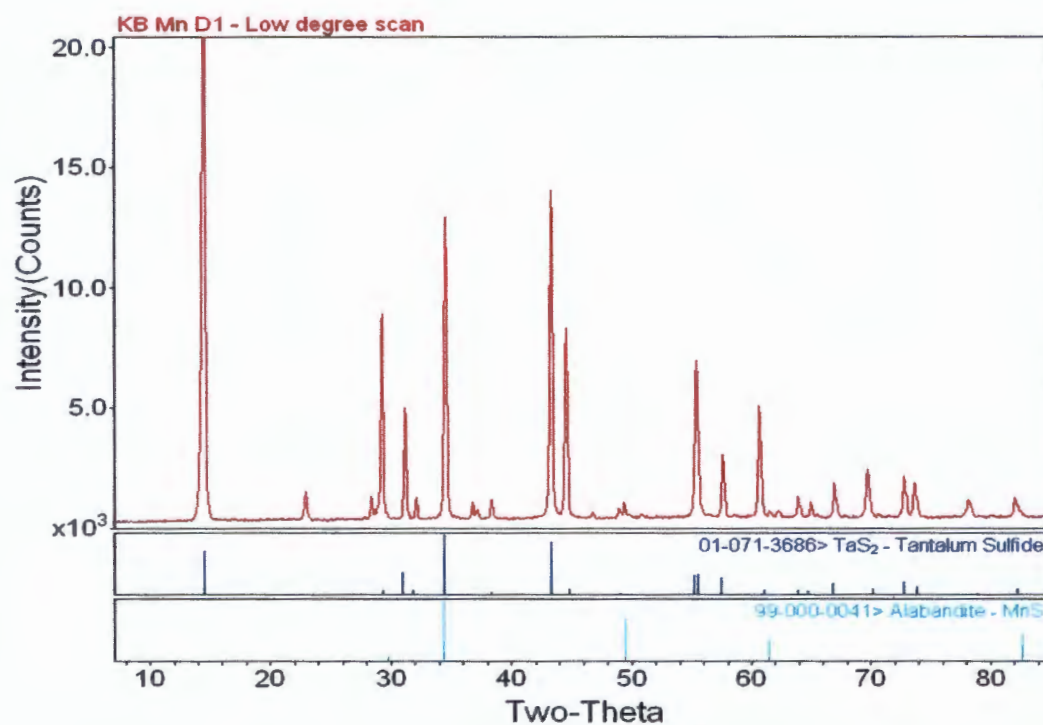
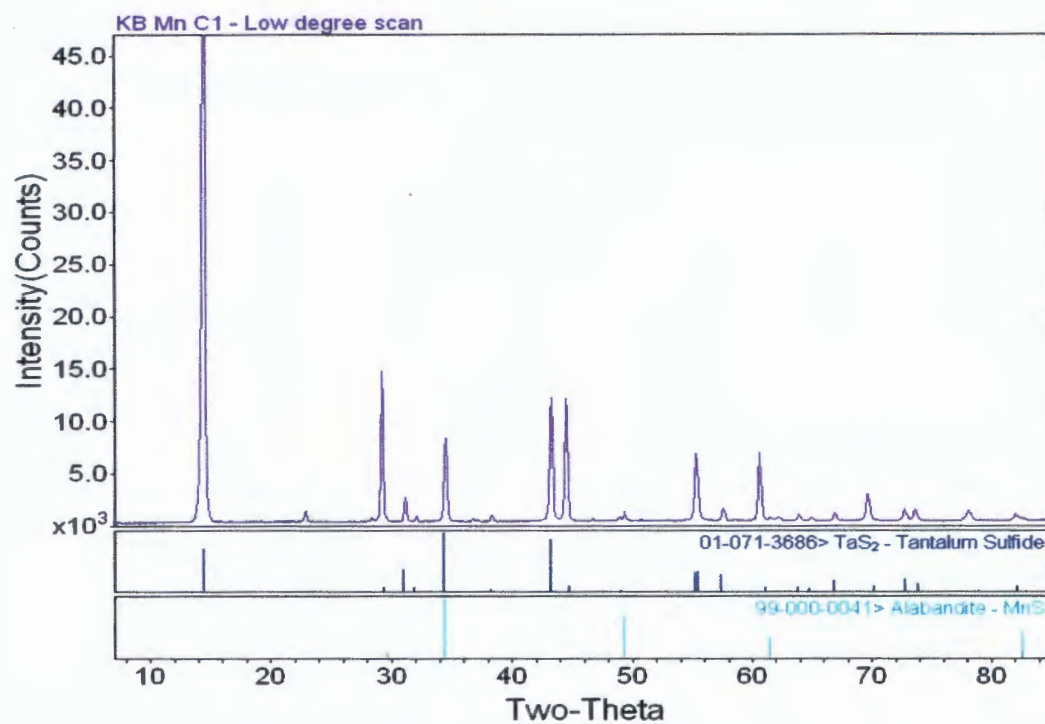
Method B, Pure

Methods C and D, Pure

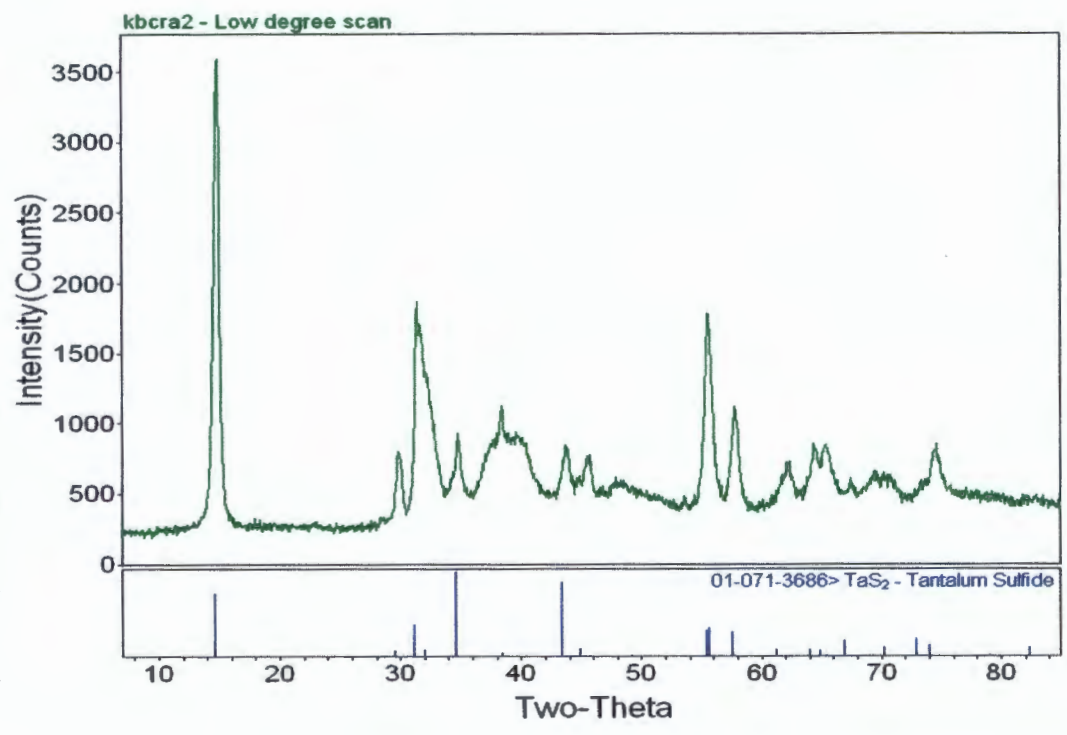
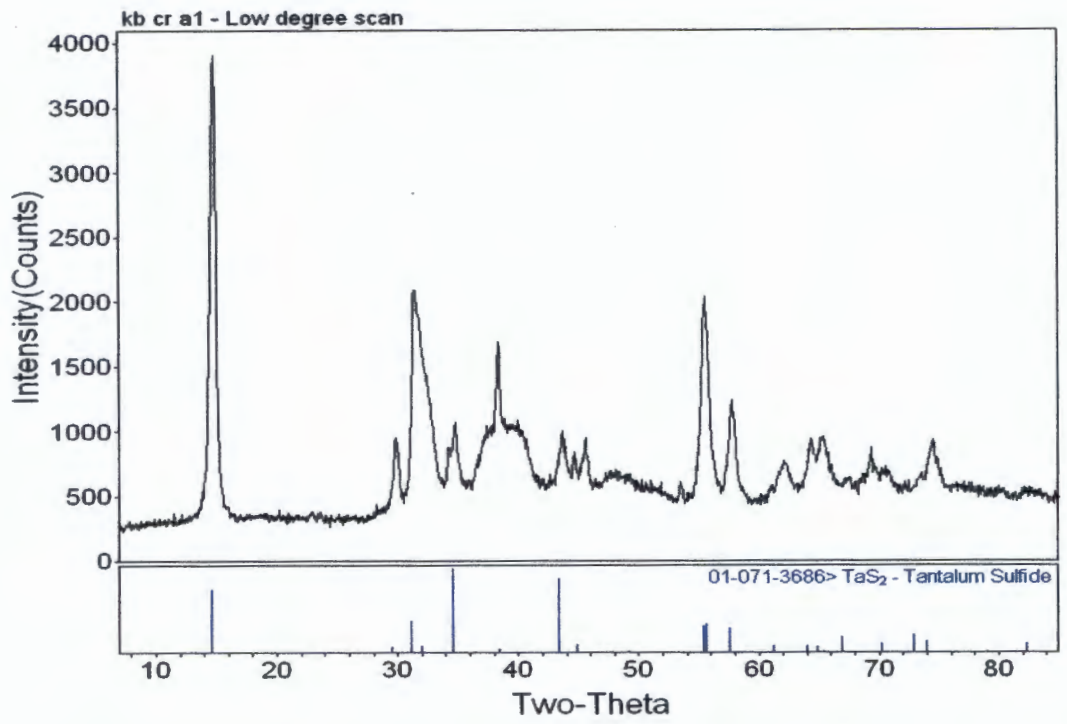
Method A, Mn intercalation

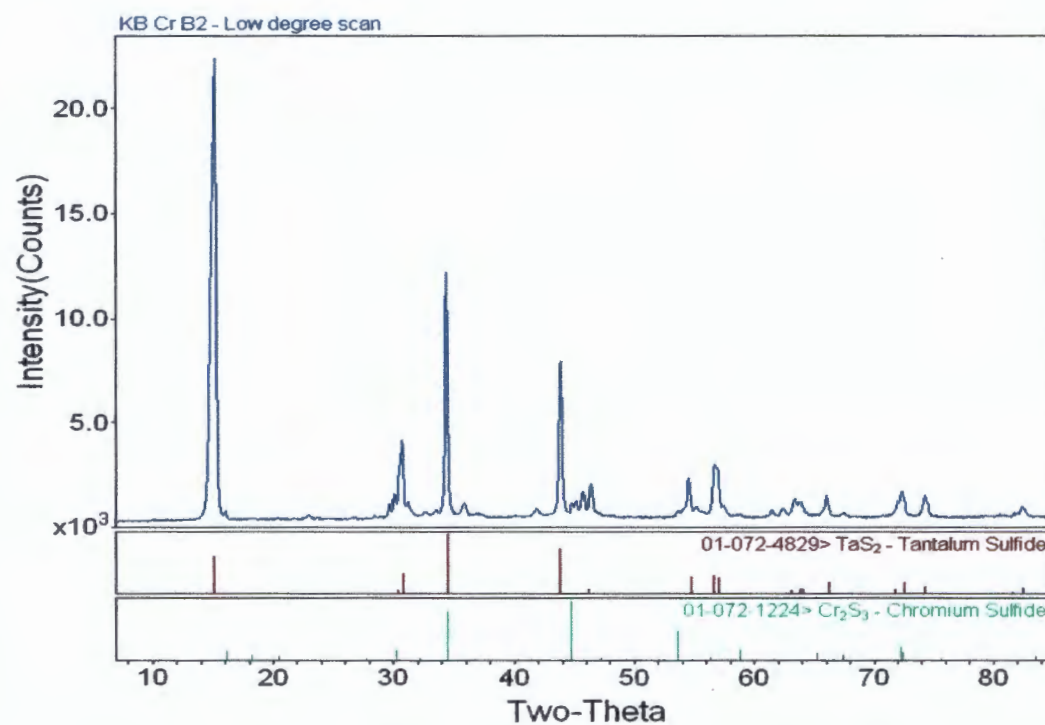
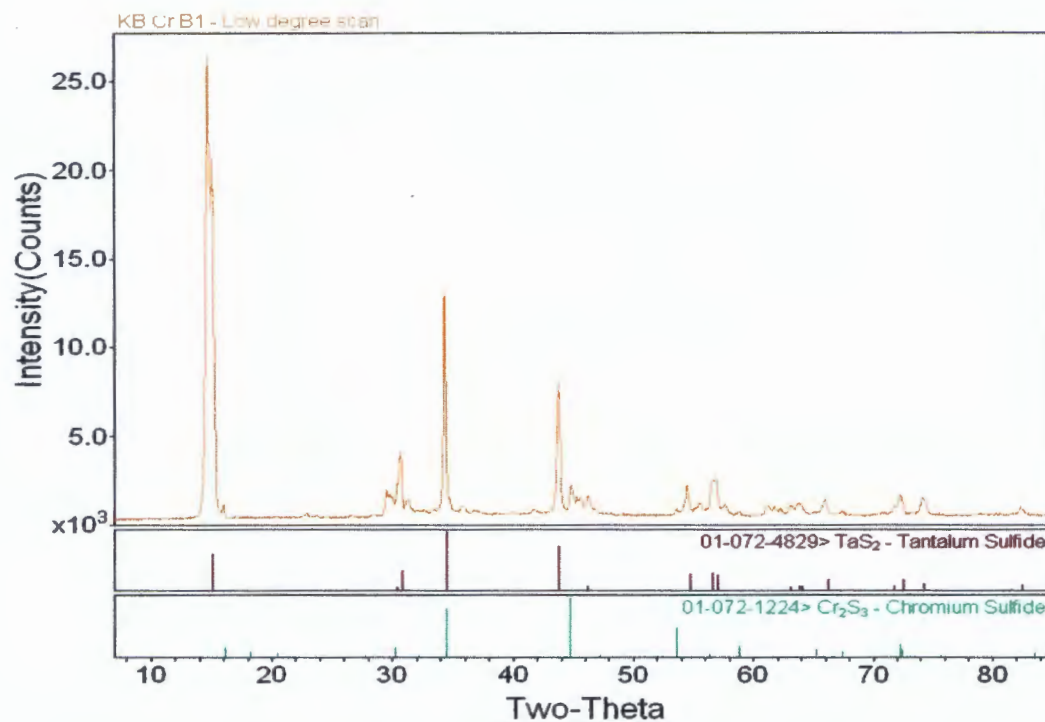
Method B, MnS seeded

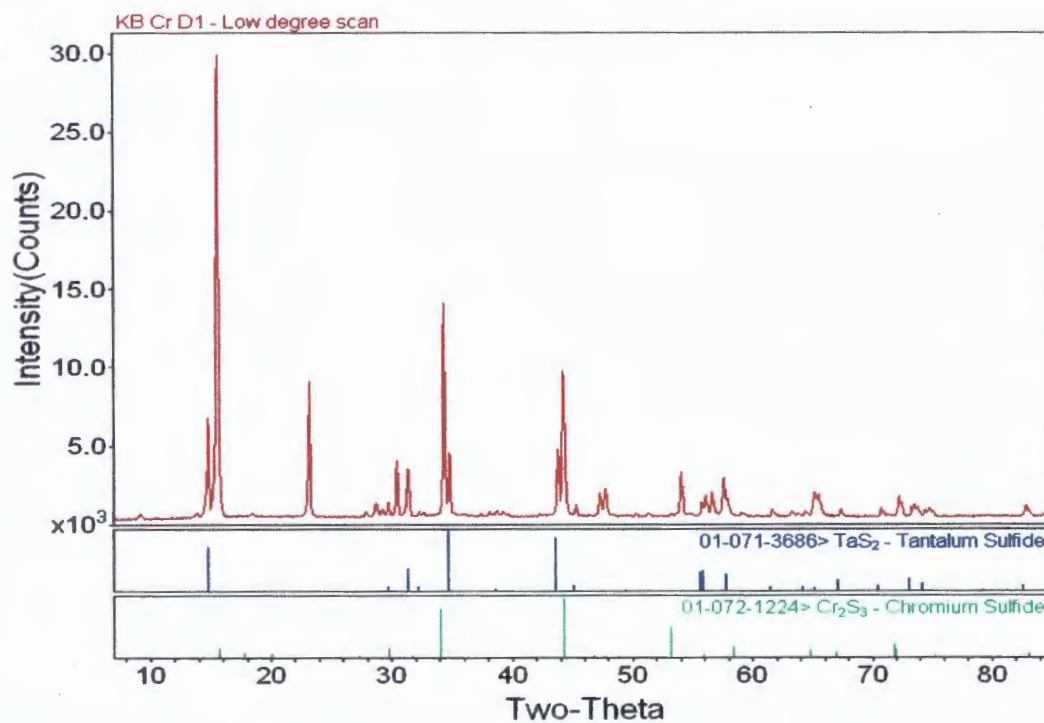
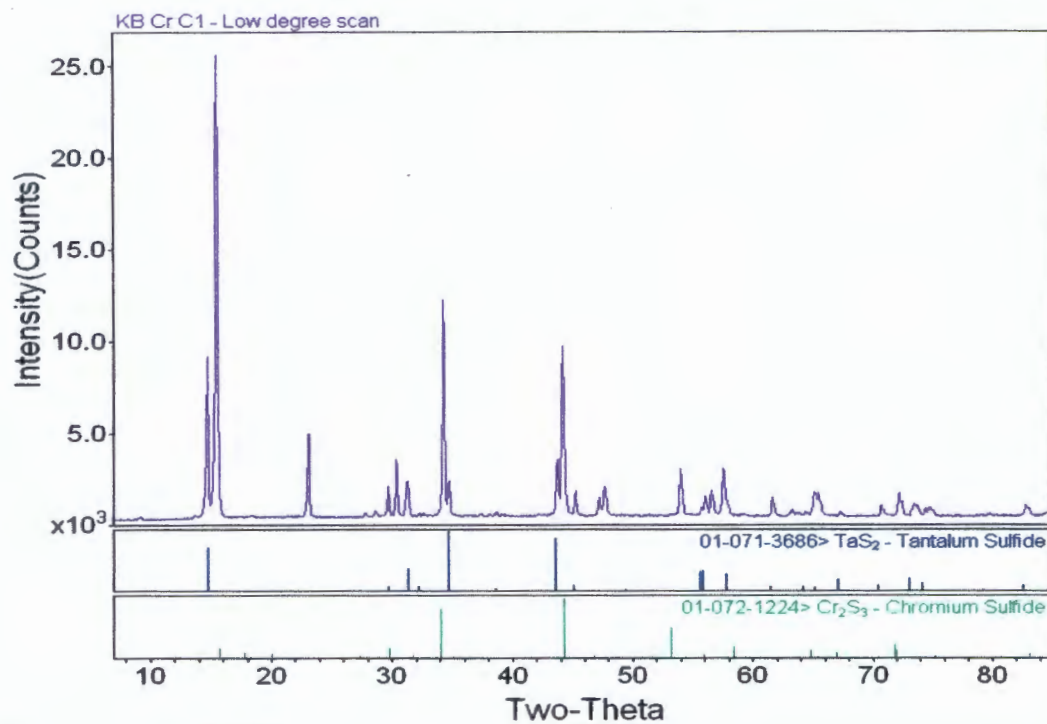


Methods C and D, MnS seeded as base

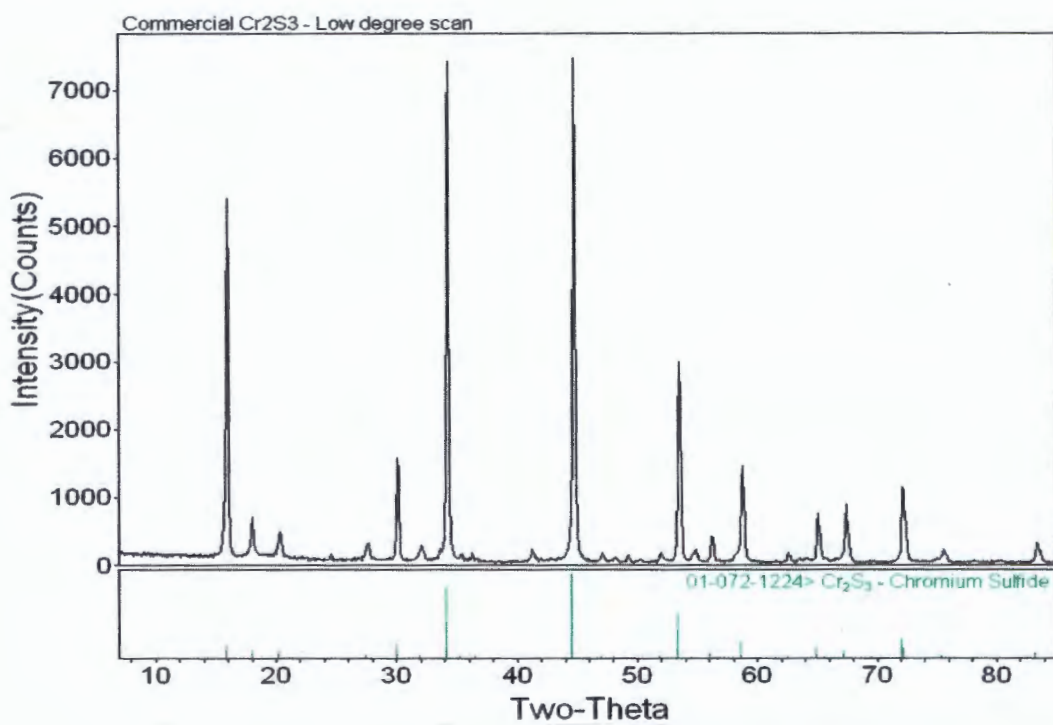
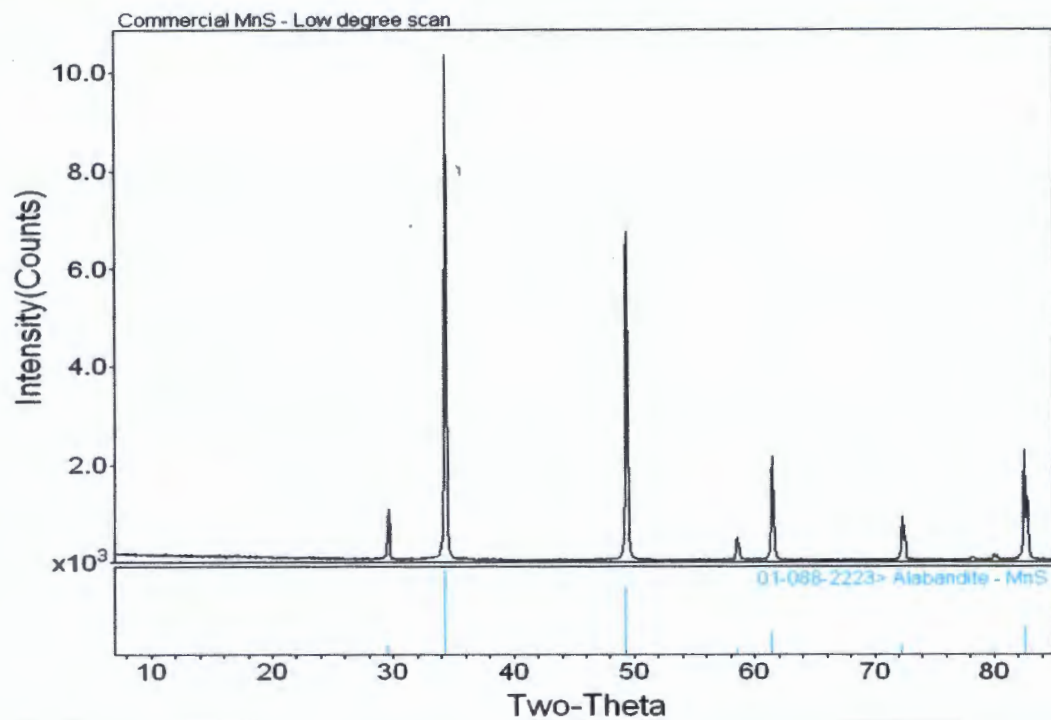
Method A, Cr intercalation



Method B, Cr₂S₃ seeded

Methods C and D, Cr₂S₃ seeded as base

Commercial Seeding Powders



APPENDIX B: IDENTIFIED DATA CARDS FROM THE INTERNATIONAL CENTER FOR DIFFRACTION DATA

PDF#01-071-3686(RDB); QM=Blank(B); d=Calculated; I=Calculated

PDF Card

Tantalum Sulfide

TaS₂

Radiation=CuKα1

Lambda=1.540599

Filter=

Calibration=

2θ=14.630-149.037

Mo(R/R)=13.0

Ref: Jellinek, F.

J. Less-Common Met., v4 p8 (1962)

Hexagonal - Powder Diffraction, P6₃/mmc (194)

Z=2

mp=

CELL: 3.315 x 3.315 x 12.1 <90.0 x 90.0 x 120.0>

P 5=n#6 00

Density(c)=7.068

Density(m)=

Mwt=245.07

Vol=115.16

F(30)=899.9(0.000,300)

Ref: Ibid.

ANX: AX2, ICSD Collection Code: 52116, Polymorphism/Phase Transition: 2H, Calculated Pattern Original Remarks: ICSD entry Z52116 is Name: FIZZ52116, Minor Warning: No R value given in the paper. No s.d. reported/abstracted on the cell dimension. Significant Warning: ICSD Warning: The coordinates are those given in the paper but the atomic distances do not agree with those calculated during testing. The coordinates are probably correct. Wyckoff Sequence: f b (P6₃/MMC), Unit Cell Data Source: Powder Diffraction.

Strong Lines: 6 05/0 2 87/2 2 79/1 2 58/6 2 08/4

63 Lines, Wavelength to Compute Theta = 1.54059A(Cu), I%-Type = Peak Height

#	d(A)	I(v)	(hkl)	2-Theta	Theta	1/(2d)	#	d(A)	I(v)	(hkl)	2-Theta	Theta	1/(2d)
1	6.0500	75.0	(002)	14.630	7.315	0.0826	33	1.0478	0.9	(213)	94.637	47.319	0.4772
2	3.0250	7.4	(004)	29.505	14.752	0.1653	34	1.0412	4.8	(208)	95.432	47.716	0.4802
3	2.8709	38.4	(100)	31.129	15.564	0.1742	35	1.0272	0.4	(1,0,1)	97.166	48.593	0.4868
4	2.7933	8.1	(101)	32.015	16.007	0.1790	36	1.0214	20.0	(214)	97.907	48.954	0.4895
5	2.5937	100.0	(102)	34.554	17.277	0.1928	37	1.0083	0.5	(0,0,12)	99.824	49.912	0.4959
6	2.3389	5.0	(103)	38.458	19.229	0.2138	38	0.9901	0.9	(215)	102.153	51.077	0.5050
7	2.0824	88.4	(104)	43.420	21.710	0.2431	39	0.9813	0.5	(209)	103.443	51.721	0.5096
8	2.0167	9.5	(006)	44.911	22.455	0.2479	40	0.9773	6.0	(1,1,10)	104.034	52.017	0.5116
9	1.8503	2.5	(105)	49.203	24.601	0.2702	41	0.9570	6.6	(300)	107.209	53.605	0.5225
10	1.6575	32.0	(110)	55.386	27.693	0.3017	42	0.9555	12.3	(216)	107.439	53.719	0.5233
11	1.6502	34.6	(106)	55.652	27.826	0.3030	43	0.9540	4.8	(301)	107.690	53.848	0.5241
12	1.5986	29.5	(112)	57.814	28.907	0.3128	44	0.9514	8.6	(1,0,12)	108.129	54.065	0.5256
13	1.5125	7.8	(008)	61.233	30.616	0.3306	45	0.9452	5.8	(302)	109.165	54.582	0.5290
14	1.4609	1.2	(107)	62.687	31.343	0.3376	46	0.9311	0.5	(303)	111.642	55.821	0.5370
15	1.4536	8.4	(114)	64.001	32.000	0.3440	47	0.9252	5.4	(2,0,10)	112.735	56.368	0.5404
16	1.4354	7.0	(200)	64.909	32.454	0.3483	48	0.9190	0.5	(217)	113.895	56.947	0.5441
17	1.4254	1.3	(201)	65.421	32.710	0.3508	49	0.9124	2.0	(304)	115.185	57.593	0.5490
18	1.3957	19.2	(202)	66.944	33.472	0.3580	50	0.8654	0.5	(1,0,13)	120.917	60.458	0.5647
19	1.3524	1.0	(203)	69.444	34.722	0.3697	51	0.8617	6.7	(218)	121.779	60.889	0.5671
20	1.3382	10.9	(108)	70.289	35.145	0.3737	52	0.8731	0.5	(2,0,11)	123.827	61.914	0.5727
21	1.2988	21.3	(204)	72.880	36.440	0.3856	53	0.8646	5.8	(306)	125.991	62.995	0.5783
22	1.2805	14.2	(116)	73.963	36.982	0.3905	54	0.8646	5.8	(0,0,14)	125.991	62.995	0.5783
23	1.2346	0.7	(205)	77.207	38.604	0.4050	55	0.8615	2.1	(1,1,12)	126.807	63.404	0.5804
24	1.2176	0.7	(109)	78.493	39.247	0.4107	56	0.8444	0.5	(219)	131.639	65.819	0.5921
25	1.2100	1.9	(0,0,10)	79.079	39.539	0.4132	57	0.8298	5.5	(220)	136.704	68.352	0.6033
26	1.1594	10.5	(206)	82.400	41.200	0.4276	58	0.8276	5.5	(1,0,14)	137.108	68.554	0.6042
27	1.1173	17.9	(118)	87.174	43.587	0.4475	59	0.8251	8.2	(2,0,12)	137.997	68.999	0.6060
28	1.1150	14.7	(1,0,10)	87.393	43.697	0.4484	60	0.8211	5.0	(222)	139.465	69.743	0.6090
29	1.1043	0.4	(207)	88.458	44.229	0.4528	61	0.8087	10.7	(308)	144.548	72.274	0.6183
30	1.0651	5.4	(210)	90.452	45.226	0.4606	62	0.8078	10.7	(2,1,10)	144.928	72.464	0.6189
31	1.0808	1.3	(211)	90.917	45.458	0.4628	63	0.7993	1.7	(224)	149.037	74.519	0.6256
32	1.0681	15.7	(212)	92.310	46.155	0.4681							

PDF#01-072-4829(RDB): QM=Indexed(I); d=Calculated; I=Calculated

PDF Card

Tantalum Sulfide

TaS₅Radiation=CuK_α1

Lambda=1.5405999

Filter=

Calibration=

2 θ =15.004-148.860

1/(c(F)R)=12.2

Ref: Jellinek, F.

J. Less-Common Met., v4 p9 (1962)

Hexagonal - Powder Diffraction, P3m1 (164)

Z=1

mp=

Cell: 3.36 x 3.36 x 5.9 (90.0 x 90.0 x 120.0)

P.S.=hP3.00

Density(c)=7.055

Density(m)=

Mwt=245.07

Vol=57.68

F(30)=999.9(1.000,3000)

Ref: Ibid.

Additional Patterns: See PDF 09-002-0137, ANX: AX2, Formula from original source: Ta S₂, ICSD Collection Code: 52115. Test from ICSD: At least one temperature factor missing in the paper. Minor Warning: No R factors reported/abstracted. No e.s.d reported/abstracted on the cell dimension. Minor test comments from ICSD exist. Unit Cell Data Source: Powder Diffraction.

Strong Lines: 5.90(X) 2.95(1) 2.91(3) 2.61(7) 2.07(4) 1.63(1) 1.63(1)

45 Lines, Wavelength to Compute Theta = 1.54059(A)(Cu), I%-Type = Peak Height

#	d(A)	h(v)	(hkl)	2-Theta	Theta	1/(2d)	#	d(A)	h(v)	(hkl)	2-Theta	Theta	1/(2d)
1	5.9000	63.0	(001)	15.004	7.502	0.0847	24	1.0305	17.7	(122)	96.744	48.372	0.4852
2	2.9500	6.3	(002)	30.273	15.136	0.1695	25	0.9633	0.4	(006)	103.137	51.568	0.5085
3	2.9099	34.1	(100)	30.701	15.350	0.1716	26	0.9699	5.4	(300)	105.152	52.576	0.5155
4	2.6097	100.0	(011)	34.335	17.167	0.1916	27	0.9656	5.4	(115)	105.827	52.914	0.5178
5	2.0716	75.6	(012)	43.657	21.829	0.2414	28	0.9599	11.6	(213)	106.732	53.366	0.5209
6	1.9667	7.7	(003)	46.117	23.059	0.2542	29	0.9571	8.5	(301)	107.188	53.593	0.5224
7	1.6600	28.5	(110)	54.582	27.291	0.2976	30	0.9316	7.2	(016)	111.557	55.779	0.5367
8	1.6294	30.3	(103)	56.425	28.213	0.3069	31	0.9214	1.6	(032)	113.438	56.719	0.5426
9	1.6156	26.7	(111)	56.945	28.472	0.3095	32	0.9165	5.3	(205)	114.367	57.193	0.5456
10	1.4750	6.3	(004)	62.964	31.482	0.3390	33	0.9817	5.9	(214)	121.771	60.886	0.5671
11	1.4599	7.6	(112)	63.894	31.847	0.3425	34	0.8699	4.7	(033)	124.625	62.312	0.5748
12	1.4549	7.7	(200)	63.935	31.968	0.3437	35	0.8486	1.8	(116)	130.371	65.186	0.5892
13	1.4126	19.2	(201)	66.090	33.045	0.3540	36	0.8429	0.9	(007)	132.103	66.051	0.5932
14	1.3156	9.0	(104)	71.676	35.838	0.3800	37	0.8400	4.4	(220)	132.988	66.494	0.5952
15	1.3049	18.8	(202)	72.361	36.180	0.3832	38	0.8316	4.5	(221)	135.720	67.860	0.6012
16	1.2774	12.2	(113)	74.174	37.087	0.3914	39	0.8147	6.4	(206)	141.989	70.994	0.6137
17	1.1600	1.6	(005)	81.505	40.752	0.4237	40	0.8104	9.2	(304)	143.768	71.894	0.6170
18	1.1696	10.2	(023)	82.382	41.191	0.4275	41	0.8096	5.5	(107)	144.156	72.078	0.6176
19	1.1084	14.7	(114)	86.047	44.024	0.4511	42	0.8079	3.7	(222)	144.906	72.453	0.6189
20	1.0998	5.1	(210)	88.915	44.458	0.4546	43	0.8070	3.7	(310)	145.285	72.643	0.6195
21	1.0935	8.2	(016)	89.566	44.783	0.4572	44	0.8046	10.2	(125)	146.445	73.222	0.6215
22	1.0612	15.8	(121)	90.869	45.435	0.4625	45	0.7996	9.8	(311)	148.880	74.440	0.6253
23	1.0356	4.3	(024)	96.069	48.045	0.4827							

PDF#01-073-2201(ROB): QM=Indexed(I); d=Calculated; I=Calculated

PDF Card

Tantalum Sulfide

TaS₂Radiation=CuK_α1

Lambda=1.54059810

Filter=

Calibration=

ZT=7.373-89.802

Wc(RIR)=12.5

Ref: Haeggi, G., Schoenberg, N.

Ark. Chem., v7 p371 (1954)

Rhombohedral - (Unknown), R $\bar{3}m$ (166)

Z=6

mp=

CELL: 3.34 x 3.34 x 35.94 <90.0 x 90.0 x 120.0>

P.S.=hR6.00 (Å)

Density(c)=7.032

Density(m)=

Mwt=245.07

Vol=347.22

F(30)=612.3(0.001,33.0)

Ref: Ibid.

ANX: AX2. ICSD Collection Code: 24757. Other Cell: Cell of J. Less-Common Met., 4 9-15 (1962): 3.335, 35.85. Calculated Pattern Original Remarks: Ta partly in trigonal prism. Test from ICSD; At least one TF missing. No R value given. Calc. density unusual but tolerable. Minor Warning: No R value given in the paper. No d reported/abstracted on the cell dimension. Wyckoff Sequence: c3 (R3-MHR).

Strong Lines: 5.96X 3.901 2.682 2.751 2.681

51 Lines, Wavelength to Compute Theta = 1.54059Å/Cu, I% - Type = Peak height

#	d(Å)	I(v)	(hkl)	2-Theta	Theta	1/(2d)	#	d(Å)	I(v)	(hkl)	2-Theta	Theta	1/(2d)
1	11.9600	0.1	(003)	7.373	3.687	0.0417	27	1.4416	6.6	(202)	64.597	32.299	0.3468
2	5.9900	100.0	(006)	14.777	7.389	0.0835	28	1.4279	5.0	(024)	65.295	32.647	0.3502
3	3.9933	0.2	(009)	22.244	11.122	0.1252	29	1.4226	1.7	(1,0,22)	65.575	32.788	0.3515
4	2.9950	10.0	(0,0,12)	29.807	14.904	0.1669	30	1.4179	4.2	(205)	65.815	32.907	0.3528
5	2.8832	50.8	(101)	30.991	15.496	0.1734	31	1.3921	18.5	(027)	67.193	33.596	0.3592
6	2.8556	9.6	(012)	31.297	15.648	0.1751	32	1.3767	3.0	(208)	68.047	34.023	0.3632
7	2.7634	27.8	(104)	32.492	16.246	0.1816	33	1.3748	7.4	(0,1,23)	68.161	34.076	0.3637
8	2.6834	19.0	(015)	33.364	16.682	0.1863	34	1.3701	3.9	(1,1,15)	68.422	34.211	0.3650
9	2.5201	96.4	(107)	35.596	17.798	0.1984	35	1.3417	4.9	(0,2,10)	70.076	35.036	0.3727
10	2.4320	10.3	(018)	36.931	18.465	0.2056	36	1.3225	9.5	(2,0,11)	71.247	35.624	0.3781
11	2.3960	0.3	(0,0,15)	37.506	18.753	0.2087	37	1.2874	7.0	(1,0,25)	73.503	36.752	0.3684
12	2.2534	22.1	(1,0,10)	39.978	19.989	0.2219	38	1.2810	26.7	(0,2,13)	73.929	36.965	0.3903
13	2.1658	41.5	(0,1,11)	41.669	20.835	0.2309	39	1.2810	26.7	(1,1,18)	73.929	36.965	0.3903
14	1.9986	40.8	(0,0,18)	45.340	22.670	0.2502	40	1.2601	4.3	(2,0,14)	75.369	37.685	0.3968
15	1.9986	40.8	(1,0,13)	45.340	22.670	0.2502	41	1.2472	1.4	(0,1,26)	76.264	38.142	0.4009
16	1.9200	16.2	(0,1,14)	47.305	23.653	0.2604	42	1.2160	1.0	(0,2,16)	78.612	39.306	0.4112
17	1.7741	3.7	(1,0,16)	51.467	25.733	0.2818	43	1.1980	2.5	(0,0,30)	80.029	40.015	0.4174
18	1.7068	33.3	(0,1,17)	53.655	26.827	0.2929	44	1.1937	11.0	(2,0,17)	80.379	40.189	0.4189
19	1.6700	44.1	(110)	54.938	27.468	0.2994	45	1.1732	2.0	(1,0,28)	82.075	41.036	0.4262
20	1.6087	41.0	(116)	57.220	28.610	0.3108	46	1.1489	2.1	(0,2,19)	84.204	42.102	0.4352
21	1.5631	6.4	(1,0,19)	58.230	29.115	0.3158	47	1.1392	1.6	(0,1,29)	85.095	42.548	0.4389
22	1.5407	0.4	(119)	59.995	29.998	0.3245	48	1.1267	2.7	(2,0,20)	86.264	43.132	0.4438
23	1.5264	6.7	(0,1,20)	60.615	30.308	0.3276	49	1.1149	23.6	(1,1,24)	87.403	43.702	0.4485
24	1.4975	10.4	(0,0,24)	61.913	30.957	0.3339	50	1.0926	7.1	(211)	89.843	44.922	0.4576
25	1.4586	11.5	(1,1,12)	63.758	31.878	0.3428	51	1.0913	2.2	(122)	89.802	44.901	0.4582
26	1.4451	9.1	(021)	64.423	32.211	0.3480							

PDF#01-070-2612(RDB): QM=Blank(B); d=Calculated; l=Calculated

PDF Card

Manganese Tantalum Sulfide

Mn₂₃TaS₇Radiation=CuK α 1

Lambda=1.540599

Filter=

Calibration=

2 θ =14.148-89.960I₀(RIR)=10.4

Ref. van-Laar, B., Rietveld, H.M., Jds. D.J.W.

J. Solid State Chem., v3 p154 (1971)

Hexagonal - Powder Diffraction, P6₃/mmc (194)

Z=8 mp=

CELL: 6.64 x 6.64 x 12.51 <90.0 x 90.0 x 120.0>

P. S=H26.00

Density(c)=7.197

Density(m)=

Mwt=256.8

Vol=477.67

F(30)=999.9(0.000,300)

Ref. Ibd.

ANX: AB4XB ICSD Collection Code: 42660 Temperature of Data Collection: 4.2 K. Test from ICSD: REF. Journal of Solid State Chemistry CLAS 6/mmm (Riemann-Mauguin) - D6h (Schoenflies), PRS: H26. No R value given in the paper. (Code 5). At least one temperature factor missing in the paper. (C. Minor Warning. No R value given in the paper. No e.s.d. reported/abstracted on the cell dimension. Significant Warning. ICSD Warning: The coordinates are those given in the paper but the atomic distances do not agree with those calculated during testing. The coordinates are probably correct. Wyckoff Sequence: k h f a (P6₃/MMC). Unit Cell Data Source: Powder Diffraction.

Strong Lines: 6.26/X 3.13/1

91 Lines, Wavelength to Compute Theta = 1.54059Å(Cu), I%-Type = Peak Height

#	d(Å)	I(v)	(hkl)	2-Theta	#	d(Å)	I(v)	(hkl)	2-Theta	#	d(Å)	I(v)	(hkl)	2-Theta
1	6.2550	62.1	(002)	14.148	32	1.6600	33.2	(220)	55.295	63	1.2668	0.3	(316)	74.901
2	5.7504	1.5	(100)	15.396	33	1.6408	0.7	(215)	55.999	64	1.2578	0.9	(323)	75.529
3	5.2249	0.7	(101)	16.956	34	1.6343	0.2	(304)	56.242	65	1.2548	0.6	(410)	75.736
4	4.2333	1.8	(102)	20.968	35	1.6045	23.0	(272)	57.383	66	1.2510	2.2	(209)	76.012
5	3.3758	0.3	(103)	26.390	36	1.5821	0.2	(311)	58.273	67	1.2510	2.2	(0,0,10)	76.012
6	3.3200	0.7	(110)	26.632	37	1.5638	9.4	(006)	59.023	68	1.2486	1.6	(411)	76.186
7	3.1275	10.0	(004)	28.517	38	1.5454	0.3	(312)	59.793	69	1.2465	0.9	(405)	76.336
8	2.9325	1.1	(112)	30.456	39	1.5216	0.5	(305)	60.827	70	1.2303	0.3	(412)	77.524
9	2.8752	44.9	(200)	31.090	40	1.5179	1.8	(207)	60.995	71	1.2224	0.3	(1,0,10)	78.122
10	2.8022	7.8	(201)	31.911	41	1.5090	0.3	(106)	61.392	72	1.2155	0.3	(324)	78.650
11	2.7474	1.0	(104)	32.564	42	1.5046	0.3	(216)	61.586	73	1.2117	0.3	(306)	78.948
12	2.6124	62.4	(202)	34.296	43	1.4896	0.3	(313)	62.276	74	1.2016	0.3	(413)	79.740
13	2.3671	5.2	(203)	37.982	44	1.4663	10.1	(224)	63.383	75	1.1899	0.3	(317)	80.683
14	2.2542	0.2	(105)	38.237	45	1.4378	7.6	(400)	64.799	76	1.1835	8.5	(406)	81.210
15	2.2765	0.5	(114)	38.555	46	1.4282	1.1	(401)	65.278	77	1.1710	0.3	(219)	82.286
16	2.1735	0.7	(210)	41.515	47	1.4208	0.5	(314)	65.661	78	1.1710	0.3	(1,1,10)	82.266
17	2.1414	1.8	(211)	42.166	48	1.4147	0.3	(116)	65.981	79	1.1670	1.0	(325)	82.614
18	2.1167	100.0	(204)	42.682	49	1.4111	0.3	(306)	66.169	80	1.1648	0.7	(414)	82.817
19	2.0850	8.9	(006)	43.363	50	1.4011	15.0	(402)	66.705	81	1.1471	8.5	(2,0,10)	84.366
20	2.0530	0.6	(212)	44.073	51	1.3804	0.5	(217)	67.838	82	1.1453	4.4	(501)	84.536
21	1.9601	0.4	(106)	46.280	52	1.3737	13.6	(208)	68.213	83	1.1382	19.4	(226)	85.179
22	1.9274	1.0	(213)	47.114	53	1.3591	1.1	(403)	69.050	84	1.1253	0.3	(309)	86.399
23	1.9168	0.2	(300)	47.390	54	1.3511	0.3	(109)	69.516	85	1.1217	0.3	(415)	86.744
24	1.8947	1.2	(301)	47.977	55	1.3449	0.3	(315)	69.886	86	1.1202	0.7	(407)	86.891
25	1.8874	2.7	(205)	48.173	56	1.3192	0.3	(320)	71.450	87	1.1166	0.3	(318)	87.240
26	1.8327	0.4	(302)	49.706	57	1.3120	1.5	(321)	71.906	88	1.1148	0.3	(326)	87.412
27	1.7849	0.4	(214)	51.137	58	1.3062	22.9	(307)	72.274	89	1.1087	0.7	(503)	88.019
28	1.7657	0.2	(116)	51.731	59	1.3062	22.9	(404)	72.274	90	1.1067	0.4	(330)	88.222
29	1.7416	0.7	(303)	52.500	60	1.2987	12.5	(226)	72.781	91	1.0997	0.4	(332)	88.980
30	1.7066	0.2	(107)	53.662	61	1.2908	0.3	(322)	73.273					
31	1.6879	27.6	(206)	54.305	62	1.2694	0.3	(216)	74.723					

PDF#01-072-0601(ROB); QM=Blank(B); d=Calculated; I=Calculated

PDF Card

Hausenite, syn (Manganese Sulfide)

MnS₂Radiation=CuK α 1

Lambda=1.5405619

Filter=

Calibration=

ZT=25.230-87.380

I/c(RIR)=3.59

Ref: Offner, F.

Z. Kristallogr., Kristallgeom., Kristallphys., Kristallchem., v89 p182 (1934)

Cubic - (Unknown), Pa $\bar{3}$ (205)

Z=4 mp=

CELL: 6.109 x 6.109 x 6.109 <90.0 x 90.0 x 90.0>

P.S.=cP12.00

Density(c)=3.469

Density(m)=

Mwt=119.06

Vol=227.99

F(23)=999.9(0.000,2310)

Ref: Ibid.

Additional Patterns: See PDF 01-076-2050 and PDF 00-025-0549. ANX. AX2. ICSD Collection Code: 15991. Test from ICSD. No R value given. A: at least one TF missing. Minor Warning: No R value given in the paper. Significant Warning: ICSD Warning: The coordinates are those given in the paper but the atomic distances do not agree with those calculated during testing. The coordinates are probably correct. Wyckoff Sequence: c a (PA3-)

Strong Lines: 3.5311 3.051X 2.7313 2.4913 2.1614 1.8415 1.7611

23 Lines, Wavelength to Compute Theta = 1.54056Å(Cu), I%-Type = Peak Height

#	d(Å)	I(v)	(hkl)	2-Theta	Theta	1/(2 θ)	#	d(Å)	I(v)	(hkl)	2-Theta	Theta	1/(2 θ)
1	3.5270	9.1	(111)	25.230	12.615	0.1418	13	1.4399	3.2	(411)	64.682	32.341	0.3472
2	3.0545	100.0	(200)	29.214	14.607	0.1637	14	1.4015	19.2	(331)	66.682	33.341	0.3568
3	2.7320	37.3	(210)	32.753	16.377	0.1830	15	1.3660	9.6	(420)	66.652	34.326	0.3660
4	2.4940	39.4	(211)	35.961	17.981	0.2005	16	1.3331	8.0	(421)	70.596	35.298	0.3751
5	2.1590	57.7	(220)	41.788	20.894	0.2315	17	1.3024	1.9	(332)	72.516	36.258	0.3839
6	2.0363	3.5	(221)	44.454	22.227	0.2455	18	1.2470	11.8	(422)	76.300	38.150	0.4010
7	1.8419	86.7	(311)	49.442	24.721	0.2715	19	1.2216	4.0	(430)	78.168	39.084	0.4092
8	1.7635	18.2	(222)	51.799	25.900	0.2835	20	1.1981	5.1	(431)	80.024	40.012	0.4173
9	1.6943	26.1	(323)	54.582	27.041	0.2951	21	1.1757	44.7	(511)	81.868	40.934	0.4253
10	1.6327	32.4	(123)	56.301	28.151	0.3062	22	1.1344	19.0	(432)	85.535	42.768	0.4408
11	1.5273	0.2	(402)	60.579	30.289	0.3274	23	1.1154	5.2	(125)	87.360	43.680	0.4483
12	1.4617	6.2	(410)	62.650	31.325	0.3375							

PDF#99-000-0041; QM=Uncommon(?); d=Other/Unknown; I=(Unknown)

PDF Card

Alabandite

MnS

Radiation=CuK α 1

Lambda=1.5406

Filter=

Calibration=

ZT=29.605-137.675

I/c(RIR)=

Ref: JADE's Userfile

Cubic: Fm $\bar{3}m$ (225)

Z=4 mp=

CELL: 5.214 x 5.214 x 5.214 <90.0 x 90.0 x 90.0>

P.S.=

Density(c)=4.0

Density(m)=

Mwt=

Vol=141.7

Ref: Ibid.

NOTE: Hardness range is 3.5-4. Locality: Sacaromb (Nagyag), Transylvania, Romania. Submetallic black; grey in reflected light. Min-Group: Galena. PDF: 06-0518. Ref: Neues Jahrbuch für Mineralogie, Abhandlungen 144 (1982), 107. Ref: USA National Bureau of Standards Circular 539, 4 (1955), 11. Ref: American Journal of Science ser. 4, 2 (1921), 239. Ref: Handbook of Mineralogy (Anthony et al.), 1 (1990), 5.

Strong Lines: 2.611X 1.8515 1.5112 1.1112 1.0112 0.8111 0.8311 3.0211

8 Lines, Wavelength to Compute Theta = 1.54059Å(Cu), I%-Type = (Unknown)

#	d(Å)	I(v)	(hkl)	2-Theta	Theta	1/(2 θ)	#	d(Å)	I(v)	(hkl)	2-Theta	Theta	1/(2 θ)
1	3.0150	9.0		29.605	14.802	0.1858	5	1.1680	45.0		82.523	41.262	0.4261
2	2.6120	100.0		34.304	17.152	0.1914	6	1.0680	49.0		92.540	46.270	0.4690
3	1.8470	71.0		49.297	24.649	0.2707	7	0.8700	30.0		124.601	62.300	0.5747
4	1.5090	35.0		61.390	30.695	0.3313	8	0.8260	32.0		137.675	68.838	0.6053

PDF#01-072-1223(ROB); OM=Indexed(I); d=Calculated; I=Calculated

PDF Card

Chromium Sulfide

Cr₇S₇Radiation=CuK α 1

Lambda=1.5405969

Filter=

Calibration=

Zf=15 824-89 556

Wc(RIR)=3.08

Ref: Jelinek, F.

Acta Crystallogr., v10 p620 (1957)

Hexagonal - (Unknown); P $\bar{3}1c$ (163)

Z=4

mp=

CELL: 5.939 x 5.939 x 11.192 <90.0 x 90.0 x 120.0>

P.S.=bP20.00

Density(c)=3.889

Density(m)=4.075

Mwt=200.17

Vol=341.87

F(30)=999.910.000.32:0

Ref: Ibsd.

Additional Patterns: See PDF 00-011-0007, ANX. A2X3, ICSD Collection Code: 16720, Test from ICSD. No R value given. At least one TF missing. Calc. density unusual but tolerable. Minor Warning: No R value given in the paper. Wyckoff Sequence: i f c b (P3-1C)

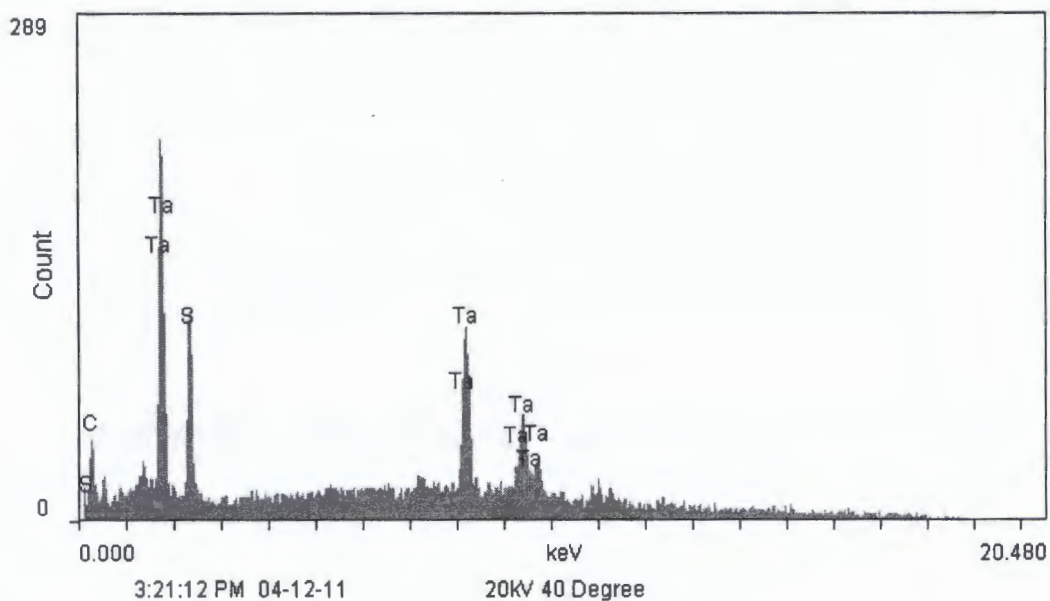
Strong Lines: 5 60/4 5 14/1 4 67/3 3 79/1 3 92/1 2 97/2 2 62/X

68 Lines, Wavelength to Compute Theta = 1.54059Å(Cu), % - Type = Peak Height

#	d(Å)	I(v)	(hkl)	2-Theta	Theta	1/(2d)	#	d(Å)	I(v)	(hkl)	2-Theta	Theta	1/(2d)
1	5.9980	16.2	(002)	15.824	7.912	0.0683	35	1.4151	1.4	($\bar{3}\bar{1}1$)	65.962	32.981	0.3533
2	5.1433	2.7	(100)	17.227	8.613	0.0972	36	1.3690	6.5	(008)	66.817	33.408	0.3574
3	4.5735	13.4	(101)	18.974	9.487	0.1070	37	1.3623	0.5	($\bar{3}12$)	67.732	33.866	0.3617
4	3.7666	3.0	(102)	23.473	11.737	0.1320	38	1.3576	0.5	(207)	69.124	34.562	0.3682
5	3.0199	5.8	(103)	29.556	14.778	0.1656	39	1.3500	0.2	(108)	69.566	34.793	0.3704
6	2.9695	16.2	(110)	30.069	15.035	0.1684	40	1.3459	0.5	($\bar{2}\bar{1}6$)	69.823	34.911	0.3716
7	2.7980	0.2	(004)	31.950	15.980	0.1787	41	1.3324	1.1	($\bar{3}\bar{1}3$)	70.636	35.318	0.3753
8	2.6231	82.6	($\bar{1}\bar{1}2$)	34.155	17.077	0.1906	42	1.3115	23.0	($\bar{2}\bar{2}4$)	71.935	35.967	0.3812
9	2.5717	1.0	(200)	34.859	17.430	0.1944	43	1.2858	0.2	(400)	73.606	36.803	0.3889
10	2.5084	3.8	(201)	35.798	17.899	0.1995	44	1.2774	0.5	(401)	74.171	37.085	0.3914
11	2.4679	1.2	(104)	36.529	18.264	0.2034	45	1.2709	0.3	($\bar{3}\bar{1}4$)	74.618	37.309	0.3934
12	2.3367	1.0	(202)	38.495	19.247	0.2140	46	1.2656	2.4	($\bar{1}\bar{1}8$)	74.964	37.482	0.3951
13	2.1174	2.5	(203)	42.668	21.334	0.2361	47	1.2623	3.4	(306)	75.215	37.607	0.3961
14	2.0525	3.4	(105)	44.066	22.043	0.2436	48	1.2532	0.2	(402)	75.857	37.928	0.3990
15	2.0364	100.0	($\bar{1}\bar{1}4$)	44.452	22.226	0.2455	49	1.2349	0.7	($\bar{2}\bar{1}7$)	77.168	38.584	0.4049
16	1.9440	0.7	(210)	46.867	23.444	0.2572	50	1.2289	0.2	(208)	77.630	38.815	0.4069
17	1.9153	3.7	($\bar{2}\bar{1}1$)	47.429	23.714	0.2611	51	1.2157	0.4	(403)	78.640	39.320	0.4113
18	1.8934	0.6	(204)	48.012	24.006	0.2641	52	1.2087	0.4	(109)	79.178	39.589	0.4137
19	1.8653	1.5	(006)	48.761	24.381	0.2680	53	1.2030	0.7	($\bar{3}\bar{1}5$)	79.632	39.816	0.4156
20	1.8363	1.1	($\bar{2}\bar{1}2$)	49.603	24.801	0.2723	54	1.1600	0.2	(320)	81.508	40.754	0.4237
21	1.7536	0.5	(106)	52.115	26.057	0.2851	55	1.1736	0.7	(321)	82.066	41.028	0.4261
22	1.7240	3.4	($\bar{2}\bar{1}3$)	53.079	26.539	0.2900	56	1.1684	0.2	(404)	82.492	41.246	0.4280
23	1.7144	51.4	(300)	53.397	26.699	0.2916	57	1.1617	6.9	($\bar{2}\bar{2}6$)	83.072	41.536	0.4304
24	1.6884	1.4	(205)	54.268	27.144	0.2961	58	1.1546	0.2	(322)	83.698	41.849	0.4331
25	1.6392	5.9	(302)	56.057	28.028	0.3050	59	1.1355	0.2	($\bar{2}\bar{1}8$)	85.432	42.716	0.4403
26	1.5965	0.8	($\bar{2}\bar{1}4$)	57.897	28.848	0.3132	60	1.1331	0.2	($\bar{3}\bar{1}6$)	85.855	42.828	0.4413
27	1.5796	18.9	($\bar{1}\bar{1}6$)	58.375	29.187	0.3165	61	1.1250	0.6	($\bar{3}\bar{2}3$)	86.422	43.211	0.4444
28	1.5266	0.9	(107)	60.599	30.299	0.3275	62	1.1224	1.7	(410)	86.578	43.339	0.4455
29	1.5100	0.3	(206)	61.347	30.674	0.3311	63	1.1195	1.2	(209)	86.952	43.478	0.4466
30	1.4846	2.3	(220)	62.504	31.252	0.3368	64	1.1165	1.2	(0,0,10)	86.952	43.478	0.4466
31	1.4677	1.5	($\bar{2}\bar{1}5$)	63.312	31.656	0.3407	65	1.1166	0.4	(411)	87.222	43.611	0.4477
32	1.4618	0.3	(304)	63.597	31.799	0.3420	66	1.1150	0.4	(405)	87.398	43.699	0.4484
33	1.4351	13.7	(222)	64.926	32.463	0.3484	67	1.1025	11.6	(412)	88.851	44.425	0.4544
34	1.4265	0.5	(310)	65.366	32.683	0.3505	68	1.0936	0.2	(1,0,10)	89.556	44.778	0.4572

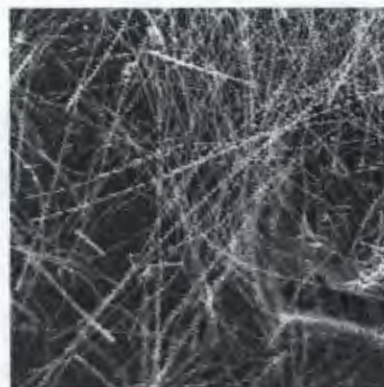
APPENDIX C: ENERGY DISPERSIVE X-RAY SPECTROSCOPY REPORTS

KB Pr A1



Identification result: KB Pr A1

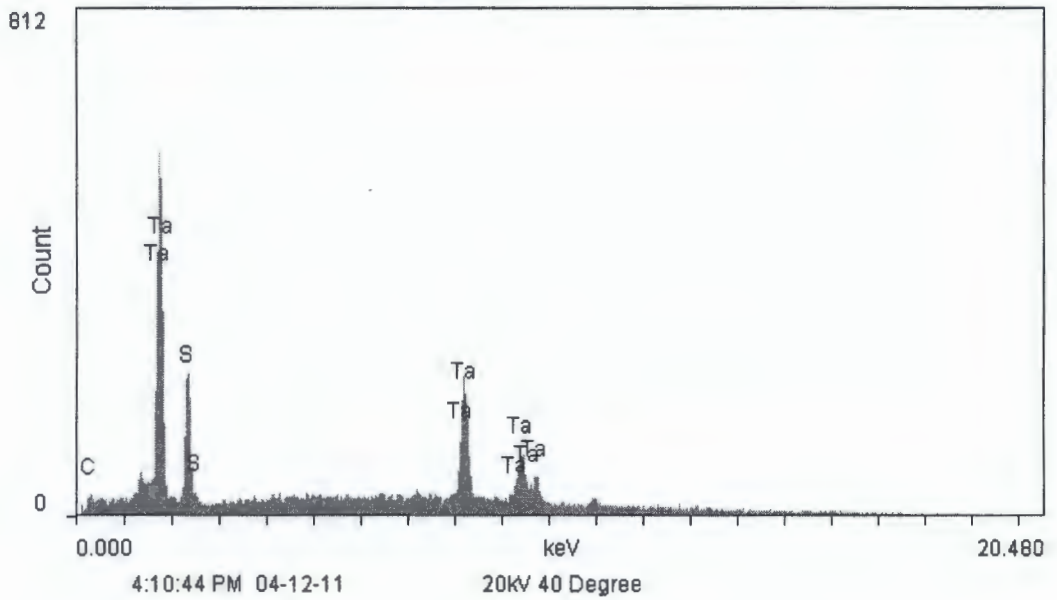
S	0.160 keV
C	0.270 keV
Ta	1.700 keV
Ta	1.770 keV
S	2.310 keV
Ta	8.089 keV
Ta	8.150 keV
Ta	9.210 keV
Ta	9.350 keV
Ta	9.500 keV
Ta	9.650 keV



Quant result: KB Pr A1

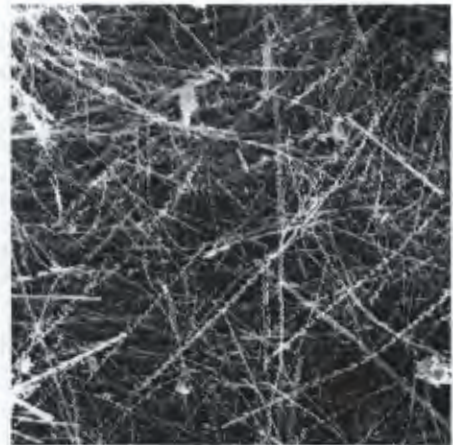
Elements:	WT%	AT%	K_A	K_F	K_Z	Intensity	P/bkg
TaM	17.78	13.16	1.027	1	0.97	6.309	6.8
S K	7.56	31.58	0.508	1	1.357	3.67	4.5
TaL	74.66	55.26	1.002	1	0.961	4.944	5.3

KB Pr B1



Identification result: KB Pr B1

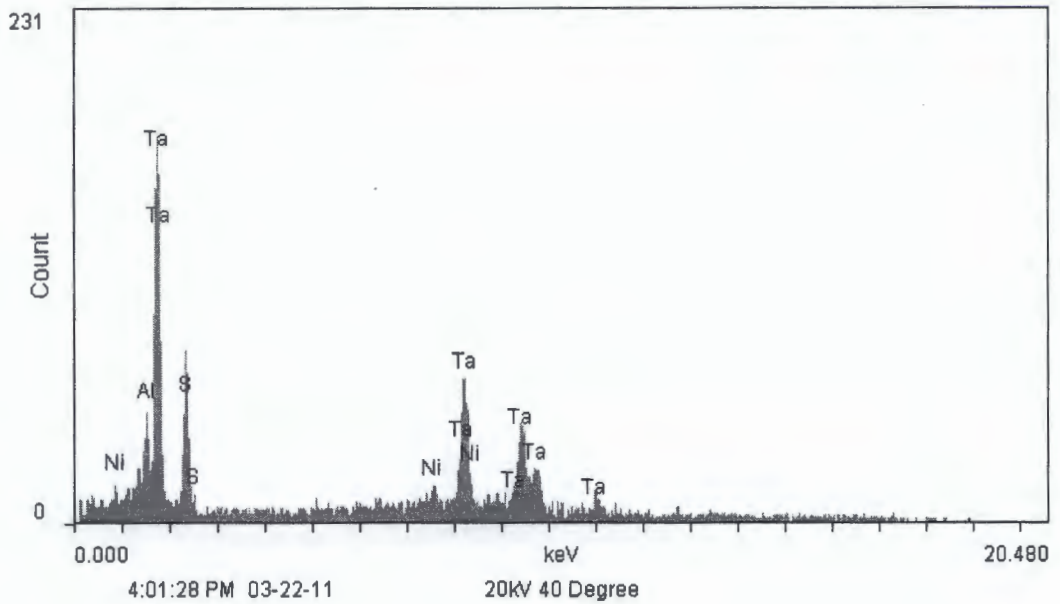
C	0.270 keV
Ta	1.700 keV
Ta	1.770 keV
S	2.310 keV
S	2.460 keV
Ta	8.089 keV
Ta	8.150 keV
Ta	9.210 keV
Ta	9.350 keV
Ta	9.500 keV
Ta	9.650 keV



Quant result: KB Pr B1

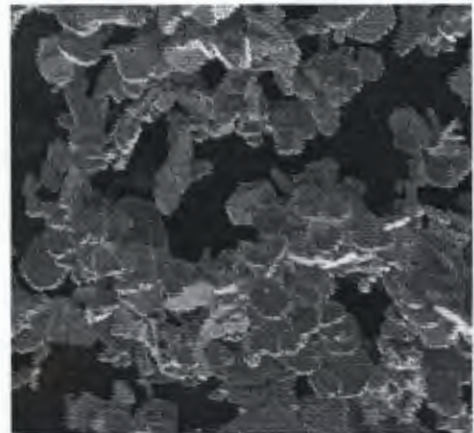
Elements:	WT%	AT%	K_A	K_F	K_Z	Intensity	P/bkg
TaM	23.57	17.36	1.028	1	0.969	47.065	9.4
S K	7.7	32.02	0.509	1	1.356	21.062	5.3
TaL	68.73	50.62	1.002	1	0.96	25.601	5.3

KB Pr C1



Identification result: KB Pr C1

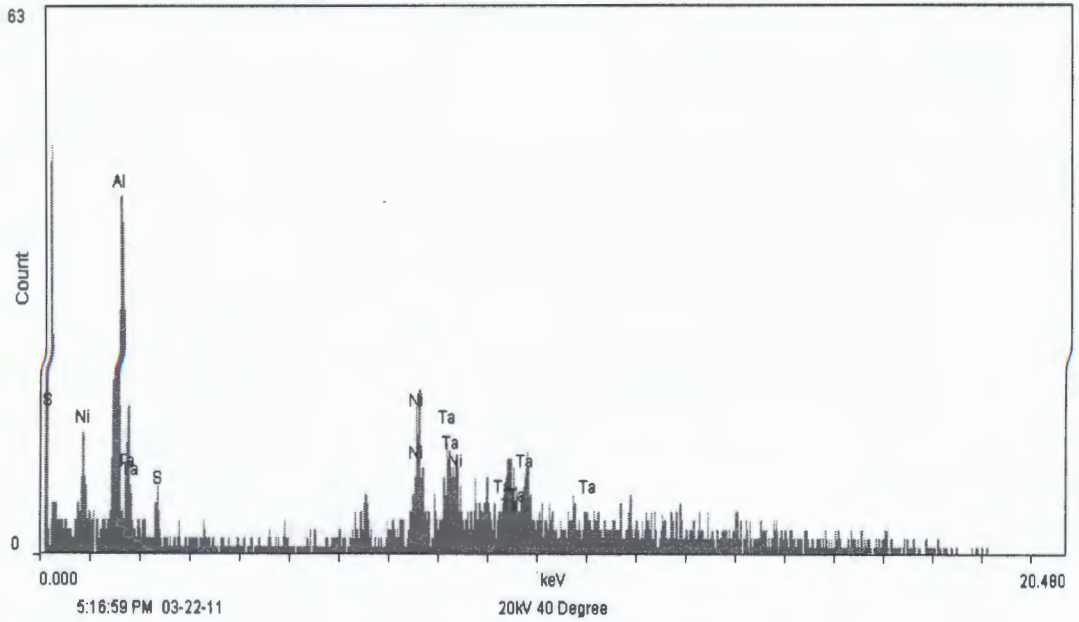
Ni	0.851 keV
Al	1.500 keV
Ta	1.730 keV
Ta	1.771 keV
S	2.299 keV
S	2.450 keV
Ni	7.470 keV
Ta	8.080 keV
Ta	8.161 keV
Ni	8.271 keV
Ta	9.190 keV
Ta	9.351 keV
Ta	9.649 keV
Ta	10.879 keV



Quant result: KB Pr C1

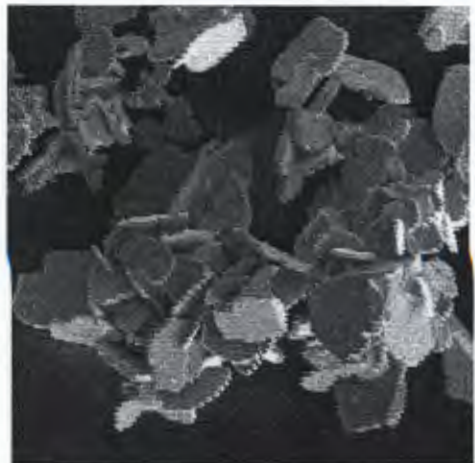
Elements:	WT%	AT%	K_A	K_F	K_Z	Intensity	P/bkg
TaM	26.69	19.9	1.026	1	0.97	10.581	15.8
S K	7.35	30.93	0.508	1	1.358	3.985	5.5
TaL	65.95	49.17	1.002	1	0.962	4.883	3.1

KB Pr D1



Identification result: KB Pr D1

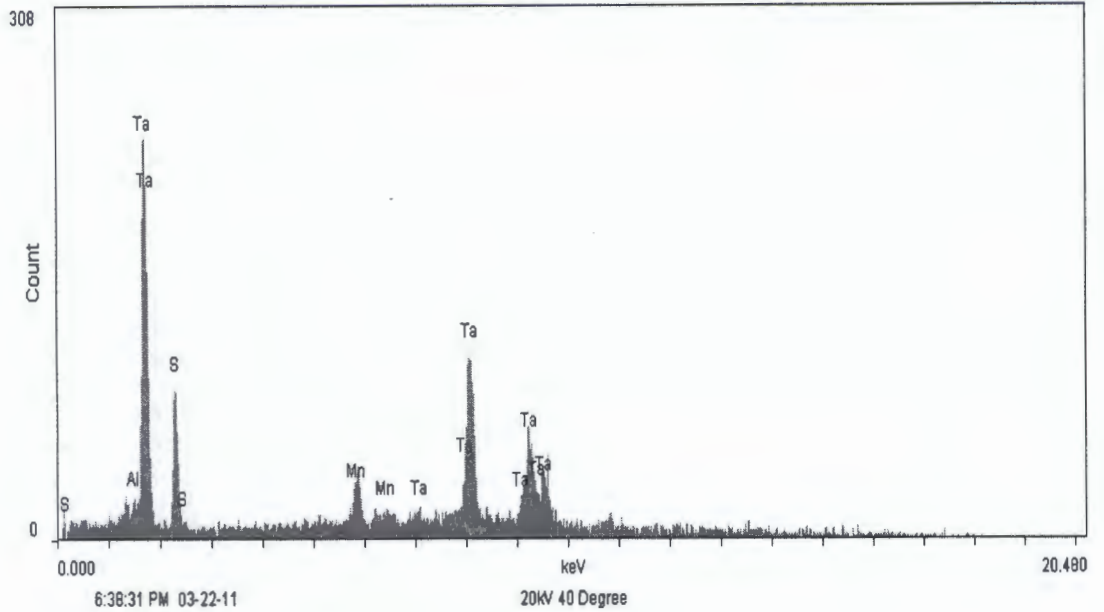
- S 0.150 keV
- Ni 0.850 keV
- Al 1.508 keV
- Ta 1.710 keV
- Ta 1.770 keV
- S 2.311 keV
- Ni 7.450 keV
- Ni 7.471 keV
- Ta 8.090 keV
- Ta 8.150 keV
- Ni 8.260 keV
- Ta 9.200 keV
- Ta 9.330 keV
- Ta 9.490 keV
- Ta 9.640 keV
- Ta 10.890 keV



Quant result: KB Pr D1

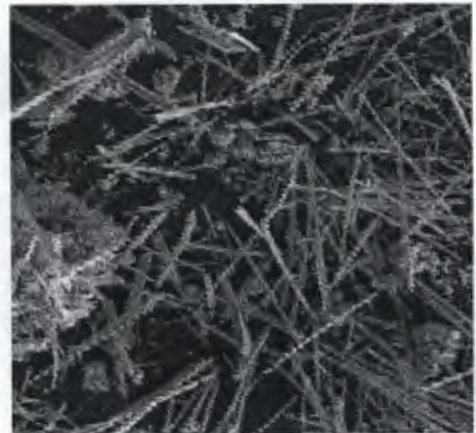
Elements:	WT%	AT%	K_A	K_F	K_Z	Intensity	P/okg
TaM	12.95	11.59	1.009	1	0.989	0.069	1
S K	2.53	12.77	0.49	1	1.392	0.018	0.4
TaL	84.52	75.64	1.001	1	0.967	0.086	1

KB Mn A1



Identification result: KB Mn A1

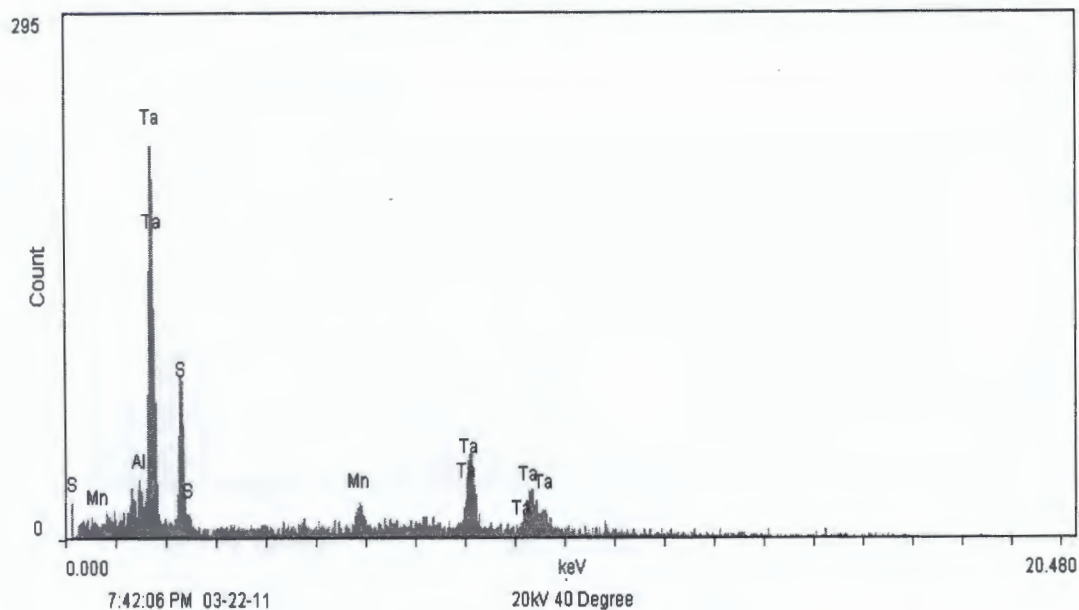
S	0.150 keV
Al	1.500 keV
Ta	1.721 keV
Ta	1.761 keV
S	2.320 keV
S	2.459 keV
Mn	5.910 keV
Mn	6.490 keV
Ta	7.161 keV
Ta	8.080 keV
Ta	8.161 keV
Ta	9.190 keV
Ta	9.351 keV
Ta	9.500 keV
Ta	9.639 keV



Quant result: KB Mn A1

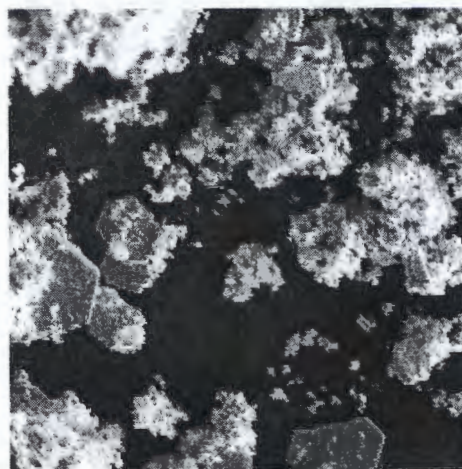
Elements:	WT%	AT%	K_A	K_F	K_Z	Intensity	P/bkg
TaM	19.18	14.45	1.012	1	0.972	7.453	13.8
TaM	0.84	0.63	1.012	1	0.972	0.327	0.6
S K	5.25	22.34	0.509	1	1.359	2.835	5.9
MnK	3.65	9.05	0.931	1.053	1.165	1.321	1.7
TaL	71.07	53.53	1	1	0.963	5.218	3.4

KB Mn B1



Identification result: KB Mn B1

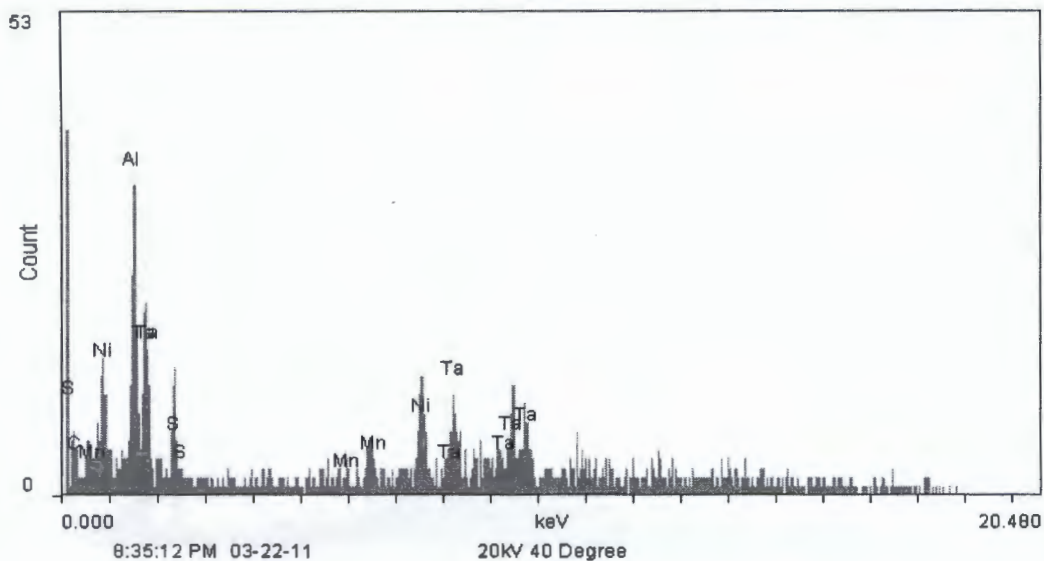
S	0.139 keV
Mn	0.630 keV
Al	1.490 keV
Ta	1.730 keV
Ta	1.771 keV
S	2.321 keV
S	2.450 keV
Mn	5.900 keV
Ta	8.090 keV
Ta	8.150 keV
Ta	9.210 keV
Ta	9.340 keV
Ta	9.660 keV



Quant result: KB Mn B1

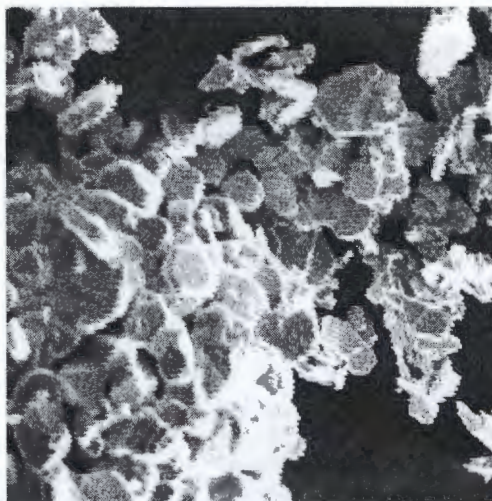
Elements:	WT%	AT%	K_A	K_F	K_Z	Intensity	P/bkg
MnL	0	0.01	0.383	1	1.107	0	0
TaM	34.54	22.31	1.032	1	0.954	6	18
SK	10.56	38.5	0.526	1	1.329	2.572	9.1
MnK	2.51	5.34	0.933	1.052	1.141	0.398	0.9
TaL	52.39	33.85	1.002	1	0.941	1.681	3.3

KB Mn C1



Identification result: KB Mn C1

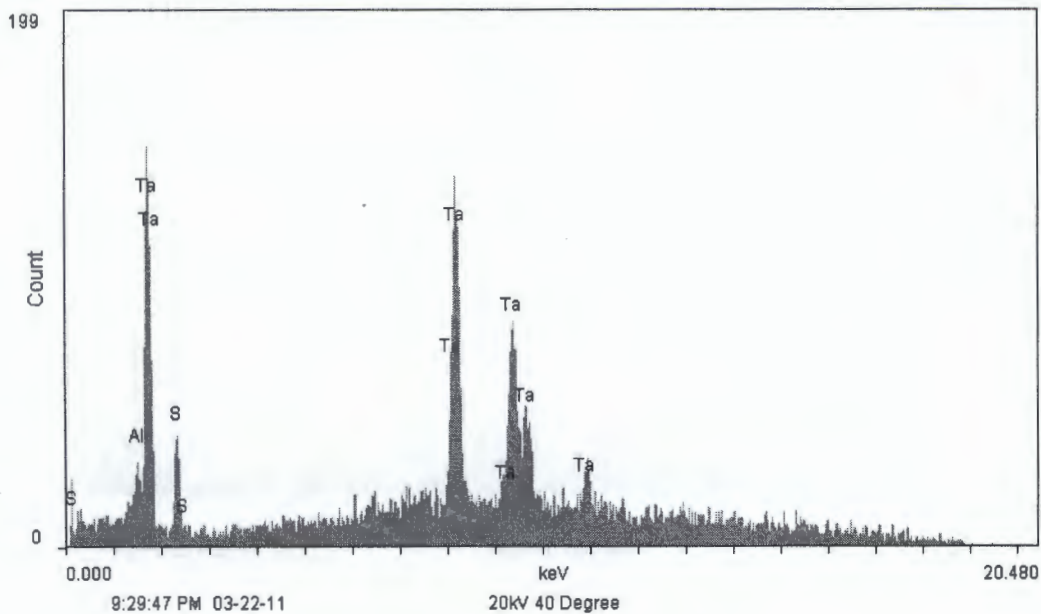
S	0.151 keV
C	0.291 keV
Mn	0.640 keV
Ni	0.840 keV
Al	1.511 keV
Ta	1.699 keV
Ta	1.770 keV
S	2.310 keV
S	2.461 keV
Mn	5.900 keV
Mn	6.490 keV
Ni	7.470 keV
Ta	8.081 keV
Ta	8.159 keV
Ta	9.210 keV
Ta	9.340 keV
Ta	9.661 keV



Quant result: KB Mn C1

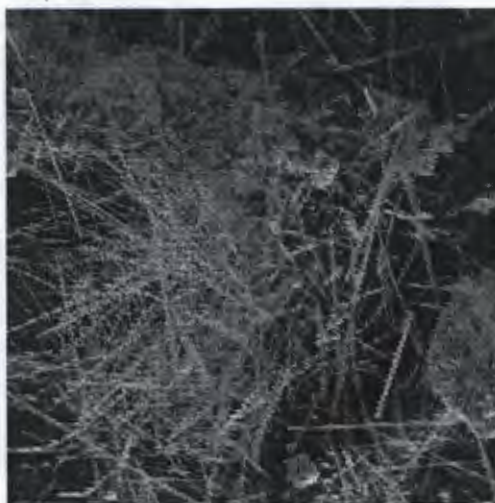
Elements:	WT%	AT%	K_A	K_F	K_Z	Intensity	P/bkg
MnL	6.8	14.44	0.391	1	1.107	0.012	0.3
TaM	29.38	18.94	1.016	1	0.955	0.238	6.6
S K	8.5	30.94	0.529	1	1.328	0.099	2.3
MnK	0.01	0.03	0.935	1.05	1.141	0	0
TaL	55.3	35.65	1	1	0.939	0.084	0.9

KB Cr A1



Identification result: KB Cr A1

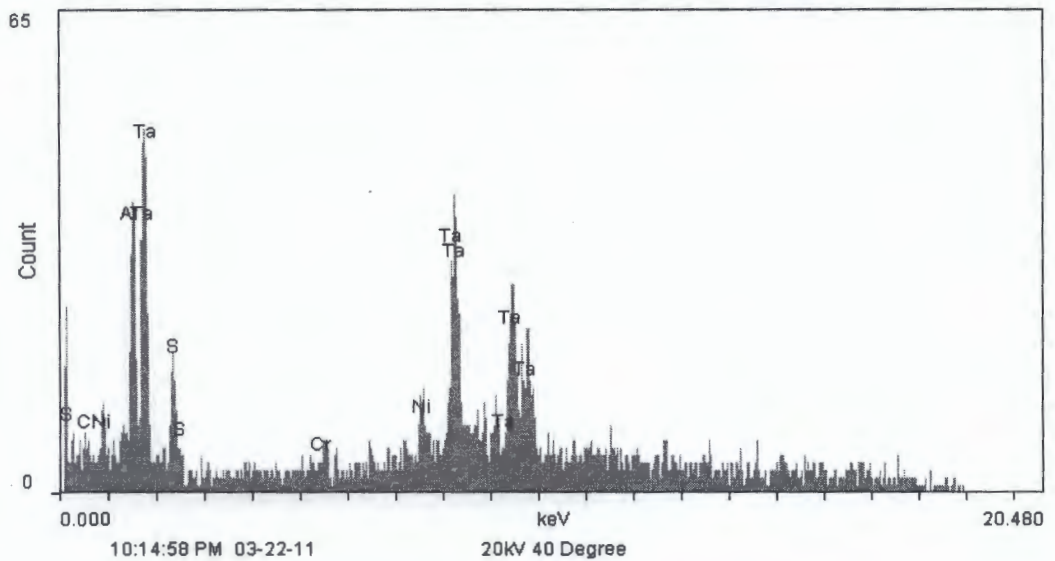
S	0.140 keV
Al	1.500 keV
Ta	1.711 keV
Ta	1.770 keV
S	2.320 keV
S	2.450 keV
Ta	8.081 keV
Ta	8.150 keV
Ta	9.210 keV
Ta	9.351 keV
Ta	9.639 keV
Ta	10.890 keV



Quant result: KB Cr A1

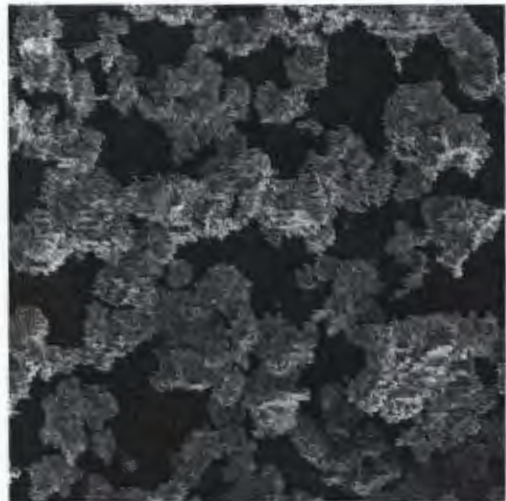
Elements:	WT%	AT%	K_A	K_F	K_Z	Intensity	P/bkg
TaM	11.94	10.63	1.01	1	0.989	4.13	6.1
S K	2.65	13.32	0.49	1	1.391	1.236	4
TaL	85.41	76.04	1.001	1	0.986	5.632	6

KB Cr B1



Identification result: KB Cr B1

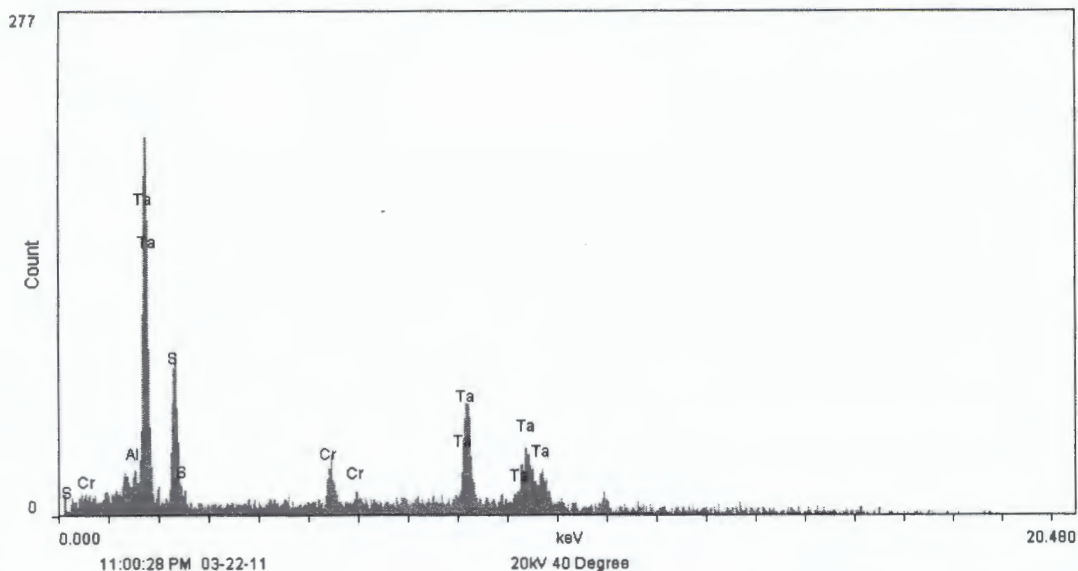
S	0.150 keV
Cr	0.570 keV
Ni	0.841 keV
Al	1.506 keV
Ta	1.700 keV
Ta	1.770 keV
S	2.309 keV
S	2.460 keV
Cr	5.410 keV
Ni	7.490 keV
Ta	8.101 keV
Ta	8.161 keV
Ta	9.210 keV
Ta	9.330 keV
Ta	9.650 keV



Quant result: KB Cr B1

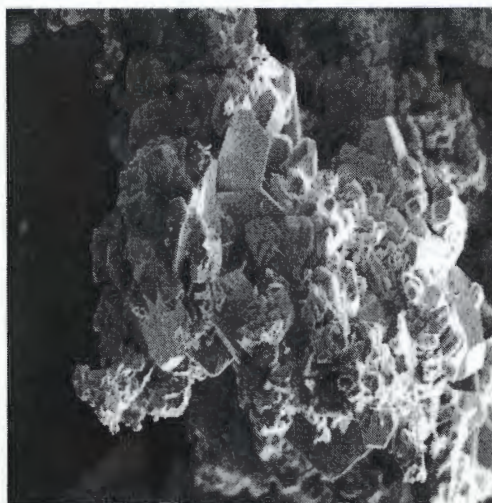
Elements:	WT%	AT%	K_A	K_F	K_Z	Intensity	P/bkg
CrL	5.12	13.68	0.341	1	1.149	0.054	0.9
TaM	15.89	12.21	1.008	1	0.974	1.152	7.7
SK	3.78	16.36	0.508	1	1.362	0.381	2.3
TaL	0.01	0.01	1	1	0.964	0	0
TaL	75.21	57.75	1	1	0.964	1.034	2.2

KB Cr C1



Identification result: KB Cr C1

S	0.160 keV
Cr	0.570 keV
Al	1.491 keV
Ta	1.710 keV
Ta	1.780 keV
S	2.300 keV
S	2.460 keV
Cr	5.400 keV
Cr	5.939 keV
Ta	8.101 keV
Ta	8.140 keV
Ta	9.220 keV
Ta	9.349 keV
Ta	9.650 keV



Quant result: KB Cr C1

Elements:	WT%	AT%	K_A	K_F	K_Z	Intensity	P/bkg
CrL	5.26	11.07	0.362	1	1.116	0.399	1.3
TaM	29.7	17.95	1.023	1	0.946	14.7	15.4
S K	9.52	32.46	0.539	1	1.313	6.803	8.6
CrK	3.33	7	0.917	1.031	1.143	1.701	1.9
TaL	52.19	31.53	1.001	1	0.928	4.781	2.3